INVESTIGATING MULTI-SPECIES INTERACTIONS AND SPATIAL STRUCTURE OF GUT-BACTERIAL COMMUNITIES USING LIVE IMAGING

by

DEEPIKA SUNDARRAMAN

A DISSERTATION

Presented to the Department of Physics
and the Division of Graduate Studies of the University of Oregon
in partial fulfillment of the requirements
for the degree of
Doctor of Philosophy

September 2022

DISSERTATION APPROVAL PAGE

Student: Deepika Sundarraman

Title: Investigating Multi-Species Interactions and Spatial Structure of Gut-Bacterial Communities using Live Imaging

This dissertation has been accepted and approved in partial fulfillment of the requirements for the Doctor of Philosophy degree in the Department of Physics by:

Stephanie A. Majewski	Chairperson
Raghuveer Parthasarathy	Advisor
Jayson Paulose	Core Member
Karen Guillemin	Institutional Representative

and

Krista M. Chronister	Vice Provost of Graduate Studies

Original approval signatures are on file with the University of Oregon Division of Graduate Studies.

Degree awarded September 2022

DISSERTATION ABSTRACT

Deepika Sundarraman

Doctor of Philosophy

Department of Physics

September 2022

Title: Investigating Multi-Species Interactions and Spatial Structure of Gut-Bacterial Communities using Live Imaging

Animal intestines harbor hundreds of microbial species that play a crucial role in host health and development. Despite their importance, many questions about the rules that govern community assembly in these complex environments remain unanswered and almost impossible to study in humans. For example, is it possible to construct multi-species communities from an understanding of pairwise interactions? What is the role of spatial structure and timing in community assembly? How do species' spatial structure and interactions affect the host? We focus on addressing these questions using a consortium of gut bacterial species, native to the vertebrate model organism of larval zebrafish. We first characterize pairwise interactions between a consortium of 5 gut bacterial isolates in 2-species and 5-species competition experiments using an interaction model and find evidence for higher order interactions that dampened strong pairwise competition and enabled coexistence in 5-species communities.

We next focus on a specific pair showing strong pairwise competition in 2-species experiments. Using light sheet fluorescence microscopy, we illuminate on the role of spatial structure in the competition between two highly aggregated species localized in the intestinal midgut, namely strains of genera *Aeromonas* (AE) and *Enterobacter* (EN). We test whether altering aggregation and localization behavior impact this interaction using a bacterial strain *Aeromonas-MB4*, derived from parental AE and composed mostly of planktonic cells that are anterior localized. When AE-MB4 invades fish colonized with EN, it induces disaggregation of the highly aggregated EN strain, an effect weakened in the presence of the other 4 species. Additionally, we observe that AE-MB4 induces increased inflammation compared to the aggregated parental AE strain, suggesting possible links between spatial structure and host inflammation.

These studies illustrate the complex ways in which species interact with each other and impact the host and that multi-species gut bacterial communities are capable of showing resilience by dampening strong competition effects.

This dissertation contains previously published and unpublished material.

CURRICULUM VITAE

NAME OF AUTHOR: Deepika Sundarraman

GRADUATE AND UNDERGRADUATE SCHOOLS ATTENDED:

University of Oregon, Eugene, Oregon
The College of Wooster, Wooster, Ohio

DEGREES AWARDED:

Doctor of Physics, 2022, University of Oregon
Bachelor of Arts, (1) Physics (2) German Studies, 2014

AREAS OF SPECIAL INTEREST:

Biophysics of microbial interactions, 3D live imaging, image analysis, machine learning

PROFESSIONAL EXPERIENCE:

Graduate Employee, University of Oregon, 2017-22

Teach for India Fellow, Teach for India, 2015-17

GRANTS, AWARDS AND HONORS:

Selected Speaker, Physics of Life Symposium, 2022

First Prize, Oregon Bioengineering Symposium Talk Competition, 2020

Diversity Equity and Inclusion grant, UO Department of Biology, 2018

First Year Fellowship, University of Oregon, 2017

Arthur H. Compton Prize, The College of Wooster, 2014

Copeland Award, The College of Wooster, 2013

Mary A. Sanborne Prize, The College of Wooster, 2013

PUBLICATIONS:

Sundarraman, D., Hay, E. A., Martins, D. M., Shields, D. S., Pettinari, N. L. & Parthasarathy, R., Higher-Order Interactions Dampen Pairwise Competition in the Zebrafish Gut Microbiome. *mBio*, **11**: e01667-20 (2020)

Leary, C. C., Lankford, M. & Sundarraman, D., Polarization-based control of spin-orbit vector modes of light in biphoton interference, *Opt. Express* **24**, 14227-14241 (2016)

Leary, C. C., Lankford, M. & Sundarraman, D., Coupling of spin and orbital degrees of freedom in tunable Hong-Ou-Mandel interference involving photons in hybrid spin-orbit modes. *Proc. SPIE, Quantum Optics and Quantum Information Transfer and Processing*, 95050T (2015)

Leary, C. C., Gilliss, T. & Sundarraman, D., Bimodal Hong-Ou-Mandel Interference in Symmetric and Asymmetric Optical Systems, *The Rochester Conferences on Coherence and Quantum Optics and the Quantum Information and Measurement meeting, Optical Society of America*, M6.05.(2013)

Brückner, U. & Sundarraman, D., Engagement with Civil Society EU India Relations in the Field of Education and Labour Migration: The Case of Germany, *FPRC Journal*, **13** 228-237 (2013)

ACKNOWLEDGEMENTS

I appreciate a number of people who have made it possible for me to do this work. A sincere thanks to my dissertation adviser, Raghu Parthasarathy who served as an excellent mentor and introduced me to the fascinating world of biophysics and quantitative image analysis. The consistent guidance and opportunities for growth and learning have been instrumental in my PhD experience. All my fellow colleagues, within the Parthasarathy lab and in other labs affiliated with the META center at UO, energized me with their ideas and feedback. Working collaboratively with other scientists such as Jarrod Smith and mentors such as Karen Guillemin has enabled me to push my science to new levels.

I thank my friends, both near and afar, and from different walks of life for their support and encouragement. I appreciate my family, in particular, my mother, who encourages me to pursue all my dreams and leads with extraordinary strength and grace. My sister has always been a source of constant guidance throughout life.

I've been fortunate to have many mentors from different facets of life, both within and outside of science. I appreciate Cody Leary, Jeremy Wegner and Rajender Shah for their support at different points in my education.

TABLE OF CONTENTS

LIST OF FIGURES

Figure Page

CHAPTER I

INTRODUCTION

1.1. Overview

Microbes are ubiquitous and intimately connected with the environments they reside in, some of which include soil, oceans, mammalian intestines and even extreme habitats such as deep sea hydrothermal vents and hot and cold deserts. They perform a variety of functions in these varied environments, ranging from biodegradation to nitrogen fixation, carbon dioxide sequestration, plant nutrition and more [1]. Realization of their significance and functionality has prompted an increased interest in the role of microbes within host intestines. Recent work has illustrated that microbes are involved in aspects of host immunity, development, and a variety of diseases [2–11]. For instance, microbes can be linked to functions such as dietary fat uptake, proliferation of insulin-producing beta cells responsible for regulating glucose levels in our body, and development of immune cell types such as T, B and Treg cells [12–26]. Multiple diseases, including inflammatory bowel disease(IBD), rheumatoid arthritis and Crohn's disease have been linked to dysbiosis of the microbiome [27–31]. As studies continue to uncover the various ways in which microbes impact our lives, there is still a limited understanding of the determinants of microbial composition, especially in an environment like the vertebrate gut, where there is great complexity in chemical composition and anatomy as well as physical flows [32, 33].

Different parts of the gastro-intestinal tract have been shown to differ in microbial composition [34], indicative of the various selection pressures at play

within the gut. The members of this spatially varying composition comprise a wide variety of bacteria, archaea, fungi as well as viruses [35]. When cataloging bacteria alone, almost 2000 distinct taxa have been detected to date [36]. The enormous diversity and functionality of these microbes warrants the question; how do these members interact with each other within the vertebrate gut and what rules govern microbial composition? Several studies have described how the initial residents can determine which microbes are allowed to cohabit and the potential benefits to resistance against pathogenic invasion [37, 38]. Controlled studies in model systems allow us to infer general rules for community structure and gather information on the mechanisms by which multi-species intestinal communities assemble and impact the host.

In the era of interdisciplinarity, several different approaches are useful to tackle this question. As a physicist, the gut with its spatiotemporally varying features and composition, peristaltic flows and bacterial residents serves as a fascinating model system to study complex interactions. In this dissertation, I bring a quantitative perspective to studying inter-species bacterial interactions in the larval zebrafish gut combining techniques of 3D live imaging, image analysis and biophysical modeling. In the remaining text of this chapter, I set a foundation for this work by describing model systems, relevant ecological concepts, interaction models and tools used in this study.

In the subsequent chapter, Chapter II, adapted from published work, I characterize inter-species interactions in the larval zebrafish gut using an interaction model and address whether multi-species interactions can be predicted from a pairwise additive model.

In Chapter III, adapted from work recently submitted for publication, I delineate a novel mechanism for interaction between two bacterial species that have been found to have spatially distinct localizations.

In Chapter IV, I zoom out to focus on the host and host-bacteria interactions by describing some results on immune activity for different gut-bacterial species.

Finally, I draw conclusions from all my PhD work and map out various directions for further exploration in Chapter V.

1.2. Model systems

Studies in humans have revealed novel insights into how factors such as diet, social environment and age impact gut microbial composition [39–45]. Although these studies reveal correlations, experiments in controlled systems are necessary to find evidence for causation and gain mechanistic insights. Various model organisms have been used to this end, a few examples being mice, fruit flies (*Drosophila melanogaster*), nematodes (*Caenorhabditis elegans*) and zebrafish (*Danio rerio*). Each of these model systems have been exploited for their own advantages.
Mice are often preferred for their genetic similarity to humans, however a single experiment can often span months with most studies usually timed between the 6-20 week age range. Given the intensive task of maintaining mice for long periods, some of the largest datasets involve only about 10 mice.

In other model systems such as *Drosophila melanogaster* and *Caenorhabditis elegans* experiments are often more tractable than in mice, since these animals develop on a shorter time scale i.e approximately days and require less maintenance. It's unclear however whether the results in these invertebrate animals will translate into humans as the intestines of these animals differ more

compared to the vertebrate gut [46]. For example, zebrafish possess organs like the liver and pancreas, which have similar functionality to that in humans [46]. Such specialized organs are missing in *Drosophila melanogaster* or *Caenorhabditis elegans*. For both these organisms, data is obtained from dissection of the gut, fixation of fish or chemical information from stool samples typically in the form of RNA or DNA sequences from which it is not possible to infer spatial structure or dynamic information on microbial communities in the gut.

In recent decades, the zebrafish has turned out to be an excellent model system to investigate host-microbe interactions within the vertebrate gut. These organisms are amenable to gnotobiotic techniques i.e. can be easily raised devoid of microbes, which allows for controlled studies on bacterial interactions. In addition, its optical transparency at larval stages and a wide variety of transgenic strains makes it an ideal system to visualize bacterial dynamics and relationships to different host characteristics [47–49]. Recent work generating fluorescently tagged bacterial isolates allows for visualization of bacterial dynamics in the native gut environment in live fish [50]. This work has yielded 3D live imaging studies illuminating specific spatiotemporal features of gut bacterial populations and competition dynamics, mechanisms of *Vibrio cholera* invasion, and effects of antibiotics on the gut microbiota [51–53]. All these features make larval zebrafish an ideal system for controlled studies of bacterial interactions and their dynamics.

1.3. Quantifying species interactions and types of abundance data

The German zoologist Ernst Haeckel introduced the term ecology as the study of the relationships of organisms with their environment. Darwin pioneered some of the earliest comparative ecological studies in the field that led

to revolutionary findings on evolution [54]. During the 20th century, experiments in ecology involved cataloging species in their natural settings [55–57]. It wasn't until the notable work of Robert Paine that simple perturbative experiments on ecosystems to infer species interactions become popular. Rob Paine's seminal experimental studies on tidepool ecosystems paved the way for the idea of a 'keystone species' [58–61]. To extract the role of a single species on the ecosystem, Paine removed all the starfish inhabiting one site and left them undisturbed in another. He observed that the site that lacked the starfish population saw a loss of species diversity over a period of two years. As starfish preyed on mussels, when starfish were present, the mussel population was in check. In the absence of starfish, the mussel population takes over all the available space, eliminating other species from the community. In this case, the keystone species starfish was responsible for maintaining diversity in tidepools. Paine's species-removal approach was able to isolate individual species' effects on the remaining species in the ecosystem.

In the context of the gut microbiome, a variety of approaches have been used to infer species effects or interactions. Developments in DNA sequencing technologies have resulted in easy procurement of relative abundance data, often derived from stool samples. Relative abundance data is a measure of what fraction of the total population is composed of a given species, not giving information about absolute abundance. Such data is used to calculate correlation coefficients, such as Pearson or Spearman correlations, that indicate whether two species are likely to be found simultaneously or not. It is often assumed that positively correlated species have cooperative interactions and negatively correlated species have competitive interactions, which may not necessarily be accurate [62]. Positive

correlations between species can also come from scenarios in which two species are non-interacting or competing, but show an overall increase in abundance. Moreover, species interactions are in general asymmetric, i.e. the effect of a species A on B is not the same or equal to that of B on A. These correlation coefficients are unable to capture this as they are inherently symmetric.

Compared to relative abundance, absolute abundance data give a thorough representation of the constituent members and their numbers. Studies collecting absolute abundance information are, however, difficult, and usually not feasible for large scale microbiome studies, especially related to humans. Obtaining such data is however more tractable in in vitro settings or in model system experiments that sample the entire population of the gut to map interactions.

1.4. Interaction types, models and stability

As described earlier, ecological systems such as the gut microbiome, more often than not, comprise a large number of players. Among any two species, interactions may be competitive, cooperative, or neutral. Within this realm of interaction types, one can also expect asymmetric interaction states such as amensalism and commensalism, where one species is unaffected while the other is positively or negatively affected . The simplest interspecies interaction to characterize is that between a pair of species in isolation. The addition of another member results in a trio that quickly complicates the landscape for interaction types. Now, for a trio A,B and C, the interaction between A and B is context dependent and may be impacted by the presence of the species C. This is true for each of the different permutations in the trio. As communities become more diverse, mapping interactions becomes an increasingly complex problem.

To measure interactions in such multi-species communities, an approach is to use a well-defined model with limited assumptions. Since two-species/pairwise interactions form the foundation for all other interaction types, we can investigate the question of whether interactions in complex communities are a cumulative effect of multiple pairwise interactions between species pairs. If such an approach applies, it simplifies the complexity in the community and allows for a bottom-up approach to designing synthetic communities by simply using information from pairwise studies. Interactions that do not stem from a pairwise additive model are termed higher order or indirect interactions [63].

Investigating the pairwise additivity of interactions has taken precedence in multiple ecological studies [64–67]. Of particular relevance are those centered around the gut microbiome, done in various animal model systems. In a study using *C. Elegans*, the presence of additional species did not imply higher order interactions and microbial composition was found to be predictable from two-species competitions [68]. In a different study involving the *Drosophila* microbiome, higher order interactions were found to be present and responsible for shaping host-fitness traits [69].

Higher order interactions have come up in numerous studies and have been attributed to stability in complex ecosystems [70–73] The concept of stability itself has significant bearing in studies of the gut microbiome. Stability has direct implications for pathogen resistance and a stable resilient microbiome has been attributed to multiple benefits to host health and well-being [74]. Studies characterizing species interactions are an essential step to develop a better understanding of what properties constitute microbiome stability.

In recent decades, an increasing number of studies related to modeling species interactions and community stability have been piloted by physicists. Theoretical work in Pankaj Mehta's lab has developed a wide variety of statistical tools and models to study interaction networks [62, 75, 76]. Some of these tools have been used to infer interactions and 'keystone species' in large microbiome datasets [62]. Other notable work is the quantitative modeling work by Ned Wingreen's group to study metabolic interaction dynamics of microbial consortia including trade-offs and spatial structure to predict diversity in complex microbiomes [73, 77, 78]. This work showed that multi-species coexistence is more widespread than previously known and stems from the many ways in which species partition metabolic tradeoffs. Experimental work on microbial communities of *C. Elegans* and soil ecosystems from Jeff Gore's lab enabled studies of higher order interactions in controlled systems, realizing the construction of a desired microbial consortia [65, 68]. Many of the tools used by physicists in these fields translate from interaction studies in other areas of physics.

In Chapter II, we use similar quantitative approaches in the form of an interaction model and investigate the rules governing species interactions in diverse bacterial communities in a controlled set of species in the vertebrate model system of larval zebrafish, something not been attempted previously. The study by Lopez et al. using the invertebrate *C. elegans* model system found that interactions in multi-species communities were pairwise additive [68]. These results are in fact contradictory to those I describe in Chapter II.

1.5. Spatial structure and its significance in the host gut environment

Spatial information is thought to be a key determinant of interaction outcomes. For example, a study comprising three-soil derived bacteria showed that by simply manipulating spatial structure, competition outcomes were altered [79]. By controlling the microscale spatial structure of three species using a microfluidic device, the study showed that when the habitats of the species were connected, one ensured the survival of all species, as opposed to the outcome when their habitats were isolated [79]. It is also hypothesized that such structuring could explain observations such as the existence of 4000-500,000 distinct microbial taxa found in as little as 30g of soil [55, 80, 81]. Spatial structure can thus be responsible for promoting diversity in complex communities. This may be of particular relevance in the gut microbiome, where it is known that distinct regions of the intestine harbor distinct environments [82–85] and that gradients of nutrients and oxygen can result in microbial reservoirs in regions such as the colonic crypts [84]. How the hundreds of species in the human intestine exploit these habitats to coexist and sustain diverse communities remains to be understood. The exploration of microbial spatial structure within the gut can thus shed insight into mechanisms of interactions.

Apart from the variations in the locations and the potential composition of microbes in different regions in the gut, there are also differences relating to how microbes may socially organize themselves. Members of a species may be planktonic, i.e. existing as discrete individuals, either motile or non-motile. Microbes of the same species may also choose to aggregate i.e. form a collective clump of cells. When such aggregates of cells unify their resources and act as a collective entity often adhering to surfaces, these clusters of cells are referred to as

biofilms. One well known example is the biofilms of the pathogen *Pseudomonas aeruginosa* that are often found to be resistant to antibiotics due in part to this biofilm forming property. [86, 87]. In other cases, bacterial motility can be beneficial for infection spread and can cause inflammation in cases such as *Vibrio cholerae, Helicobacter pylori* and *Salmonella typhirium* [88].

The spatial organization of bacteria plays a role in determining community structure as well as their impact on the host, yet its characterization remains challenging. A vast amount of data in microbiome research uses sequencing methods applied to fecal samples that don't retain spatial information. Imaging of in vivo spatial structure in organisms such as mice entails intestinal dissection which does not reveal dynamics and assumes that the structure within the gut in live animals is preserved upon removal. Zebrafish, due to its optical transparency at larval stages, has emerged as a powerful model to study spatial structure. In our lab, the live imaging of commensal microbial communities in germ-free zebrafish has led to the discovery of characteristic spatial domains for certain microbial members [51–53, 89–91]. Such work has led to the discovery of correlations between aggregation behaviors and location in the intestine and dynamics that shape the structure of intestinal communities [91, 92].

The variance in spatial structure across species leads to several unexplored questions in the sphere of community structure in the gut microbiome. For instance, what is the connection between spatial structure and competition? How are species interactions impacted by their spatial distribution? And alternatively, how is spatial structure impacted by interactions? In Chapter III, adapted from work currently under revision for publication, I delve into this question by dissecting the dynamics, spatial structure and interactions between two zebrafish-

native gut bacterial species with overlapping spatial domains, *Aeromonas veronii* (ZOR0001) (AE) and *Enterobacter* (ZOR0014) (EN) and two species with distinct aggregation and distribution, *Aermonas*-MB4 (AE-MB4) and EN.

1.6. The host: Mucus and the immune system

As previously noted, varied chemical and nutrient gradients exist along the gut that may be important to determining microbial spatial organization and interactions. A critical constituent of this environment is host mucus, composed of glycoproteins and serving multiple functional roles [93]. The lumenal mucosal layer within the gut acts as a barrier against microbes as well as a source of nutrition for certain intestinal species [84]. This complex relationship has been illustrated through several studies. For instance, the pathogen *Vibrio cholera* has been found to degrade intestinal mucus [94, 95]. Other bacterial species are known to stimulate the differentiation of mucus-producing goblet cells [96]. In the case of *Pseudomonas aeruginosa*, several studies have found that mucin proteins can stimulate bacterial aggregation and biofilm formation [97, 98]. Thus mucus-bacteria interactions can have significant consequences for the host and the microbiota. Through investigations described in Chapter III and IV, I address how a specific bacterial species (AE-MB4) that is deficient in sensing mucus has altered interactions compared to its wild-type counterpart (AE), and induces intestinal inflammation.

The cross-talk between the immune system and the microbiota is another crucial determinant of host health. Certain microbes have been known to promote immune system development, while the immune system itself can act as an ecological filter for microbes [99, 100]. Studies in zebrafish have revealed species-

specific immune responses, where a zebrafish commensal *Shewenella* secretes potent anti-inflammatory factors that can mute strong inflammation caused by other abundant pro-inflammatory members [101]. Further, studies also illustrate that immune responses are linked to motility behaviors of specific strains and their spatial organization [90]. To explore the connection between the host immune system, mucus sensing, and bacterial spatial structure, I characterized the immune response of specific commensal members in single-species and two-species experiments and qualitatively document unique instances of immune-bacteria interactions, described in Chapter IV.

1.7. Light sheet fluorescence microscopy

3D imaging at a high resolution is necessary for studies of the dynamics of bacterial populations and immune cells in the gut of live animals. Some of the commonly used approaches for 3D imaging are confocal and light sheet fluorescence microscopy. Confocal imaging works on the principle of exciting the entire imaging volume using a laser and then scanning a single focal point in three dimensions while using a pinhole to block any out-of-focus light. Although this approach can generate images at high resolution, image acquisition is slow as a single point is being scanned in three dimensions. Advancements to this approach such as spinning disk confocal can speed up imaging by using multiple pinholes that scan multiple points simultaneously. Confocal microscopy of all sorts, however, expose a large volume to large amounts of light which can lead to phototoxic effects. Such phototoxicity can result in abnormal dynamics of live organisms as shown in the case of skeletal morphogenesis [102].

Our lab uses a light sheet fluorescence microscope to obtain 3D images at a high resolution for studies of the dynamics of bacterial populations and immune cells in the gut of live animals. Light sheet fluorescence microscopy involves illuminating and imaging an entire plane of the sample at a given point of time and then scanning only in one dimension, perpendicular to the plane, i.e. through the depth of the specimen. This combination results in high resolution as well as fast imaging. Since only a single plane is excited at a given time, we reduce photobleaching and phototoxicity. The microscope in the lab described later has been customized for imaging bacterial populations in the larval zebrafish gut over long periods of time. Other light sheet microscopes with varying designs, such as passing a collimated beam through a cylindrical lens are widely used and described elsewhere [103–106]. This technique has had a wide variety of applications in live imaging, with examples ranging from imaging host-microbe interactions to developmental dynamics and even neuronal firing in live animals [51, 107, 108].

The microscope in the lab comprises a light source (laser) that is scanned using a galvo mirror oscillating at a frequency of 500 Hz, much faster than the camera exposure time of 30ms, which results in a time-averaged sheet covering the entire field of view. The sheet is transmitted through a lens which provides it a thickness of a few microns, the depth excited within the specimen. Perpendicular to the sheet, a detection lens captures fluorescence emission. For the imaging experiments described in this dissertation, lasers at 488nm and 568nm were used to excite fluorescent proteins in the specimen in series to image pairs of bacterial species or a combination of immune cells (TNFα+ cells or macrophages) and bacteria. A single 3D image of an entire fish gut comprising 4 scans in 1 fluorescence channel takes about 45s to obtain. This microscope thus allows

one to combine fast image acquisition with high resolution allowing for robust characterization of bacterial population dynamics in live fish.

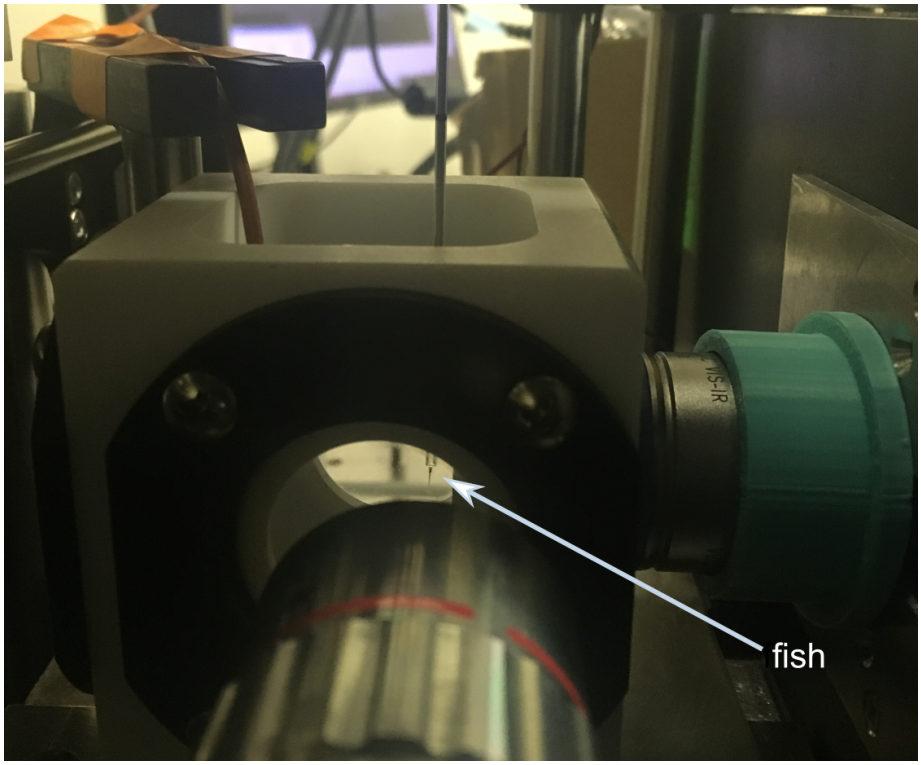

FIGURE 1.1. Image showing a live fish mounted within the custom sample chamber on the lab's light sheet microscope.

A detailed description of the setup is provided elsewhere [89]. In brief, the mounting setup comprises a custom designed sample chamber that is filled with sterile embryo medium and MS-222 anesthetic (20µL/mL). Anesthetized fish are mounted using agar (0.6% in sterile embryo medium) in glass capillaries as in Fig 1.1. Each capillary is inserted into the sample chamber and held by a mount connected to a stage that is controlled with custom-built software. The fish are extruded from the glass capillary before imaging. For time lapse experiments, involving imaging fish overnight, up to 6 fish can be mounted for imaging at for

up to 16 hours. The data is saved and analyzed using a customized image analysis pipeline described below.

1.8. Image analysis

The studies described in Ch. III and IV used image analysis approaches for quantification of spatial structure, dynamics and immune response from 3D images. A single scan through the larval zebrafish gut comprises a set of 2D images of approximate size (2500x1500) pixels, an area of (406x244)µm. Consecutive 2D images in the scan are taken with a step size of 1 micron. A typical 3D scan comprises about 150-300 2D images. An exemplar 2D image of a wild-type zebrafish gut inoculated with EN is shown in Fig 1.2, showing objects including planktonic or individual bacterial cells, aggregates or clumps of bacterial cells, autofluorescent zebrafish cells, background autofluorescence that varies due to the amount of mucus in the gut, and other background noise. The bacteria in these fish could either be planktonic i.e. exist as single individual cells or form large multicellular aggregates shown in Fig 1.2.

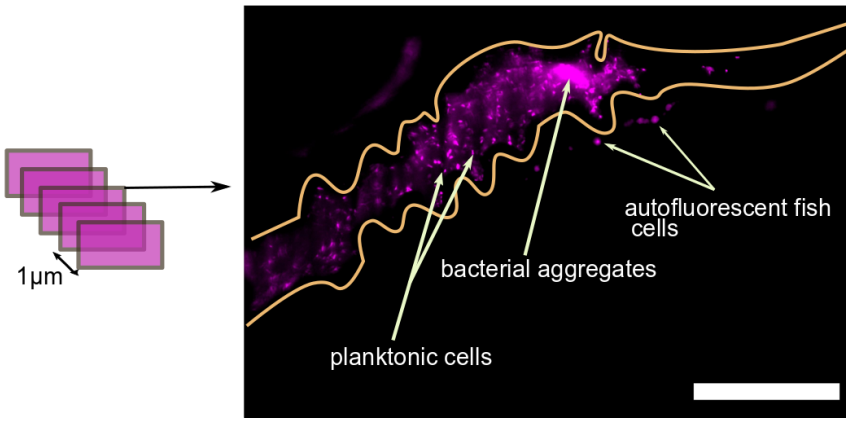

FIGURE 1.2. An example 2D image (right) of the midgut region from a 3D scan (left) illustrating some of the different objects detected in these images. The gut is outlined in yellow. Scale bar: 50µm

The general aspects of the image analysis pipeline are described here, while the specific quantification tasks are described in Ch. II and III.

1.8.1. Individual bacteria detection

Individual bacteria detection is performed in two steps. The first step involves identifying all potential bacteria objects using a blob detection algorithm. The second step uses a convolutional neural network to classify all objects as bacteria and noise blobs. The network was developed and has been described in detail in earlier published work [109].

The initial process of identifying various potential bacteria in the images uses a local maxima finder to detect objects of the size of a bacteria within each 2D image of the 3D scan. The 2D masks of identified objects are stitched in the depth dimension to generate a 3D mask for the image stack. The center of mass of each of the identified regions is then used to define a (30x30x10) pixel sized voxel or (5x5x10)µm, a cube large enough to encompass a single bacterial cell. Each individual voxel from the original image is saved after being normalized to have 0 mean and unit standard deviation before being passed onto the neural network.

Labeling for training the neural network was done using software developed in Python that displays each saved voxel displaying the potential bacteria object and allows the user to assign a 'b' for bacteria or 'nb' for not-bacteria label to it, thus allowing for binary classification. In prior work, the convolutional neural network was trained on a bacterial species of the genus *Vibrio* [109]. For the study described in Ch. II, a new labeled set of 18,013 images (5239 bacteria and 12774 blobs) was generated for training on *Aeromonas-MB4* (AE-MB4) species.

The labeled data was input into the network described in [Hay 2019] for a total of 120 epochs. Cross- validation on the training set was performed to minimize and assess overfitting to the data. A test set of 1548 bacteria and 11,163 noise blobs yielded a classification accuracy of 91% for AE-MB4.

Each of the models trained is amenable to transfer learning, in which the network is initially trained on one of these species and then the final fully connected layer is trained on new data from another species. This approach seems to work well for training a *Vibrio* network on *Pseudomonas* data [109]. For AE-MB4 however, the accuracy of the classification results was considerably better when the network was independently trained on the species itself and no transfer learning was performed. The same network was trained for another species, Enterobacter (EN) using data labeled specifically for EN. The resulting trained models for AE-MB4 and EN are applied to the new data for predictions.

The saved x, y, z locations and the predicted label from the network output are visualized using software written in Python. Objects that are misclassified are manually filtered during the visualization step.

1.8.2. Gut and aggregate segmentation

For segmentation of the gut and bacterial aggregates in the larval zebrafish gut in 3D images, we use a widely used algorithm developed for biomedical images, U-net [110]. Details of the network architecture are provided in [110]. The implementation for zebrafish gut datasets was done by a previous lab member which involved slight modifications described in [111]. For the fluorescence microscopy images, approximately N=1340 2D images of the gut were hand-labeled. After the initial training, the algorithm is used to identify the mask in

a test set and outputs a mask with a binary pixel-wise prediction for each pixel in the image. A limited amount of post-processing stitches various regions in the mask. The mask is visualized using custom software and edited if need be.

For images of bacterial aggregates, a combination of thresholding based on background intensity and manual labeling was done to determine aggregate objects. This manually labeled data has primarily been used in analysis in Chapter III.

In the next few chapters, I use tools from image analysis, live imaging and quantitative modeling to probe (i) the rules governing species interactions in multi-species communities within the vertebrate gut (Chapter 2), (ii) the connection between spatial structure and inter-species interactions (Chapter 3) (iii) host immune response for species with different spatial structure (Chapter 4).

CHAPTER II

MAPPING INTERACTIONS IN MULTI-SPECIES COMMUNITIES

This work is adapted from previously published co-authored work by D. Sundarraman, E. A. Hay, D. M. Martins, D. S. Shields, N. L. Pettinari, and R. Parthasarathy, *Higher-Order Interactions Dampen Pairwise Competition in the Zebrafish Gut Microbiome*, mBio **11**, e01667 (2020). I was involved in the experiments, analysis and writing of this work.

2.1. Introduction

Intestinal microbes exist in complex and heterogeneous communities of interacting, taxonomically diverse species. The composition of these communities varies across individuals and is crucial to the health of the host, having been shown in humans and other animals to be correlated with dietary fat uptake [13, 14], organ development [12, 20], immune regulation [10, 16–18, 21, 23] and a wide range of diseases [3–9, 11, 15, 22].

Despite the importance of intestinal communities, the determinants of their composition remain largely unknown. A growing number of studies map the effects of external perturbations, such as antibiotic drugs [112, 113] and dietary fiber [114] and fat [19, 115] on the relative abundance of gut microbial species. Intrinsic inter-microbial interactions, however, are especially challenging to measure and are important not only for shaping community composition in the absence of perturbations but also for propagating species-specific perturbations to the rest of the intestinal ecosystem.

The considerable majority of studies of the gut microbiota have been performed on naturally assembled microbiomes by sequencing DNA extracted from fecal samples, an approach that provides information about the microbial species and genes present in the gut, but that imposes several limitations on the inference of inter-species interactions. The high diversity of natural intestinal communities, and therefore the low abundance of any given species among the multitude of its fellow residents, implies that stochastic fluctuations in each species' abundance will be large, easily masking true biological interactions. The accuracy of inference is considerably worse if only relative, rather than absolute, abundance data is available [62, 116–118], as is typically the case in sequencing-based studies. Finally, we note that fecal sampling assesses only the microbes that have exited the host, which may not be representative of the intestinal community [119].

An alternative approach to using DNA sequencing and naturally assembled host-microbiota systems is to build such systems from the bottom-up using model organisms. This is accomplished by using techniques for generating initially germ-free animals, and well-defined sets of small numbers of microbial species, and then measuring the populations of these species resident in the intestine. Recent work along these lines has been performed using the nematode *Caenorhabditis elegans* [68] and the fruit fly *Drosophila melanogaster* [69, 120]. However, as described further below, these studies imply different principles at play in the different systems. Moreover, it is unclear whether conclusions from either model platform translate to a vertebrate gut, which has both greater anatomical complexity and more specific microbial selection [121]. To address this, we measure bacterial interactions in larval zebrafish (Fig 2.1A), a model vertebrate organism amenable to gnotobiotic techniques [47–49, 122], which has enabled in earlier work

that investigated pairs of bacterial species the discovery of specific interbacterial competition mechanisms related to intestinal transport [51, 52]. The experiments described below involve several hundred fish, each with 1-5 resident bacterial species, enabling robust inference of inter-species interactions.

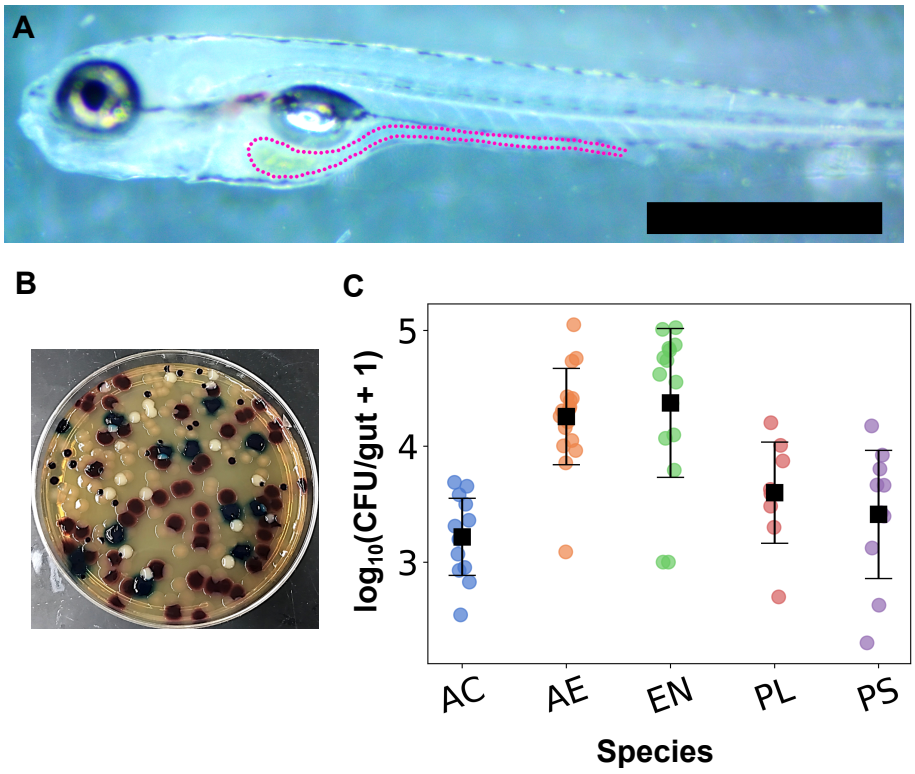

FIGURE 2.1. (A) A 7 day post fertilization larval zebrafish, with a dotted line outlining the intestine. Scale bar: 500 µm. (B) Chromogenic agar plate showing colonies of all the candidate five species (AC: milky opaque, AE: reddish purple, EN: blue, PL: dark purple and PS: colorless translucent) (C) The abundance per zebrafish gut of each of the five bacterial species when colonized in mono-association with the host, assessed as colony forming units (CFU) from plated gut contents. Each circular datapoint is a CFU value from an individual fish (N = 13, 17, 15, 8, and 10, from left to right), with the mean and standard deviation indicated by the square markers and error bars.

The ability to quantify species abundance and to manipulate it by controlled addition or subtraction of species is commonplace in macroscopic ecological

investigations. Its implementation here enables connections between intestinal microbiome research and a large literature on ecosystem dynamics. An issue whose importance has been realized for decades is the extent to which interspecies interactions are pairwise additive, or whether higher-order (often called indirect) interactions are necessary to explain community structure [123, 124]. The term 'higher-order interactions' has been defined in various ways in the ecological literature [124, 125], in some cases referring specifically to non-additive changes in a species' growth rate given the presence of additional species or to changes in the nature of the interaction between two species induced by additional species, but in others referring more generally to any interaction that cannot be captured by a pairwise model. We adopt the latter, commonly used, definition, which is agnostic to underlying mechanisms [63]. In our analyses below, we consider various pairwise models and assess their ability to describe data from multi-species communities; mismatch is indicative of the existence of higher-order interactions. Pairwise additivity, if dominant, simplifies the prediction of ecosystem composition, which would be desirable for therapeutic applications of microbiome engineering. Higher-order interactions may stabilize multi-species communities according to several recent theoretical models described further in the Discussion [70–73], implying that quantifying and controlling indirect effects may be necessary for reshaping gut microbiomes.

Whether host-associated or not, microbial communities have shown a variety of interaction types. A classic study involving cultured protozoan species found good agreement between the dynamics of four-species consortia and predictions derived from measurements of pairs of species [64]. Similarly, Friedman and colleagues showed that the outcomes of competitions among three species

communities of soil-derived bacteria could be simply predicted from the outcomes of pairwise combinations [65]. In contrast, experiments based on the cheese rind microbiome found significant differences in the genes required for a non-native *E. coli* species to persist in a multi-species bacterial community compared to predictions from pairwise coexistence with community members [67]. A closed ecosystem consisting of one species each of an algae, bacteria, and ciliate exhibited a strong non-pairwise interaction, in which the bacteria is abundant in the presence of each of the algae or ciliate alone, but is subject to strong predation in the three-species system [66].

Within animals, the interaction types observed in the few studies to date that make use of controlled microbial communities in gnotobiotic hosts are also disparate. Competitive outcomes of three-species communities from subsets of eleven different bacterial species in the gut of the nematode *C. elegans* could be predicted from the outcomes of two-species experiments, with indirect effects found to be weak [68]. In contrast, work using well-defined bacterial assemblies of up to five species in the fruit fly *D. melanogaster* found strong higher-order interactions governing microbe-dependent effects on host traits such as lifespan [69].

To our knowledge, there have been no quantitative assessments of inter-bacterial interactions using controlled combinations of microbial species in a vertebrate host, leaving open the question of whether higher-order interactions are strong, or whether pairwise characterizations suffice to predict intestinal community structure. We therefore examined larval zebrafish, inoculating initially germ-free animals with specific subsets of five different species of zebrafish-derived bacteria and assessing their subsequent absolute abundances. Though the number of species is considerably fewer than the hundreds that may be present

in a normal zebrafish intestine, it is large enough to sample a range of higher-order interactions, yet small enough that the number of permutations of species is tractable.

As detailed below, we find strong pairwise interactions between certain bacterial species. However, we find weaker interactions and a greater than expected level of coexistence in fish colonized by four or five bacterial species. This suggests that measurements of pairwise inter-microbial interactions are insufficient to predict the composition of multi-species gut communities, and that higher-order interactions may dampen strong competition and facilitate diversity in a vertebrate intestine.

2.2. Results

Zebrafish (Fig 2.1A) were derived to be germ-free, and then were inoculated at 5 days post-fertilization (dpf) with the desired combination of microbial species by addition of bacteria to the flasks housing the fish. Approximately 48 hours later, fish were euthanized and their intestines were removed by dissection. Intestines and their contents were homogenized, diluted, and plated onto chromogenic agar (Methods). Secreted enzymes from each of the five candidate bacterial species generate particular colors due to substrates in the chromogenic medium, allowing quantification of colony forming units (CFUs) and therefore absolute intestinal abundance (Fig 2.1B).

The five species examined were selected as diverse representatives of genera commonly found in the zebrafish intestine. Full names and species identifiers are given in Methods; we will refer to these through most of the text by genus name or two letter abbreviation: *Acinetobacter* (AC), *Aeromonas* (AE), *Enterobacter* (EN),

Plesiomonas (PL), and *Pseudomonas* (PS). As expected given their association with the zebrafish gut microbiome, each species in mono-association, i.e. as the sole species inoculated in germ-free fish, colonizes robustly to an abundance of 10^3-10^4 CFU/gut, corresponding to an in vivo density of approximately 10^9-10^{10} bacteria/ml (Fig 2.1C).

Pairwise interactions in di-associations.

We first examined all ten possible co-inoculations of two species, which enables assessment of pairwise interactions in the absence of higher-order effects. Intestinal CFU data shows a wide range of outcomes for different species pairs. As exemplars, the CFUs per gut for each of two species, AC and EN, in the presence of each of the other four are displayed in Fig 2.2A and Fig 2.2B respectively. The abundance of AC is similar in the presence of any second species to its value in mono-association. In contrast, the mean EN abundance is similar to its mono-association value if co-inoculated with PL or PS, about 10 times lower if co-inoculated with AC, and over two orders of magnitude lower if co-inoculated with AE, implying in the latter cases strong negative interactions.

Parameterizing the strength of interactions between species is necessarily model dependent, contingent on the functional form of the relationship between one species' abundance and the other's. We show that the conclusions we reach regarding interaction strengths, especially their shifts when multiple species are present, are qualitatively similar and therefore robust for a wide range of models. We first consider a phenomenological interaction coefficient C_{ij}^{II} that is linear in

log-abundance, characterizing the effect of species j on species i as:

$$\log_{10} P_i^{II} = \langle \log_{10} P_i^{I} \rangle + C_{ij}^{II} \log_{10} P_j^{II} \tag{2.1}$$

where P_i denotes the abundance of species i and the superscript I or II denotes a mono- or di-association experiment. This form is motivated by the distribution of gut bacterial abundances being roughly log-normal, with species addition capable of inducing orders-of-magnitude changes (Fig 2.2A,B). This C_{ij}^{II} can be derived as the interaction parameter in a competitive Lotka-Volterra model modified to act on log-abundances (Methods). Qualitatively, a positive C_{ij} implies that the abundance of species i increases in the presence of j. Similarly a negative C_{ij} indicates that the abundance of species i declines in the presence of species j. Subsampling from the measured sets of bacterial abundances gives the mean and standard deviation of the estimated interaction parameters (Methods).

We plot in Fig 2.2C the C_{ij}^{II} defined by Eq. 3.1 calculated from all di-association data of all species pairs (N = 190 fish in total). For determining C_{ij}^{II}, we only use data from fish in which both species were detected so that abundance changes of one species can definitively be ascribed to the presence of the other within the gut. Uncertainties in C_{ij}^{II} are estimated from bootstrap subsampling (see Methods). The interactions are predominantly negative. Thirteen out of twenty coefficients differ from zero by over three standard deviations, indicating both a large magnitude and a less than 0.001 probability that the interaction strength is zero or of the opposite sign. The total bacterial load, i.e. the sum of the bacterial abundances, is similar for all the di-associations suggesting that the interaction effects do not stem from changes in intestinal capacity (Fig 2.2D).

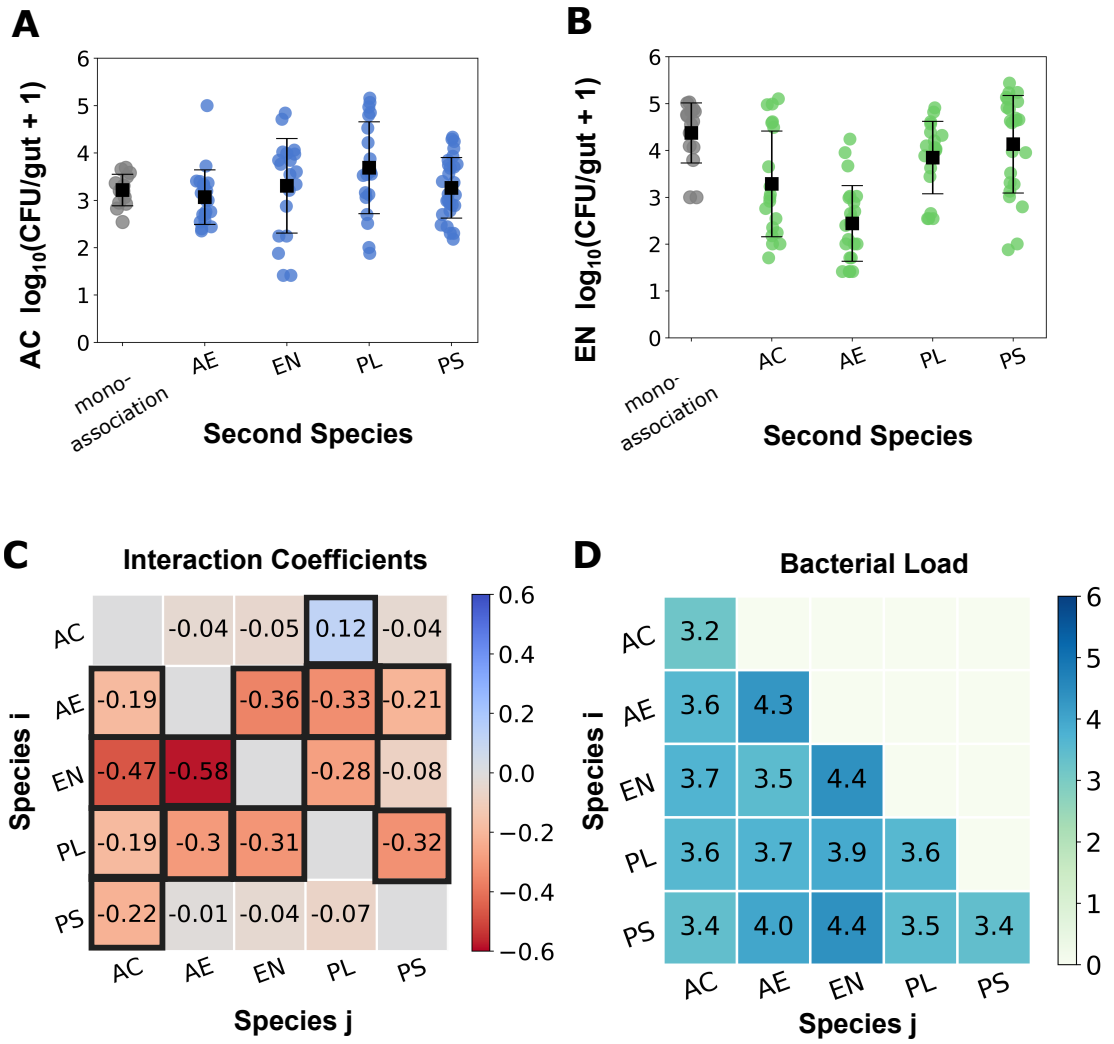

FIGURE 2.2. Abundances per zebrafish gut of (A) AC and (B) EN in mono-association (grey) and in di-association with each of the other bacterial species (blue/green). Each circular datapoint is a CFU value from an individual fish ((A) N = 13, 21, 19, 20, and 27 and (B) N = 15, 19, 22, 18, and 23 from left to right), with the mean and standard deviation indicated by the square markers and error bars. (C) Matrix of pairwise interaction coefficients C_{ij}^{II} characterizing the effect of species j on the abundance of species i. Coefficients that differ from zero by more than three standard deviations (provided in Fig A.2A) are outlined in black. (D) The average bacterial load per zebrafish in each of the di-association combinations, expressed as $\log_{10}$ of total CFUs. The standard deviations are between 0.3 and 1.1 and are displayed in Fig A.2A). Values on the diagonal are the mono-association load for each of the five species.

Though the physical and chemical environment of the zebrafish gut is likely very dissimilar to test tubes of standard growth media, we examined abundances of each of the pairs of species in in vitro competition experiments, growing overnight cultures in Lysogeny broth (LB) media and plating for CFUs (see Methods). Assessing C_{ij}^{II} as above, we find, as expected, that interaction coefficients calculated from the in vitro experiments are markedly different than those measured in vivo (see Fig A.3 and Fig 2.3B).

Our characterizations of interactions within the zebrafish gut are not qualitatively altered by using a more general power law model to compute C_{ij}^{II} from absolute abundance data, discussed below (Interactions under more general models) following the presentation of measurements of interactions between more than two species.

2.2.1. Pairwise interactions in multi-species communities.

To assess whether the strong competitive interactions we found in two-species experiments are conserved in multi-species communities, we quantified pairwise interactions in experiments inoculating fish with four or five bacterial species. To assess C_{ij}^{V}, we adopted a method similar to the leave-one-out approach often used in macroscopic ecological studies, dating at least to classic experiments in which single species were removed from tide pools and the abundances of the remaining species were measured to evaluate inter-species interactions [58]. Here, we performed co-inoculation experiments leaving out one of the five species of bacteria and compared intestinal abundances for these four-species communities to those measured in five-species co-inoculation experiments.

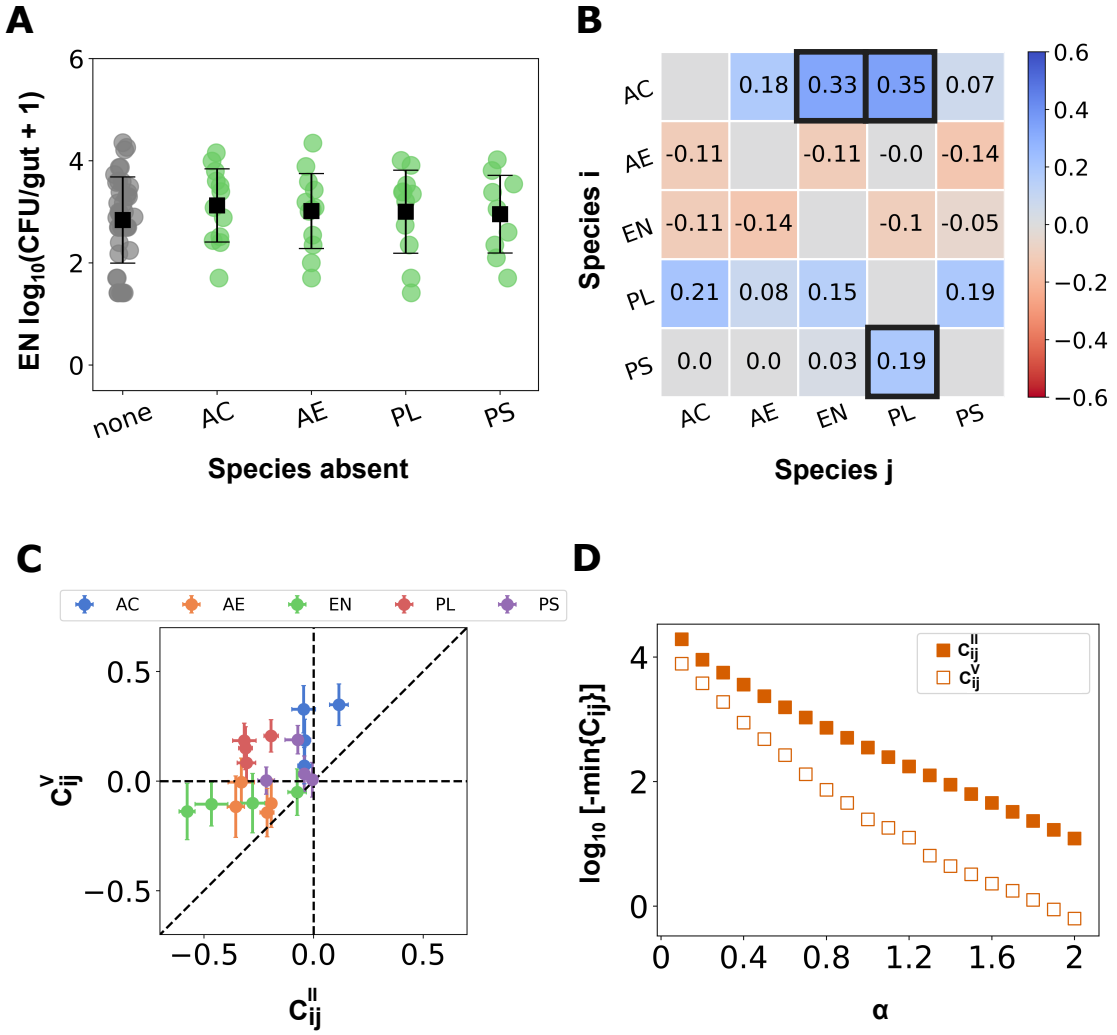

FIGURE 2.3. (A) Abundance per zebrafish gut of one of the bacterial species, EN, when all five species are co-inoculated (gray) and in each four species co-inoculation experiment (green) with the omitted species indicated on the axis. Each circular datapoint is a CFU value from an individual fish (N = 40, 12, 12, 11, and 9, from left to right), with the mean and standard deviation indicated by the square marker and error bars. (B) Matrix of pairwise interaction coefficients C_{ij}^V when 5 bacterial species are present. The coefficients outlined in black differ from zero by over three standard deviations (see Fig A.2B). (C) The pairwise interaction coefficients inferred from 4-5 species experiments versus those from 1-2 species experiments. The colors label species i for each interaction pair. (D) The minimum interaction coefficient calculated from a power-law interaction model for different values of the exponent α for the 1-2 species (square filled markers) and the 4-5 species (square markers) experiments.

In approximately N = 10 fish each, we performed all five different co-inoculations of four bacterial species. The difference in the abundance of species i in fish inoculated with all five species compared to fish inoculated with four, missing species j, gives a measure of the impact of species j on species i in the multi-species environment. As an example, EN abundance in inoculations lacking AC, AE, PL, and PS, and in five-species inoculations, are shown in Fig 2.3A. In contrast to the di-association experiments (Fig 2.2B), we see that EN does not show large abundance differences, in either its mean or its distribution, as a result of any fifth species being present. Independent of any model, this suggests that non-pairwise, i.e. higher-order, interactions are present in the multi-species community.

Again, a variety of options are possible for quantifying interaction coefficients in the multi-species system. We first consider interaction coefficients as modifying mean-log-abundances, analogous to the pairwise model of Eq. 3.1:

$$\log_{10} P_i^V = \log_{10} P_i^{IV} + C_{ij}^V \log_{10} P_j^V \tag{2.2}$$

The interaction coefficients C_{ij}^V that we obtain, displayed in Fig 2.3B, are different and in general considerably weaker than the C_{ij}^{II} found in the two-species case Fig 2.2C. There are only three interactions that differ from zero by over three standard deviations. Strikingly, all three of these interactions are positive. This shift towards weaker and more positive interactions between the two-species and multi-species interactions is further illustrated in Fig 2.3C in which the multi-species interaction coefficients, C_{ij}^V are plotted against the 2-species interaction coefficients, C_{ij}^{II}.

2.2.2. Interactions under more general models.

As noted, a model that is linearly additive in logarithmic abundances is only one of an infinite number of choices, and moreover may not adequately capture the complexity of interactions in the gut. Earlier experiments investigating the spatial structure of specific microbial communities in the larval zebrafish intestine have shown that species such as AE, EN and PS form dense three-dimensional aggregates [91]. The size and location of aggregates and the locations of cells, conspecific or otherwise, within these aggregates may impact their interactions in ways that could be sub-linear, linear, or super-linear in population size. Previous work has also established that gut bacteria may also influence intestinal mechanics [52], highlighting one of many possible indirect interaction mechanisms whose functional forms are unknown. Furthermore, other studies have shown that different modes of physical and chemical communication could result in long range interactions between different species [126–128]. To address these possibilities, we evaluated species interactions with a more general power law model, wherein the interaction effects between species could be non-linear in the abundance of the effector species. Here the interaction coefficient C_{ij} depends on a power, α, of the abundance of the effector species j, which we evaluate in the range $\alpha = 0.1$ to 2, spanning sub-linear and super-linear interactions. Modified versions of Eq. 3.1 and 3.2 give:

$$P_i^{II} = \langle P_i^I \rangle + C_{ij}^{II}(P_j^{II})^\alpha \tag{2.3}$$

and

$$P_i^V = \langle P_i^{IV} \rangle + C_{ij}^V(P_j^V)^\alpha \tag{2.4}$$

from which we can evaluate $C_{ij}^{II}$and C_{ij}^{V} respectively. Note that $\alpha = 1$ in Eq. 3.3, 2.4, i.e. interactions that are linear in abundance, is simply the steady-state behavior of the competitive Lotka Volterra model commonly used in population modeling and are shown in Fig A.5. We provide the $C_{ij}^{II}$and C_{ij}^{V} for several different α in Fig A.4. Throughout, as in the logarithmic model shown above, pairwise interactions in di-association are in many cases strongly negative, while the multi-species interactions are weaker. This is summarized by studying the trends in the most negative $C_{ij}^{II}$and C_{ij}^{V} for different values of α, depicted in Fig 2.3D, which shows that for all α the strongest C_{ij}^{V} is significantly weaker than the strongest C_{ij}^{II}, suggesting that our results are robust to choice of model.

2.2.3. Five-species coexistence.

We next consider co-inoculation of all five bacterial species. Examination of over 200 fish shows a large variety in abundances, depicted in Fig 2.4A as the relative abundance of each species in each larval gut. Multiple species are able to coexist, with the median number of species present being 4 (Fig 2.4B). The mean total bacterial load as well as its distribution (Fig 2.4C) is similar to the mean and distribution of the mono- and di-association experiments, as well as four-species co-inoculation experiments discussed earlier. We calculated the expected abundance of each bacterial species, if the interactions governing the five-species community were simply a linear combination of the pairwise interactions governing di-associations, C_{ij}^{II}. Any of the additive models we evaluated can be extended to combinations of species. Considering the model focused on above, with interaction coefficients modifying log abundances, the predicted abundance of species i in the presence of another species j is given by

$$\log_{10} P_i^V = \langle \log_{10} P_i^I \rangle + \sum_{j \neq i} C_{ij}^{II} \log_{10} P_j^V \tag{2.5}$$

where the superscript V denotes the five-species co-inoculation experiment. A model linear in species abundance ($\alpha = 1$) is also considered in Methods), and gives qualitatively similar outputs and conclusions. Sampling from the measured distributions of each of the interaction coefficients and the mean abundance in mono-association allows calculation of the distribution of expected P_i^V values.

We plot the measured and predicted distributions of intestinal abundances of each of the five species for the five-species co-inoculation experiment in Fig 2.4D. The measured distributions of each of the species are very similar to each other. In contrast, the distributions of the predicted abundances vary significantly by species. For two of the species, AC and PS, the mean of the observed and predicted distributions are similar. For the other three species, in contrast, the observed and predicted populations are in strong disagreement, with the pairwise prediction being at least an order of magnitude lower than the observed abundances. For EN and PL in particular, we would expect extinction in a large fraction of fish due to strong negative pairwise interactions; in actuality, both species are common and abundant.

Similarly, we can extract from the model the predicted frequency of occurrence of each of the species, regardless of abundance i.e. the fraction of fish with a non-zero population of that species. We find that the predicted frequency is much lower than the experimentally observed frequency for PL and EN (Fig 2.4E).

FIGURE 2.4. (A) Stacked bar plot of the relative abundances of the five bacterial species when all five were co-inoculated. Each bar is from a single dissected fish. The bars are ordered by total bacterial load. (B) Histogram of the total number of bacterial species present in the gut when all five species were co-inoculated. (C) The total bacterial load as a function of the number of inoculated species. Each circular datapoint is a CFU value from an individual fish (N = 63, 232, 187, and 202, from left to right), with the mean and standard deviation indicated by the square marker and error bars.(D) The predicted (blue Xs) and measured (brown circles) abundances of each bacterial species in the zebrafish gut when all five species are co-inoculated. Predictions are based on an interaction model that is linear in log-abundance using the pairwise C_{ij}^{II} coefficients, as described in the main text. Solid square markers indicate the mean and standard deviation of the distributions excluding null counts. The dotted line indicates the experimental detection limit of 25 cells. The experimental data is from N = 202 fish in total and the predicted distributions arise from 250 samples of the distribution of interaction coefficients. (E) The observed frequency of occurrence in the gut from the five-species co-inoculation experiment versus the predicted frequencies for each of the five species. (F) The Pearson correlation coefficients calculated from the relative abundances of pairs of species when all five species were co-inoculated.

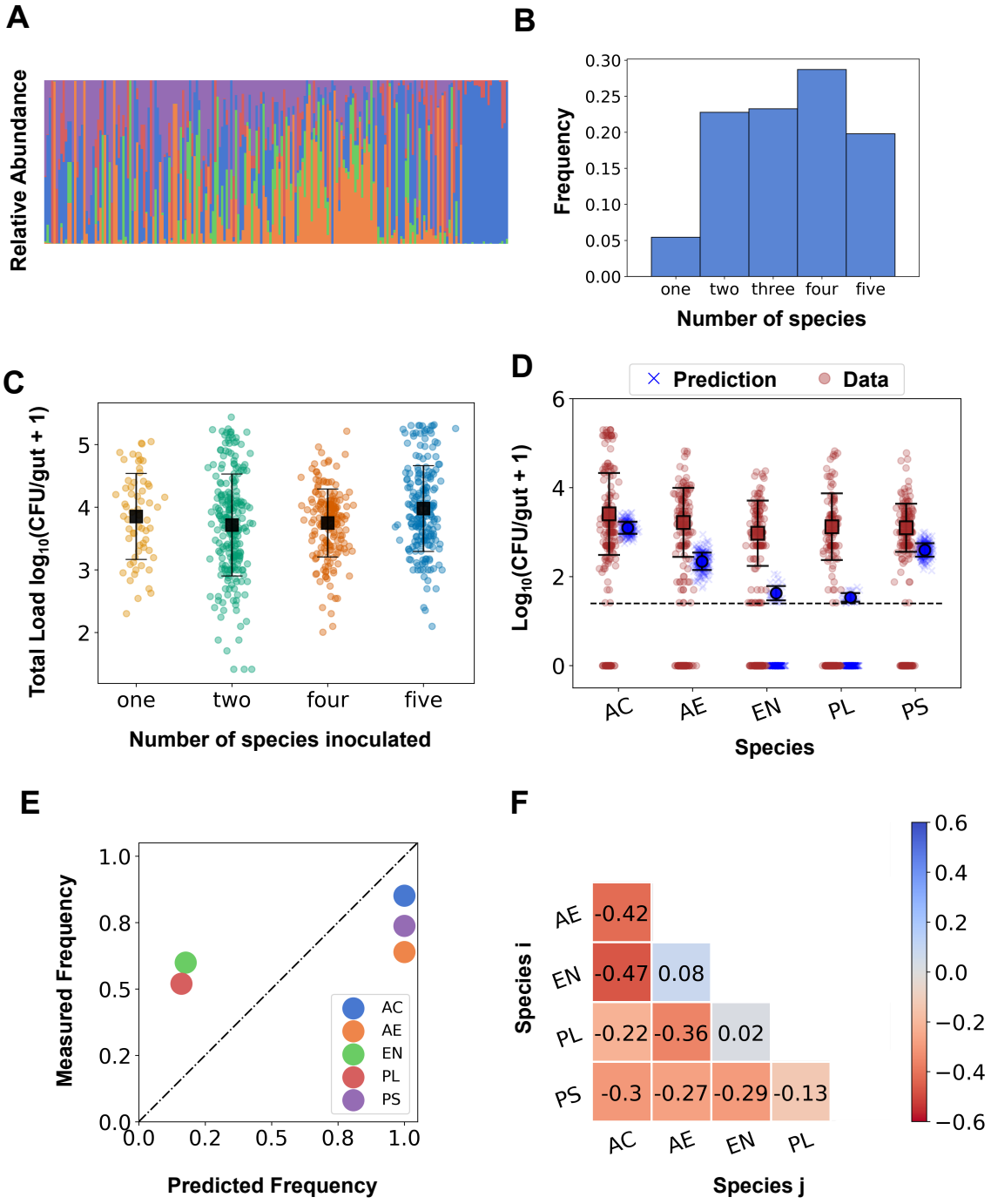
A
Relative Abundance
B
Frequency
0.30
0.25
0.20
0.15
0.10
0.05
0.00
one
two
three
four
five
Number of species
C
Total Load log10(CFU/gut + 1)
5
4
3
2
one
two
four
five
Number of species inoculated
D
Prediction
Data
Log10(CFU/gut + 1)
6
4
2
0
AC
AE
EN
PL
PS
Species
E
Measured Frequency
1.0
0.8
0.5
0.2
0.0
0.0
0.2
0.5
0.8
1.0
AC
AE
EN
PL
PS
Predicted Frequency
F
Species i
AE
EN
PL
PS
-0.42
-0.47
0.08
-0.22
-0.36
0.02
-0.3
-0.27
-0.29
-0.13
AC
AE
EN
PL
Species j
0.6
0.4
0.2
0.0
−0.2
−0.4
−0.6

FIGURE 2.4.

By measuring absolute abundances of bacterial populations in the gut, we provide direct assessments of inter-species interactions. More common sequencing-based methods, applied for example to the human gut microbiome, typically provide relative measures of species abundance, i.e. each taxonomic unit's fraction of the total load. Correlations among relative abundances are often used as measures of interaction strengths [129, 130]. Calculating the Pearson correlation coefficients of the relative abundances of each pair of species in fish inoculated with all five bacterial species, we find a strikingly different interaction matrix (Fig 2.4F) than that inferred from absolute abundance changes (Fig 2.3B), with many strong negative values. There are many likely reasons for the difference between Pearson correlations and our more directly measured interaction coefficients. The Pearson r necessarily attributes correlations between pairs of species as being indicative of the dynamics of that pair independent of other species, is confounded by overall changes in total bacterial load, and, perhaps most importantly, is necessarily symmetric ($C_{ij} = C_{ji}$). Our C_{ij} inferred from absolute abundance data are notably asymmetric (Fig 2.2C,Fig 2.3B).

2.3. Discussion

Using a model system comprising five commensal bacterial species in the larval zebrafish intestine, we have characterized aspects of gut microbiome assembly. Controlled combinations of inoculated species and measurements of absolute abundance in the gut, both challenging to perform in other vertebrate systems, reveal clear signatures of interactions among species. We find strong, competitive interactions among certain pairs in fish inoculated with two bacterial species. In contrast, pairwise interactions are weak in intestines colonized by four

to five species, and all species are present at equal or greater abundance than would be predicted based on two-species data.

Our quantification of interaction strengths relies on a minimal set of assumptions that serve as a general test of additive models. Interaction strengths are necessarily parameters of some model. In the text, we make use of a model in which the log-transformed population of a species is a linear function of the other species' log-transformed populations, and a more general power law model that spans both sub-linear and super-linear dependences on population sizes. There are good reasons to be skeptical of such frameworks. First, intestinal populations may not be well described by equilibrium, steady-state values. Second, these models lack spatial structure information. In vivo microscopy of one or two species in the zebrafish gut [51–53] underscores both of these concerns: populations are very dynamic with rapid growth and stochastic expulsions; interactions can be mediated by complex intestinal mechanics; and aggregation and localization behaviors are species-specific.

Imaging also, however, provides justifications for these rough models. Prior microscopy-based studies have shown that growth rates are rapid, with populations reaching carrying capacities within roughly 12 hours [51, 53], well below the 48 hour assessment time considered here. Because of strong aggregation observed in nearly all bacterial species, most individual bacteria residing in the bulk of clusters will not directly interact with other species, leading to interactions that are sub-linear in population size, suggesting a logarithmic or $\alpha < 1$ power-law functional form. Furthermore, stochastic dynamics can be mapped onto robust average properties for populations [51, 131]. It is therefore reasonable to make use of simple models, not as rigorous descriptions of the system but as approximations

whose parameters characterize effective behaviors. We note that all these issues also affect more commonly used models, such as standard competitive Lotka-Volterra models that are linear in population sizes. These models are often applied to gut microbiome data and used to infer interaction parameters [62, 132, 133] despite a lack of information about their realism. The power law model of interactions provides the strongest indication of the generality of our conclusions. Over a range of interaction forms extending from highly sublinear ($\alpha = 0.1$) to super-linear ($\alpha = 2.0$), strong competitive interactions are damped when four or five species are present (Fig 2.3D), suggestive of higher-order interactions among intestinal bacteria.

The ecological potential for higher-order or indirect interactions, i.e. interactions that cannot be reduced to pairwise additive components but rather result from the activities of three or more species, to be important determinants of community structure has been appreciated for decades [64, 123, 124]. Identification of higher-order interactions among constituent species is important for accurate prediction of responses to ecological perturbations such as species invasion or extinction, as well as functions of multi-species communities, as such features will not be adequately forecast by examination of direct interactions in subsystems [123, 134].

Inferring and quantifying indirect interactions in natural ecosystems is, however, challenging, calling for subtle and model-dependent statistical tests [123, 124, 135]. Constructed or manipulated systems enable more straightforward assays in which particular species are introduced or removed amid a backdrop of others. Several such systems involving macroscopic organisms [136–140], as well as microorganisms [66, 69] have uncovered significant indirect interactions.

However, some studies of microbial communities have found weak or negligible higher-order interactions [64, 65], including one study examining combinations of species introduced to the *C. elegans* gut [68]. The complexity of interactions in a vertebrate gut has remained unclear, and correlation-based methods for inferring interactions from sequencing-based data have assumed that pairwise interactions suffice [129, 141, 142].

Our measurements using gnotobiotic larval zebrafish, a model vertebrate, show strong pairwise interactions when only two bacterial species are present in the intestine and weak pairwise interactions when four to five species are present, indicating that higher-order interactions are important (Fig 2.3) . In many cases, the effect is evident from the raw data itself. For example, EN is strongly suppressed by AE if the two are inoculated together (Fig 2.2B). Comparing EN abundance in fish colonized by all species except AE with its abundance in fish colonized by all species, however, shows little difference, indicating that the EN-AE interaction is strongly attenuated by the presence of the other bacterial groups (Fig 2.3A).

Two additional observations also imply the presence of strong higher-order interactions in our intestinal ecosystem. Considering fish colonized by all five bacterial species, the mean abundance of each species is at least as high as would be predicted solely from direct interactions (Fig 2.4D). Moreover, the diversity of bacterial species is higher would be predicted, as all of the species occur in more than 50% of fish, contrary to prediction (Fig 2.4E). Considering fish colonized by all five bacterial species, the abundance of each species is at least as high and the diversity of bacterial species is higher than the values that would be predicted solely from direct interactions.

Our finding of increased species diversity than expected from pairwise interactions in a system of several gut bacterial species is consistent with recent theoretical studies that suggest, for a variety of reasons, that higher-order interactions are likely to stabilize communities and promote coexistence. The topic of multi-species coexistence has a long history in ecology. Especially since classic work by Robert May showing that a system comprising pairwise interacting constituents will, in general, be less stable as the number of species increases [143], explaining how complex communities can exist has been a theoretical challenge. There are many resolutions to this paradox, such as spatial heterogeneity, interactions across trophic levels, and temporal variation. However, even without such additional structure, incorporating higher-order terms into general random competitive interaction models leads to widespread coexistence [70–72]. Such large-scale coexistence can also emerge naturally from contemporary resource competition models [73, 144], in which cross-feeding or metabolic tradeoffs necessarily involve multiple interacting species. Intriguingly, the abundance distributions of all five of our gut bacterial species, when inoculated together, are similar to one another. The average Shannon entropy of the five species community ($H = 1.16 \pm 0.24$) (see Methods) also resembles that of a purely neutrally assembled community ($H = 1.61$), reminiscent of dynamics mimicking neutral assembly that emerge from multi-species dynamics driven by resource use constraints [73, 145].

Our findings imply that measurements of two-species interactions among microbial residents of the vertebrate gut are likely to be insufficient for predictions of community dynamics and composition. Moreover, they imply that inference from microbiome data of inter-species interactions, for example by fitting Lotka-

Volterra-type models with pairwise interaction terms [62, 132, 133, 146] should not be thought of as representing fundamental pairwise interactions that would be manifested, for example, if the constituent species were isolated, but rather as effective interactions in a complex milieu.

Our measurements do not shed light on what mechanisms give rise to higher-order interactions in our system. Likely candidates include metabolic interactions among the species, interactions mediated by host activities such as immune responses, and modulation of spatial structure by coexisting species. Immune responses are sensitive to specific bacterial species [101] and to bacterial behaviors [90]. Regarding spatial structure in particular, in vivo imaging of these bacterial species in mono-association has shown robust aggregation behaviors that correlate with location in the gut [91] Given the physical constraints of the intestinal environment, we think that modification of spatial organization due to the presence of species with overlapping distributions is a likely mechanism for higher-order interactions. Notably, both immune responses and spatial structure are amenable to live imaging in larval zebrafish [51, 52, 91]. Though the parameter space of transgenic hosts, fluorescent labels, and interaction timescales to explore in imaging studies is potentially very large, such future studies are likely to yield valuable insights into the mechanisms orchestrating the strong interactions observed here. Furthermore, examination of the roles of priority effects and other aspects of initial colonization, as well as stability of diverse communities with respect to invasion, may reveal potential routes for intentionally manipulating the vertebrate microbiome to engineer desired traits.

2.4. Materials and methods

2.4.1. Animal Care.

All experiments with zebrafish were done in accordance with protocols approved by the University of Oregon Institutional Animal Care and Use Committee and following standard protocols [147].

2.4.2. Gnotobiology.

Wild-type (ABCxTU strain) larval zebrafish (*Danio rerio*) were derived germ-free as described in [47]. In brief, embryos were washed at approximately 7 hours post-fertilization with antibiotic, bleach, and iodine solutions and then moved to tissue culture flasks of 15mL sterile embryo medium solution with approximately 1mL of sterile solution per larva. The flasks were then stored in a temperature-controlled room maintained at 28°C.

2.4.3. Bacterial Strains and Culture.

The five bacterial strains used in this study, namely *Aeromonas sp.* (ZOR0001), *Pseudomonas mendocina* (ZWU0006), *Acinetobacter calcoaceticus* (ZOR0008), *Enterobacter sp.* (ZOR0014), and *Plesiomonas sp.* (ZOR0011) were originally isolated from the zebrafish intestine and have been fluorescently labelled to express GFP and dTomato facilitating their identification in our experimental assays [50, 148]. Stocks of bacteria were maintained in 25% glycerol at -80° C.

2.4.4. Inoculation of tissue culture flasks.

One day prior to inoculation of the tissue culture flasks, bacteria from frozen glycerol stocks were shaken overnight in Lysogeny Broth (LB media, 10 g/L NaCl, 5 g/L yeast extract, 12 g/L tryptone, 1 g/L glucose) and grown for 16 h overnight at 30°C. Samples of 1mL of each of the overnight cultures were washed twice by centrifuging at 7000g/rpm for 2 min, removing the supernatant, and adding 1mL of fresh sterile embryo media. At 5 dpf, the tissue culture flasks were inoculated with this solution at a concentration of 10^6 CFU/mL. For each of the competition experiments involving 2, 4 and 5 bacterial species, equal concentrations were inoculated into the flasks. After inoculation, the flasks were maintained at 30°C until dissection at 7 dpf.

2.4.5. Dissection and Plating.

To determine the intestinal abundance of bacterial species, dissections of larval zebrafish were performed at 7 dpf. Zebrafish were euthanized by hypothermal shock. Intestines were removed by dissection and placed in 500µL of sterile embryo media and homogenized with zirconium oxide beads using a bullet blender. The homogenized gut solution was diluted to 10^{-1} and 10^{-2}, and 100µL of these dilutions were spread onto agar plates. For mono- and di-associated inoculations, tryptic soy agar (TSA) plates were used in which fluorescence could be used to differentiate up to two species. For inoculations of more than two species, Universal HiChrome Agar (Sigma-Aldrich) plates were used, allowing for visual differentiation of each species using a colorimetric indicator. The abundances of each of the species in the zebrafish gut was determined by counting the colony forming units on the plates.

2.4.6. In vitro competition experiments.

To determine the in vitro competition coefficients, all the different pairwise combinations of the five species were grown in overnight cultures of LB media as above. On the following day, cultures were plated at 10^{-7} or 10^{-6} dilutions, depending on the ability to detect both species in a given dilution. Abundances were obtained by counting the number of CFUs of each species on the plates.

2.4.7. Interaction Models

2.4.7.1. Pairwise Interactions

As noted in the main text, we aim to characterize the measured abundances of microbial species with numerical parameters that characterize their interactions. These parameters may simply be phenomenological, but may also relate to dynamical population models.

Considering two species, labeled by subscripts i and j, the commonly used competitive Lotka-Volterra model describes the behavior of the populations P by the following relationship:

$$\frac{\mathrm{d}P_i}{\mathrm{d}t} = r_i P_i \left(1 - \frac{P_i - C_{ij}P_j}{K_i}\right) \tag{2.6}$$

where r_i is the intrinsic growth rate, K_i is the carrying capacity, and C_{ij}, defined for is the interaction coefficient, negative for competitive interactions and positive for beneficial interactions.

As steady state, $\frac{\mathrm{d}P_i}{\mathrm{d}t} = 0$, hence,

$$C_{ij} = \frac{P_i - K_i}{P_j}. \tag{2.7}$$

Note that this holds even if the initial factor in the Lotka-Volterra equation, $r_i P_i$ is replaced by any generic function of P_i . As discussed in the main text, each of the bacterial species examined is known to reach its carrying capacity approximately 10-12 hours after inoculation [51], a timescale considerably shorter than the 48 hours post-inoculation of our abundance measurements. It is therefore reasonable to make use of the steady-state approximation.

In our experiments, we measure intestinal abundances in di-associations, P^{II}, and mono-associations, P^I. The carrying capacity, K_i, is unknown. We assume K_i can be well approximated by the average P_i^I across fish, i.e. that the average abundance of a species in the absence of other species is similar to its carrying capacity in the gut. Therefore:

$$C_{ij} \approx \frac{P_i^{II} - \langle P_i^I \rangle}{P_j^{II}} \tag{2.8}$$

where the angle brackets indicate the mean across fish. Eq. 3.3 provides a simple characterization of inter-species interactions in the context of the standard competitive Lotka-Volterra equations.

As discussed in the main text, there is no reason the intestinal microbial populations must be governed by Lotka-Volterra dynamics or any linear interaction model. We therefore consider a model of logarithmic interactions and a more general family of power-law models. The logarithmic model, influenced by the order-of-magnitude changes in species abundance induced by competition, can follow from a phenomenological recasting of the competitive Lotka-Volterra model in terms of log-transformed populations:

$$\frac{\mathrm{d}\log_{10} P_i}{\mathrm{d}t} = f(P_i)\left(1 - \frac{\log_{10} P_i - C_{ij}\log_{10} P_j}{\log_{10} K_i}\right), \tag{2.9}$$

where we note that the first factor on the right hand side can be any generic function of P_i. Again assuming steady state dynamics and estimating $\log_{10} K_i$ by the average of $\log_{10} P_i$, the interaction coefficients are given by:

$$C_{ij} \approx \frac{\log_{10} P_i^{II} - \langle \log_{10} P_i^{I} \rangle}{\log_{10} P_j^{II}}. \tag{2.10}$$

which is Eq. 2.6 of the main text. We note that regardless of the validity of the dynamical model, Eq. 2.9 can be considered as a phenomenological characterization in which interaction effects are logarithmically additive (i.e. multiplicative) in population size.

Finally, we consider interactions with a power-law dependence on the size of the influencing species:

$$\frac{\mathrm{d}P_i}{\mathrm{d}t} = f(P_i)\left(1 - \frac{P_i - C_{ij}(P_j)^{\alpha}}{K_i}\right), \tag{2.11}$$

from which

$$C_{ij} \approx \frac{P_i^{II} - \langle P_i^{I} \rangle}{(P_j^{II})^{\alpha}} \tag{2.12}$$

As noted in the main text, we consider sub-linear ($\alpha < 1$) and super-linear ($\alpha > 1$) interactions. Linear interactions ($\alpha = 1$) are equivalent to the standard Lotka-Volterra model.

2.4.7.2. Pairwise Interactions in the Presence of Additional Species

To compare interactions between communities of two species and communities of more species, namely four or five, we extended the above parameterization. The standard Lotka-Volterra dynamical model for an arbitrary number of species is given by

$$\frac{\mathrm{d}P_i}{\mathrm{d}t} = r_i P_i \left(1 - \frac{P_i - \sum_{j \neq i} C_{ij} P_j}{K_i} \right) \tag{2.13}$$

where the sum runs over species. Again considering steady-state,

$$P_i = K_i + \sum_{j \neq i} C_{ij} P_j \tag{2.14}$$

As discussed in the main text, we infer C_{ij}^V by comparing the abundance of species i in fish co-inoculated by a set of species excluding and including species j. Again denoting the number of species by a superscript, subtracting P_i^{IV} from P_i^V gives

$$P_i^V - P_i^{IV} = C_{ij}^V P_j^V, \tag{2.15}$$

from which

$$C_{ij}^V = \frac{P_i^V - P_i^{IV}}{P_j^V}. \tag{2.16}$$

Similar expressions follow for the multi-species interaction coefficient in the log-transformed model:

$$C_{ij}^V = \frac{\log_{10} P_i^V - \log_{10} P_i^{IV}}{\log_{10} P_j^V}. \tag{2.17}$$

and the power-law model:

$$C_{ij}^{V} = \frac{P_i^V - P_i^{IV}}{(P_j^V)^{\alpha}}. \tag{2.18}$$

The interaction matrices for calculated for the two-species experiments (C_{ij}^{II}), using Eq. 2.10 and four-to-five-species experiments (C_{ij}^{V}), using Eq. 2.17 are shown in Fig S2. As noted in the main text, we found similar patterns distinguishing C_{ij}^{II} and C_{ij}^{V}, namely weaker and more positive interactions in the latter case, throughout the full range of α examined (Fig 2.3, A.4).

2.4.8. Sampling and Parameter Estimation

For each di-association, we measured the species abundances P_i^{II} and P_j^{II} in N=10 to 30 fish and calculated C_{ij}^{II} for each according to Eq. 2.8, 2.10, 2.12 above. To ensure that the measured abundance changes can be attributed to the presence of the second species we ignored data for which either P_i^{II} or P_j^{II} was zero. Each set of abundance measurements provides a C_{ij} value via the above equations. To determine the most likely C_{ij} from this set, as well as the uncertainty in our estimation of C_{ij}, we make use of sampling. With 3000 repetitions, we randomly sampled 75% of each dataset without replacement and calculated the mean and standard deviation of the C_{ij}.

To determine the number of repetitions needed to accurately estimate C_{ij}, we performed the same analysis on simulated population data, drawing P_i^{II} from a log-normal distribution, using a fixed $\langle \log_{10} P_i^I \rangle$, and drawing C_{ij} from a normal distribution of known mean and standard deviation. Using these we compute $\log_{10} P_j^{II}$ using Eq. 2.10, and from the simulated data we calculated the mean and standard deviation of the interaction coefficient as above. We found that sampling 75% of the dataset, $\sim$ 2000 repetitions yield the standard deviation of C_{ij} to an

accuracy of 90%. The resulting mean and standard deviation of C_{ij}^{II}, one for each species pair, are shown in the figures in the main text and Fig A.2A.

Interaction parameters in multi-species experiments, i.e. C_{ij}^{V}, were similarly calculated from subsampling abundance data from both the four species and the five species experiments. The mean and standard deviation of the C_{ij}^{V} coefficients calculated using this model are shown in Fig S2B. As in the calculation of the di-association-derived C_{ij}^{II}, we considered only data from fish in which each of the species inoculated in the four and five species experiments was detected, ensuring that the effects from all other species are consistent between experiments.

In vitro interaction coefficients were also calculated using Eq. 2.10 from abundance measurements in pairwise competition experiments in Lysogeny broth (LB) medium. The parameters shown in Fig A.3 reflect the mean and standard deviation of the coefficients from six replicates for each of the pairs of species.

2.4.9. Relative Abundance Correlations

As noted in the main text, the Pearson correlation coefficients between the relative abundances of species are commonly interpreted as measures of inter-species interactions. Denoting the relative abundance of species i (i.e. the population normalized to the sum of all species populations) in fish n as $(p_i)_n$, we calculate the correlation coefficient as usual:

$$r_{ij} = \frac{\sum_{n=1}^{N} \Big((p_i)_n - \langle p_i \rangle \Big) \Big((p_j)_n - \langle p_j \rangle \Big)}{\sqrt{\sum_{n=1}^{N} \Big((p_i)_n - \langle p_i \rangle \Big)^2 \sum_{n=1}^{N} \Big((p_j)_n - \langle p_j \rangle \Big)^2}} \tag{2.19}$$

where N is the total number of fish examined. Note that by construction, r_{ij} is symmetric.

2.4.10. Predicted Five-Species Abundance Distributions

We asked whether we can recreate the experimentally observed five-species abundance distributions using only the pairwise interaction coefficients from Section 2.4.7.1. Focusing first on the logarithmically additive model, we construct a predicted abundance value for each species by linearly combining the pairwise effects of each of the other species:

$$\log_{10} P_i^V = \langle \log_{10} P_i^I \rangle + \sum_{j \neq i} C_{ij}^{II} \log_{10} P_j^V . \tag{2.20}$$

P_i^V and P_j^V are the predicted abundances of species i and j respectively. This gives, for the five bacterial species in our system, five equations with five unknowns, namely the predicted P_i. To determine the distributions of predicted abundances for each of the five species, we randomly sampled each C_{ij}^{II} from the interaction coefficient distributions obtained in Section 2.4.7.1 . We performed this sampling 250 times to generate a comparable number of points to the experimental distribution (N=202). Both the predicted and the measured distributions are shown in Fig 2.4D. To mimic the experimental detection limit of approximately 25 cells, all predicted abundances below 25 were set to zero.

Similarly, we calculated predicted abundance distributions for using the linearly additive model in absolute abundance (i.e. competitive Lotka-Volterra), for which

$$P_i^V = \langle P_i^I \rangle + \sum_{j \neq i} C_{ij} P_j^V . \tag{2.21}$$

As above, we generated predicted distributions for each of the five species, shown in Fig A.6.

As discussed in the main text, the predicted distributions from both pairwise-additive models indicate that the five species are less likely to coexist than is observed experimentally.

2.4.11. Five-Species Shannon Entropy

We calculated the Shannon entropy, a metric commonly used to measure species richness in multi-species communities. This is defined as:

$$H = -\sum_i p_i \ln p_i \tag{2.22}$$

where p_i is the relative abundance of species i. For a neutral (non-interacting) community of N species, $p_i = 1/N$, on average. For five species therefore, a neutral model gives $H = \ln(5) = 1.61$. To calculate H from measured data, we used relative abundances of each bacteria species and calculated the Shannon entropy using Eq. 2.22. The mean Shannon entropy, averaged over all fish, is reported in the Discussion section of this chapter.

CHAPTER III

SPATIAL STRUCTURE AND INTERACTION MECHANISMS

This work is adapted from co-authored work currently under revision by D. Sundarraman, T. J. Smith, , J. V. Z. Kast, K. Guillemin and R. Parthasarathy, *Disaggregation as an interaction mechanism among intestinal bacteria*, submitted to Biophysical Journal (2022). I was involved in the experiments, analysis and writing of this work.

3.1. Introduction

The vertebrate gut is home to a diverse set of interacting microbial species, with microbiome composition correlating with aspects of host metabolism, digestion, immune response, development, and more [12–26], Dysbiosis of the gut microbiota has been linked to several diseases such as obesity, IBD and rheumatoid arthritis [2–11]. Understanding the forces that shape intestinal communities is therefore of considerable importance, and many studies have explored how factors such as host diet and genetics can affect microbiome assembly and function. In general, spatial organization is a common and important aspect of microbial ecosystems; surface attached biofilms, microbial mats, and marine snow provide well-known examples [79, 149–152]. This likely holds in the gut as well, but spatial information is usually difficult to obtain. Conventional approaches based on, for example, metagenomic sequencing of fecal samples are blind to structure, and most spatially resolved methods typically involve coarse sampling or fixation methods that can drastically perturb the features present in live animals [82]. Regarding inter-microbial interactions in particular, we know little about the

mechanisms at play, which may include segregation to enable coexistence, contact-mediated competition, or more complex spatially-varying signals.

Larval zebrafish provide a model vertebrate system in which to observe spatial relationships among gut microbial species. The animals' optical transparency and amenability to gnotobiotic techniques [47–49, 122], together with a library of fluorescently tagged native gut bacterial isolates [50], allows controlled experiments involving live imaging of bacterial communities [51–53, 92, 106]. Mapping the spatial structure of a number of gut bacterial species established that each, in mono-association with its host, has a characteristic fraction of its population forming dense, three-dimensional aggregates and is preferentially localized in particular regions of the gut [91]. Given the well-established ecological principle of competitive exclusion, by which species competing for the same limited resource cannot stably coexist, we might expect that if introduced together, two species with an affinity for the same region will strongly compete, leading to greatly reduced abundance for at least one of the two relative to the mono-association value. Spatial segregation of competitors, whether static or dynamic, provides a route to co-existence [153–155]; thus we might expect that reducing spatial overlap of intestinal species should weaken competition. How these principles may or may not be manifested in a real vertebrate gut remains unknown, and as we show below, an example with a pair of zebrafish-native bacterial species confounds simple expectations.

Inter-species interactions are also influenced by timing, and the outcomes of competition can vary depending on whether species arrive simultaneously or not to an environment. Various ecological studies have shown that early colonizers can have an advantage over later species and can often resist invasion by late

competitors [55, 156, 157]. Regarding the gut microbiome, the pre-existing community is believed to contribute to resistance to pathogen invasion [38, 158], though a greater number of controlled studies in animal models are needed to uncover underlying mechanisms [37, 158].

To illuminate possible connections between spatial organization and inter-bacterial interactions in the context of a vertebrate intestine, we performed a set of live-imaging-based studies of a strongly interacting bacterial species pair, using light sheet fluorescence microscopy to visualize bacterial locations and dynamics in situ. Prior work based on measuring species abundances, without spatial information, characterized the interactions between various zebrafish-commensal gut bacterial species and found several examples of strong competitive pairwise interactions, one such pair being *Aeromonas* ZOR0001 and *Enterobacter* ZOR0014 [159], each of which form dense aggregates in mono-association [51, 53, 91]. These and other strong pairwise interactions were dampened in the presence of additional bacterial species [159].

As described here, imaging reveals that both of these species colocalize and co-aggregate in the larval midgut. We introduce a derivative of *Aeromonas* ZOR0001, *Aeromonas-MB4* that is deficient in biofilm formation in vitro in the presence of a glycan commonly found in the gut and find that in vivo, it is largely planktonic and motile. The dispersed strain leads to an even lower *Enterobacter* abundance than the co-localized wild type, and induces a striking dissociation of *Enterobacter* aggregates. In the presence of an already established community of multiple bacterial species, competition and disaggregation effects are diminished, coexistence is enhanced, and the planktonic isolate behaves more similarly to the wild-type parental strain. Overall, our observations point to a surprising and

unanticipated mechanism by which spatial structure can mediate gut bacterial interactions, namely induced disintegration of aggregates.

3.2. Results

3.2.1. Aeromonas-MB4 exhibits planktonic behavior in vitro and in vivo.

We consider two strains of *Aeromonas*. One is a zebrafish gut commensal, *Aeromonas* ZOR0001 (referred to as AE). The other is an *Aeromonas* isolate (referred to as AE-MB4), derived through directed evolution of AE in vitro. The zebrafish-native AE forms aggregates in vitro in certain growth media, including sterile embryo medium supplanted with 0.4% N-Acetylglucosamine (GlcNAc), a sugar prevalent in intestinal mucus [93, 160–162]. The AE-MB4 strain was derived from AE by repeated passaging of fractions of such media that were devoid of visible aggregates, thereby selecting for bacteria deficient in aggregation in the presence of GlcNAc (Fig A.7). The molecular genetic characterization of AE-MB4 is described elsewhere [163]; we focus here on the spatial dynamics of this strain and the consequences of this altered aggregation behavior on community structure.

FIGURE 3.1. (A) Bright field image of a 7dpf zebrafish with the gut outlined in red. Bar: 500μm (B & C) Maximum intensity projections of 3D images of the intestine of zebrafish mono-associated showing (B) zebrafish-commensal AE bacteria (orange), which forms large midgut aggregates and (C) AE-MB4 (magenta), which is largely planktonic. Dotted curves roughly indicate the gut boundary. Bar: 100μm. (D) Mean normalized intensity profiles of AE (orange) and AE-MB4 (magenta) along the anterior-posterior axis. In contrast to AE, which localizes predominantly in the midgut, much of the AE-MB4 population is in the anterior bulb. Circles indicate the center of mass. Curves are averaged from N = 6 fish each. (E) The probability of a cell being in an n-cell cluster for AE (orange) and AE-MB4 (magenta), mono-associated with zebrafish. Circles and error bars indicate the mean and uncertainties, calculated using jack-knife resampling. Tick marks indicate bin intervals, e.g. the orange and magenta bars between 0 and 10^0 correspond to AE and AE-MB4 probabilities to be in clusters of size n = (0-1]. Data are from N = 6 and 8 fish for AE and AE-MB4, respectively. (F) The cumulative cluster size distributions (p[cluster size $\geq$ n]) for AE (orange) and AE-MB4 (magenta) in mono-association calculated from all clusters found in N = 6 and 8 fish, respectively, showing power law behavior for $n < 10^2$. The dashed lines illustrate the slopes from power law fits in the range n = 1 to 10^2, with exponents 0.8 for each strain. At large n, the AE distribution plateaus, reflecting the presence of large clusters.

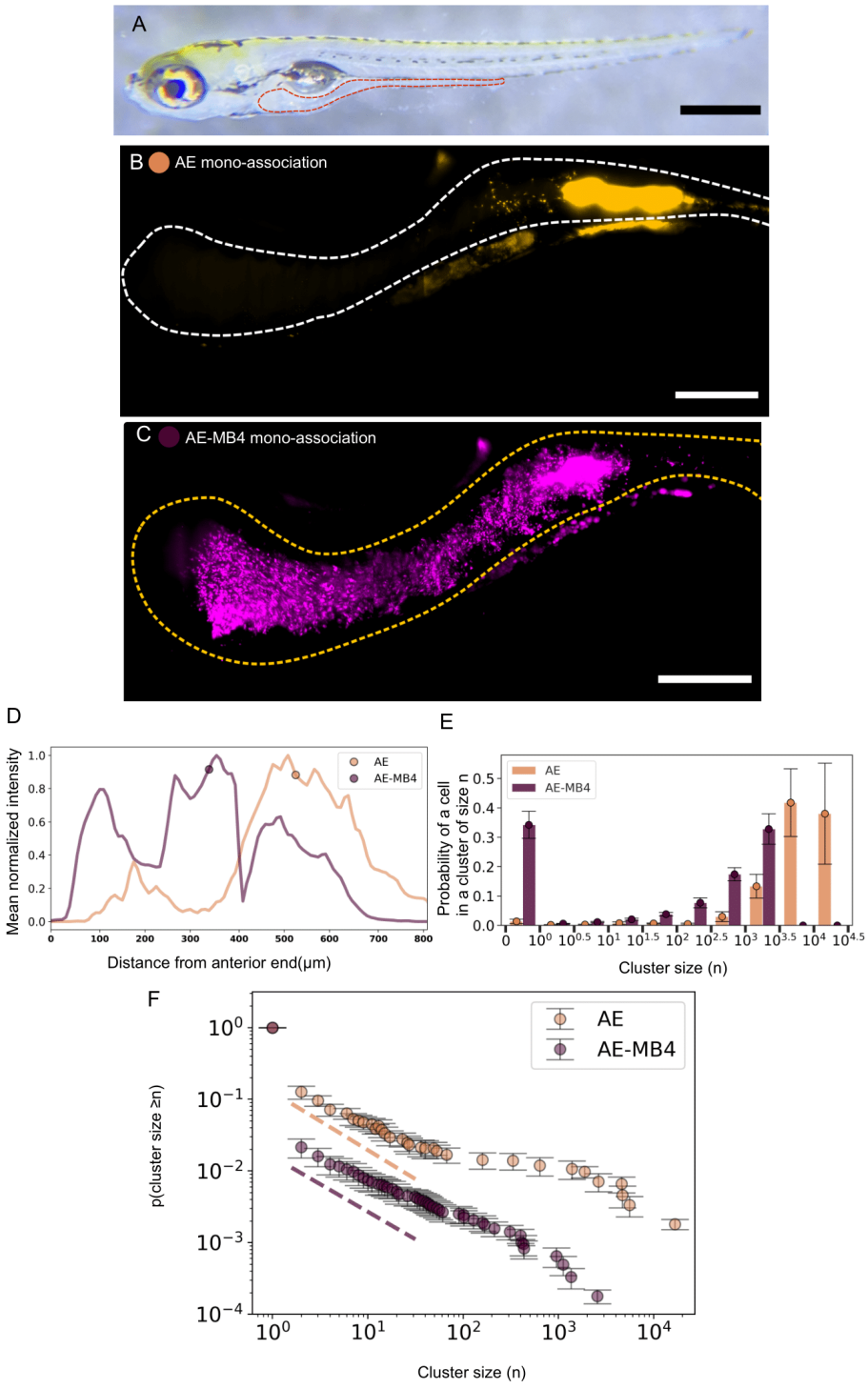
A
B
AE mono-association
C
AE-MB4 mono-association
D
Mean normalized intensity
AE
AE-MB4
Distance from anterior end(μm)
E
Probability of a cell in a cluster of size n
AE
AE-MB4
Cluster size (n)
F
p(cluster size ≥n)
AE
AE-MB4
Cluster size (n)

FIGURE 3.1.

We first characterized the spatial distribution of bacteria in initially germ-free zebrafish larvae (Fig 3.1A) mono-associated with either the commensal AE or the AE-MB4 isolate. We mono-associated initially germ-free zebrafish at 5 days post-fertilization (dpf) with each strain and imaged 48 hours later using light sheet fluorescence microscopy (Methods). Wild type AE forms dense clusters in the midgut (Fig 3.1B, D), as seen in prior work [51–53, 91, 92], whereas AE-MB4 resides primarily in the anterior with a large fraction of the population in the form of discrete planktonic cells (Fig 3.1C,D). Image analysis (see Methods) identifies individual bacterial cells and aggregated clusters and provides estimates of cluster populations. Cluster size statistics highlight the differences between the strains. After pooling measured cluster sizes from all fish, we compute the probability of a cell being in a cluster of a given size i.e. the ratio of the total number of cells found in a given cluster size bin to the net population from all clusters. For example, the bar associated with bin $(0 - 10^0]$ reflects the frequency of finding cells in clusters of size 1 in the total population. We plot this measured frequency for different cluster size bins in Fig 3.1E. AE cells are most likely to reside in large clusters (n = $10^{3.5}$), a population completely absent in AE-MB4, and AE-MB4 cells are over 30 times more likely to be planktonic than AE (Fig 3.1E). All cluster sizes are provided as supplemental Material. We also plot the reverse cumulative probability distribution of cluster sizes, p(n), i.e. the probability that a given cluster is composed of more than n bacterial cells (Fig 3.1F). The distributions for both species have characteristic power law form for small clusters ($n < 100$) with a slope of m = 0.8 ± 0.1 [92]. The disparity in p(n) between AE and AE-MB4 grows as n increases and is especially pronounced for clusters of size $n > 1000$ as the distribution of AE becomes shallower. Earlier work studying intestinal cluster

size distributions in a range of species has shown that characteristic power-law features arise from fragmentation and growth dynamics, and a shallow decline of p(n) at large n is indicative of aggregation [92], consistent with observations here.

3.2.2. A highly aggregated commensal species undergoes rapid fragmentation in the presence of the Aeromonas-MB4 isolate.

To study the role of spatial coincidence in competition in the zebrafish gut, we studied interactions of *Aeromonas* and *Aeromonas-MB4* with a different zebrafish-commensal bacterial species, *Enterobacter* ZOR0014 (referred to as EN). Past work based on abundance measurements established that the parental AE strain has strong negative interactions with EN, with the population of the latter reduced by over an order of magnitude from its mono-association value when di-associated with AE (Fig 3.2E) [159]. EN in mono-association is almost completely aggregated, with only about 10% of its population in the form of planktonic individuals, forming large clusters primarily in the midgut region of the intestine (Fig 3.2A) [53, 91]. Consistent with earlier measurements, its cluster size cumulative probability distribution and the probability of a cell being in a cluster of a given size reflect the highly aggregated spatial character of the species (Fig A.8,A.9).

FIGURE 3.2. (A-D) Maximum intensity projections of 3D images showing (A) EN (green) in mono-association forming large clusters in the midgut, (B) EN (green) in di-association with AE (orange) showing co-aggregation of both species in the midgut, (C) EN (green) in di-association with AE-MB4 (magenta) showing sparse EN amid abundant planktonic AE-MB4 cells, and (D) EN (green) after invasion by AE-MB4 (magenta) showing large populations of single cells and small clusters of EN throughout the gut. Inset: Many single cells of EN are evident. Dotted curves roughly indicate the gut boundaries. Bar (A-D): 100μm. (E) Twin axis plot showing the abundance (left axis) in $\log_{10}$(CFUs/gut + 1) and extinction fraction (right axis) for EN (green), AE (orange) and AE-MB4 (magenta) in mono-association (circles), di-association (Xs), and when EN is invaded by AE-MB4 (diamonds). Each marker indicates abundance data from a single fish. The blue line markers and black circular markers depict mean and standard deviation of the extinction fraction and abundance for EN and AE-MB4 in each of the experiments respectively. From left to right, N = 15, 12, 17, 27, 27, 36, 36, 23, and 23 fish. (F) The planktonic fraction per fish for EN in (from left to right) mono-association, dissociation with AE, dissociation with AE-MB4 and when invaded by AE-MB4. From left to right, N = 7, 10, 12, 12 fish. G. As in Fig. 3.1E, The probability of a cell being in an n-cell cluster for EN (i) in mono-association, (ii) in di-association with AE, (iii) in di-association with AE-MB4, and (iv) invaded by AE-MB4. Circles and error bars indicate the mean and uncertainties. Data are from N = 7, 10, 12, and 12 for (i)-(iv), respectively.

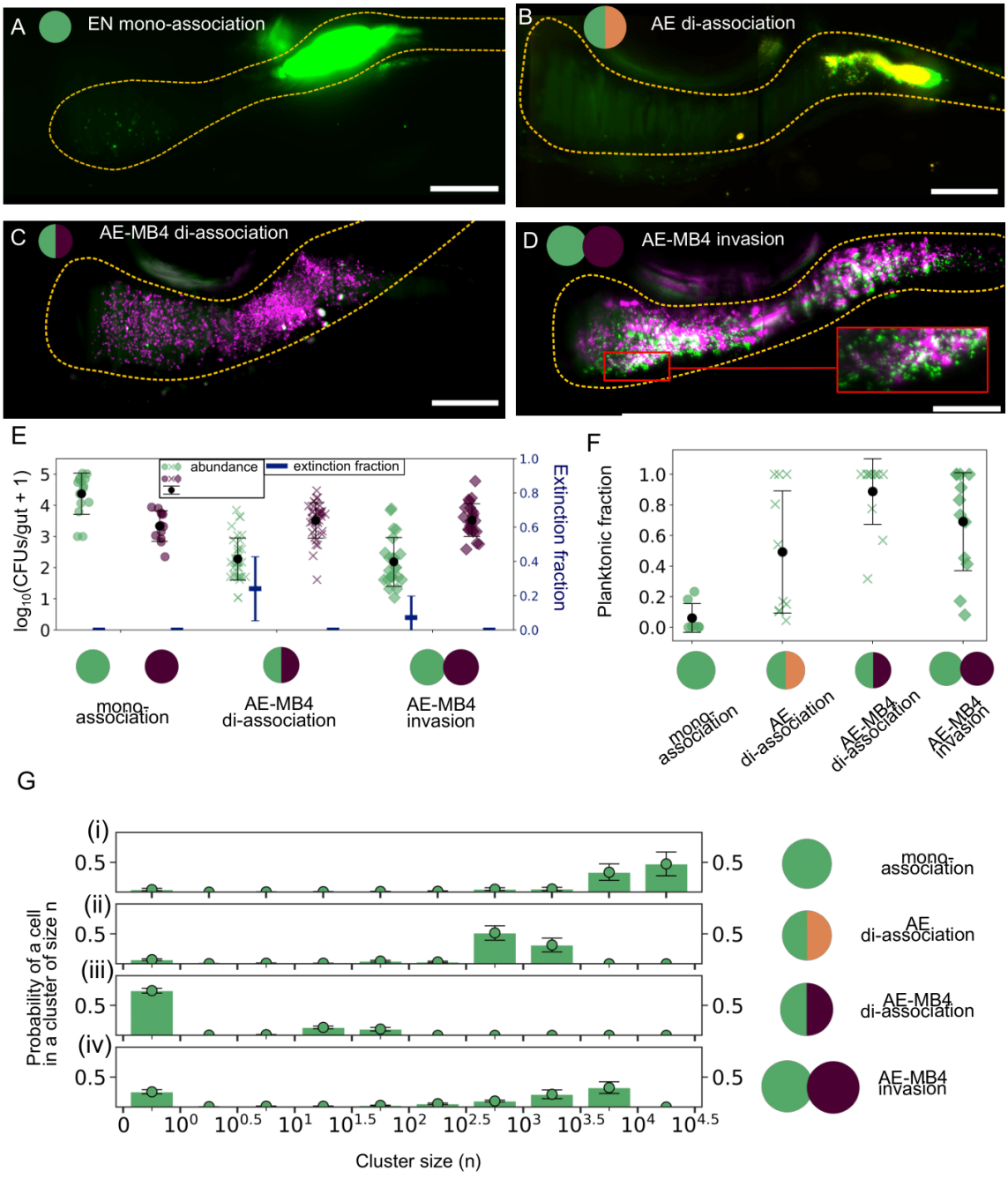
A
EN mono-association
B
AE di-association
C
AE-MB4 di-association
D
AE-MB4 invasion
E
abundance
extinction fraction
log10(CFUs/gut + 1)
Extinction fraction
mono-association
AE-MB4 di-association
AE-MB4 invasion
F
Planktonic fraction
mono-association
AE di-association
AE-MB4 di-association
AE-MB4 invasion
G
(i)
(ii)
(iii)
(iv)
Probability of a cell in a cluster of size n
Cluster size (n)
mono-association
AE di-association
AE-MB4 di-association
AE-MB4 invasion

FIGURE 3.2.

We performed di-association experiments (as in [159]) in which both AE and EN were inoculated simultaneously at 5 dpf and the spatial distribution was assessed at 7 dpf. Through imaging both species in di-association, we found that AE and EN often co-aggregate in the same region of the intestine (Fig 3.2B), suggesting that strong competition could be a consequence of both species having an affinity for similar locations. These co-aggregates of AE and EN consist of intermingled clonal clusters of each species, not well-mixed individuals of each species.

We next investigated the consequences of the AE-MB4 traits on the *Aeromonas-Enterobacter* competition. In di-association with AE-MB4, EN exhibits almost an order of magnitude lower mean abundance (2.2 ± 0.7) than with AE (3.0 ± 0.6), and roughly two orders of magnitude lower than its mono-association value (4.4 ± 0.7) (Fig 3.2E), in contrast to expectations that the species' dissimilar localizations may attenuate competition. We also note that extinction of EN is more frequent in di-association with AE-MB4 (extinction fraction = 0.2 ± 0.2), than with AE (extinction fraction = 0.1 ± 0.1). The effect on the spatial distribution of EN is striking; nearly all EN are found as discrete individuals (Fig 3.2C) , with the planktonic fraction being 0.9 ± 0.2 (mean $\pm$ std. dev.) compared to 0.1 ± 0.1 in mono-association. EN cells are never found in clusters of size $n > 10^2$, the most common range in mono-association, and in nearly 80% of the fish examined, EN shows no apparent clustering at all. The individual cells of EN rarely co-aggregate with AE-MB4 clusters, in contrast to frequently occurring co-aggregates of both species in the di-association of EN with AE.

To test how priority effects could impact interactions, we examined the abundance and spatial distribution of EN after invasion by either the AE or AE-

MB4 strains. Prior work established that EN reaches steady state abundance in approximately 8-12 hours [51, 53]. Thus, to ensure a stable pre-invasion EN population, we inoculated the second species 24 hours after the introduction of EN. When challenged with AE, the initial advantage serves to benefit EN, with most of the fish sustaining EN aggregates (Fig A.10). We anticipated priority effects to similarly impact invasion by AE-MB4. Contrary to this expectation, we found that EN is unable to persist as large aggregates in the gut (Fig 3.2D). Instead, the population consists of a large fraction of individual cells and some small clusters with a mean planktonic fraction of 0.7 ± 0.3 (Fig 3.2F,G), similar to that observed in the di-association experiments. The remaining clusters of EN in these experiments are often fragmented and sparse, unlike the dense aggregates of EN seen in other experiments.

Through time series imaging of EN-colonized fish starting 6 hrs after invasion with AE-MB4, we observed striking, rapid fragmentation of large EN aggregates into individual cells and small clusters within timescales of hours (Fig 3.3A,B). Such disintegration has not been observed in mono-association or di-association with AE and thus we attribute it to the presence of AE-MB4. The planktonic EN showed little motility. Analyzing the rate of change of isolated sub-populations identified in images as planktonic and aggregated after fragmentation of the EN aggregate, we found the growth rate (r) of individual cells ($r = 0.24 \pm 0.11$ hr^{-1}, mean $\pm$ std. dev. for N=3 fish) to be approximately three times lower than that of clusters ($r = 0.66 \pm 0.23$ hr^{-1} for N=4 fish) (Fig 3.3C). This was calculated from exponential fits of the abundance over time after identification of bacterial clusters and individuals in consecutive 3D images (Methods). This measurement takes into consideration regions where there is only growth, not influx or expulsion. The

large planktonic fraction together with the lower r of the planktonic relative to the aggregated form implies a reduced ability of EN to persist in the gut following AE-MB4 invasion. The growth rate of AE-MB4 in the invasion experiments (r = 0.76 $\pm$ 0.04 hr^{-1} for N=3 fish) was found to be higher than that of EN, consistent with the expectation that a fast growing species outcompetes a slow growing species.

To better understand the implications of a high planktonic fraction of usually aggregated EN in the gut, we simulated the dynamics of clusters in the zebrafish intestine undergoing four key processes, growth, aggregation, fragmentation and expulsion. Simulation of these processes has been shown to reproduce characteristic features of cluster size distributions observed in experimental data [92].

A detailed description of the stochastic model and its parameters is provided in Methods. In brief, growth of each cluster is logistic and the total abundance (sum of all clusters) is bound by a carrying capacity, K, equal to the mono-association abundance of the species and growth rates of individuals and clusters (r_{pl} and r_{agg}) being the experimentally measured parameters (Fig 3.3C). Aggregation or the combining of two clusters of size n, m to form a single cluster(n+m) occurs at an aggregation rate $\alpha_{nm} = \alpha\ (n*m)^{1/3}$ where the exponent 1/3 signifies collision likelihood proportional to cluster diameter. The value of α is fixed at $\log_{10}(\alpha) = -2.5$. Similar to aggregation, a cluster of size n undergoes size-dependent fragmentation of single cells at a rate $\beta = (n)^{2/3}$, corresponding to the breakup of a single cell from a cluster of size n with the 2/3 exponent reflecting that only cells on the surface have a likelihood of breaking up from the cluster. β is varied from 0.02 hr^{-1} to 1 hr^{-1} in steps of 0.025 hr^{-1}. For a cluster of size 1000, this range implies 2-100 cells fragmenting per hour. Size-independent expulsion of

aggregated clusters is fixed at a rate corroborated by previous studies, λ_{agg}=0.1 hr^{-1} while the expulsion rate of planktonic cells is varied logarithmically between $\lambda_{\text{pl}} = 0.025$ and 10 hr^{-1}.

We combine these processes in a stochastic simulation, with one of fragmentation, aggregation or expulsion reactions occurring at a given time step determined by the rates for each reaction computed for each cluster at the given time step. First, the simulation is run to determine the steady state mono-association cluster distribution for fixed α, β and λ after 24 hrs. After generating this initial EN distribution, we simulate the AE-MB4 invasion of EN aggregates by varying β. We run this for the full range of parameter values of λ_{pl} stated earlier. Averaging total abundance from 500 replicates for each pair of parameters of expulsion rate ratio $\frac{\lambda_{pl}}{\lambda_{agg}}$ and fragmentation rate β we obtain the abundance phase diagram shown in (Fig 3.3D). When $\lambda_{pl} < \lambda_{agg}$, we find that abundance corresponds to the mono-association value, irrespective of changing fragmentation rates. For $\lambda_{pl} > \lambda_{agg}$, the abundance corresponds to our experimentally observed abundance values for an expulsion rate 0.13 $\text{hr}^{-1} < \lambda_{pl} < 2.5$ hr^{-1} with the overlap more distinct in the high fragmentation regime. This is physically plausible as non-motile cells undergo a more constant efflux in the intestine, being more susceptible to flows compared to large aggregates that are removed in mass-expulsion events, also observed experimentally. This suggests that the properties of planktonic non-motile EN, with its reduced growth rate and its increased susceptibility to being expelled from the gut, can explain the low experimentally observed values of EN abundance.

FIGURE 3.3. (A) Maximum intensity projections of the midgut region from a time series showing an aggregate of EN that fragments following invasion by AE-MB4. Times indicate hours post-invasion. Dotted curves roughly indicate the gut boundary. Bar : 50 μm. (B) The planktonic fraction of the EN population over time for 3 fish measured starting 6 hrs. after invasion by AE-MB4.(C) The number of cells normalized by the initial value over time for aggregated (blue, dotted) and planktonic (teal, solid) EN populations after invasion by AE-MB4. For aggregated populations, each dataset depicts the growth of a single cluster of EN in a distinct fish (N=4). For planktonic populations, each dataset corresponds to a region comprising only planktonic cells in a distinct fish (N=3). The black curves indicate the mean growth rates: m = 0.66 $\pm$ 0.23 hr^{-1} and 0.24 $\pm$ 0.11 hr^{-1} for aggregated and planktonic cells, respectively. (D) Simulated abundance of EN as a function of the ratio of the expulsion rates for planktonic to aggregated populations ($\frac{\lambda_{pl}}{\lambda_{agg}}$) and the fragmentation rate β (hr^{-1}). Experimentally measured parameters were used for the growth rates of aggregated (r_{agg}) and planktonic (r_{pl}) EN clusters (shown in C). The shaded region corresponds to the experimentally measured abundance ($\log_{10}$(abundance) = 2.0 $\pm$ 0.9). See the Methods section for details.(E) Brightfield image of EN-AE-MB4 co-aggregates in 0.4 % GlcNAc solution. Scale bar: 1mm. (ii) Single plane of a 3D image showing co-aggregated populations of AE-MB4 (magenta), EN (green) and overlapping populations (white) in 0.4 % GlcNAc. Scale bar: 10μm.

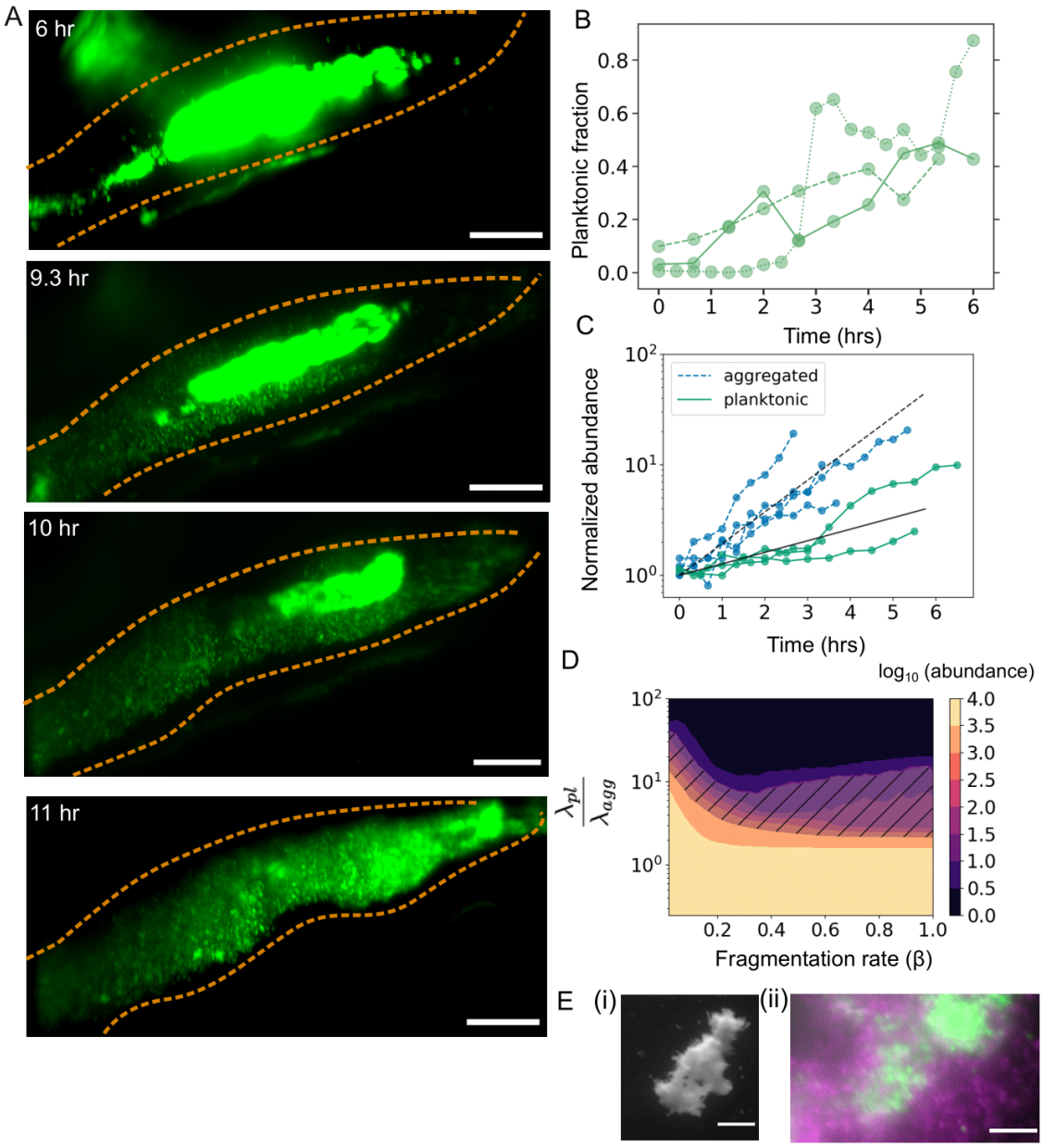
A
6 hr
9.3 hr
10 hr
11 hr
B
Planktonic fraction
Time (hrs)
C
Normalized abundance
aggregated
planktonic
Time (hrs)
D
log10 (abundance)
Fragmentation rate (β)
E
(i)
(ii)

FIGURE 3.3.

We study the aggregation of EN in the presence of AE-MB4 also in in vitro experiments, comprising 0.4 % GlcNAc solution, a medium in which AE-MB4 resists aggregation (Fig A.7). Strikingly, in co-culture experiments of AE-MB4 and EN in the same medium, AE-MB4 readily co-aggregates with EN and we observe large clusters comprising both species Fig. 3.3E. These observations show that in vivo interaction dynamics and outcome are markedly different from those in vitro.

3.2.3. The Aeromonas-MB4 isolate displaces the closely related parental AE strain

To test whether the strong competition effects and dynamics observed are specific to EN and to examine how other gut bacterial species may be impacted by AE-MB4, we studied AE-MB4's interactions with the parental zebrafish isolate AE strain. We examined intra-species interactions by inoculating, as in previous experiments, initially germ-free zebrafish with fluorescently labeled AE at 5 dpf and challenging by introduction of either AE-MB4 or differently-labeled AE 24 hours later. The abundance of AE after invasion by AE-MB4 ($\log_{10}$(abundance) = 2.8 ± 0.5) drops by over an order of magnitude compared to its mono-association value ($\log_{10}$(abundance) = 4.2 ± 0.4). Comparing the probabilities of finding AE cells in different sized clusters when invaded by itself versus when invaded with the planktonic AE-MB4, we discovered an absence of very large clusters (n = 10^4) in the presence of AE-MB4 (Fig 3.4), suggesting that the AE-MB4 isolate impacts the parental bacteria's ability to either form or maintain dense aggregates. The dynamics of interactions differ, in that we observe no dissociation of AE aggregates and instead expulsion of large AE clusters with often only small clumps persisting.

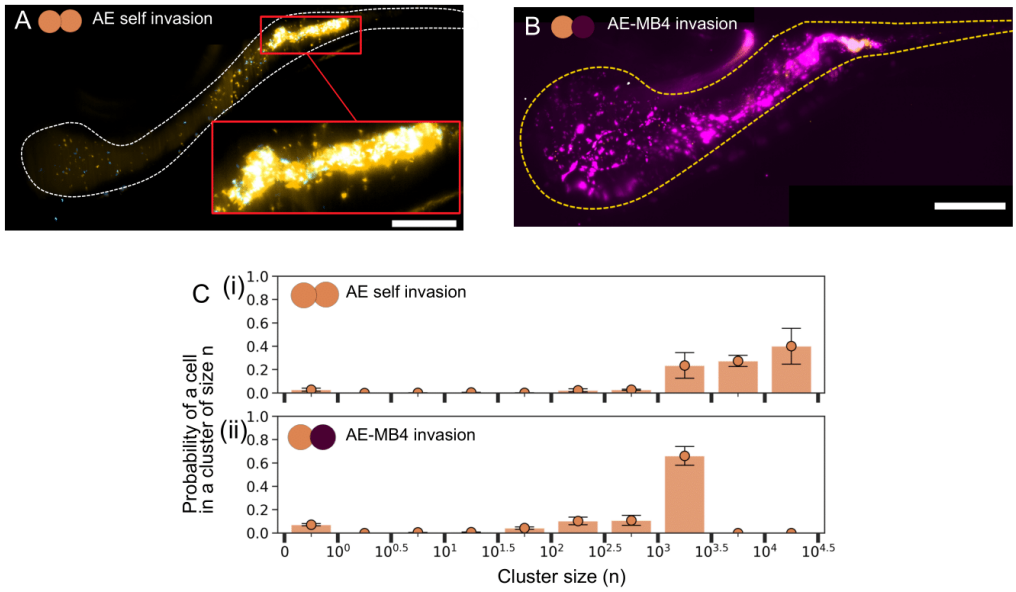

FIGURE 3.4. (A & B) Maximum intensity projections from zebrafish initially colonized by AE (orange), invaded 24 hrs. later by (A) differently labeled but otherwise isogenic AE (blue) (B) AE-MB4 (magenta). Images (A) and (B) were taken approximately 24 hrs. post-invasion. Dotted curves roughly indicate the gut boundary. Bar: 100μm. Inset to (A): a bacterial aggregate comprising both populations of AE (white overlapping regions). (C) Cluster probabilities as in Fig. 3.1E for AE (orange) when (i) invaded by others of the same strain (AE) and (ii) invaded by AE-MB4, both after 24 hrs. Circles and error bars indicate the mean and uncertainties. Data are from N = 8 and 10 fish for (i) and (ii), respectively.

3.2.4. Multi-species communities dampen strong AE-MB4-EN interactions

We next studied the interactions of EN and AE-MB4 in the presence of additional species, using a set of zebrafish commensal bacteria whose interactions have previously been characterized [159]. The additional gut community members comprised *Plesiomonas* ZOR0011 (referred to as PL), *Acinetobacter* ZOR0008 (AC), *Pseudomonas* (ZWU0006) (PS), and *Aeromonas* (AE). First, we co-inoculated four species (EN, AC, PL and PS) at 5 dpf and observed high

abundances and large populations of aggregated EN (Fig 3.5A) in the midgut region of the intestine, resembling its mono-association form (Fig 3.2A, E, G), suggesting that these species have little effect on Enterobacter's spatial structure. Then we examined the impact of AE-MB4 when also co-inoculated along with the other four species and found that on average populations of EN were more planktonic (planktonic fraction = 0.7 ± 0.2), (Fig 3.5B), as in the di-association experiments. We also noted frequent extinction of EN, with approximately 1/3 of the fish showing no trace of EN. Overall, however, EN abundance was slightly higher ($\log_{10}$(abundance) = 2.8 ± 0.5) than in the di-association experiments ($\log_{10}$(abundance) = 2.3 ± 0.7) (Fig 3.5E,G). This suggested that the negative AE-MB4 interaction effects are still present but relatively weaker in these five species co-inoculation experiments. The abundance data (Fig 3.5E) includes fish in which all species inoculated in the experiment were detected and all species excluding PL were detected. PL generally showed rare colonization across all datasets.

FIGURE 3.5. Maximum intensity projections of a larval zebrafish gut showing the spatial distribution of (A) EN (green) in the presence of four other commensal gut bacterial species forming large aggregates in the intestine (B) EN (green) in the five-species co-inoculation experiment (including AE-MB4 (magenta)) has smaller fragmented clusters and many single cells (C) EN (green) in the experiment when five species (including AE) are invaded by AE-MB4 (magenta) where EN forms larger clusters with some single cells and AE-MB4 populations show some aggregation. The dotted curve roughly defines the gut wall. Bar:100μm (D) Mean normalized intensity profiles measured along the anterior-posterior axis showing the spatial distribution of EN (green) and AE-MB4 (magenta) along the intestine when (i) EN is invaded by AE-MB4 and (ii) all five species are invaded by AE-MB4 showing large aggregates of EN persist in the midgut. The circular markers indicate the center of mass. Data are from N = 13 and 11 fish for (i) and (ii) respectively. (E) Twin axis plot showing the abundance of EN (left axis) in $\log_{10}$(CFUs/gut + 1) and extinction fraction (right axis) when in mono-association, in di-association with AE-MB4, invaded by AE-MB4, in the four-species co-inoculation experiment, in the five species co-inoculation experiment (including AE-MB4), in the five species co-inoculation experiment (including AE) invaded by AE-MB4. Abundances from individual fish are depicted with green circular markers. Mean and standard deviation for abundance and extinction fraction of EN are shown with black circular and blue line markers respectively. N (from left to right) = 15, 36, 23, 21,11, 87, 19 fish. (F) The planktonic fraction per fish for EN when invaded by AE-MB4, in the four–species co-inoculation experiment, in the five-species co-inoculation experiment (including AE-MB4) and when the five-species (including AE) are invaded by AE-MB4. Black markers indicate the mean and standard deviation. N (from left to right) = [12, 5, 2, 14] fish. (G) The probability of being in an n-cell cluster of EN when (i) invaded by AE-MB4 (ii) in the four-species co-inoculation experiment (iii) in the five-species co-inoculation experiment (including AE-MB4) (iv) in the five-species co-inoculation experiment (including AE) invaded by AE-MB4. Mean and uncertainties determined from jack-knife resampling are shown with black markers. N (top to bottom) = [12, 5, 2, 14] fish.

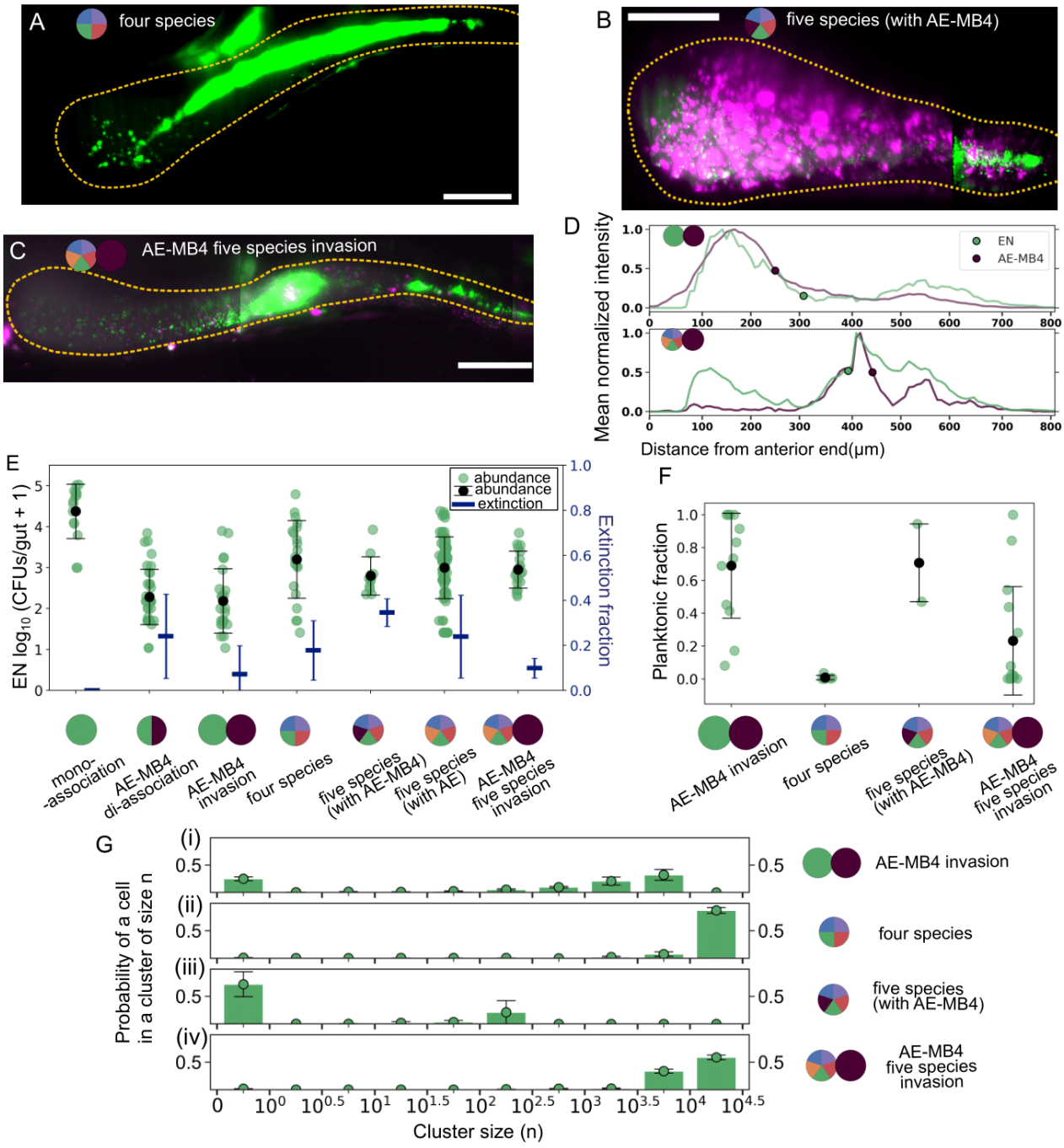
A
four species
B
five species (with AE-MB4)
C
AE-MB4 five species invasion
D
Mean normalized intensity
EN
AE-MB4
Distance from anterior end(μm)
E
EN log10 (CFUs/gut + 1)
abundance
abundance
extinction
Extinction fraction
mono-association
AE-MB4 di-association
AE-MB4 invasion
four species
five species (with AE-MB4)
five species (with AE)
AE-MB4 five species invasion
F
Planktonic fraction
AE-MB4 invasion
four species
five species (with AE-MB4)
AE-MB4 five species invasion
G
Probability of a cell in a cluster of size n
(i)
(ii)
(iii)
(iv)
Cluster size (n)
AE-MB4 invasion
four species
five species (with AE-MB4)
AE-MB4 five species invasion

FIGURE 3.5.

To determine whether these interactions persist in spite of priority effects, we performed invasion experiments with fish co-inoculated with all five species (AC, AE, EN, PL and PS), similar to mono-association EN experiments. We first studied the abundance distribution of EN in the control experiment, when no invader was introduced. We found that EN is more likely to be aggregated in these fish, resembling its typical structure with mean abundance in these fish = $10^{3.0\pm0.8}$ (Fig 3.5E).

On challenging this multi-species community with AE-MB4, we found strikingly different results from that of the mono-association invasion. Large aggregates of EN were able to persist in the presence of other species and the mean planktonic fraction of EN (0.2 ± 0.3) was lower than in the mono-association invasion experiments (0.7 ± 0.3) (Fig 3.5 D,C and F). The likelihood of a cell being in clusters of size $n > 10^3$ goes up from 67% in the mono-association invasion experiment to 97% in the multi-species challenge experiments (Fig 3.5G), while the planktonic probability is reduced from 25% to 2%. In time series experiments observing the dynamics of EN aggregates in the presence of other species, large aggregates of EN either resist breakup or undergo slower fragmentation relative to the fast timescales observed in single species mono-association invasion experiments. Together, all of these observations suggest that having a diverse and stable pre-existing community can inhibit strong interaction effects due to the invader.

To quantify the strength of interactions in different contexts, we calculated an interaction coefficient metric measuring the interaction effect of species j on species i and defined as follows as in [159]:

$$C_{ij}^{1-2} = \frac{\langle \log_{10} P_i^I \rangle - \log_{10} P_i^{II}}{\log_{10} P_j^{II}} \tag{3.1}$$

Here, P_i^I is the mono-association abundance of species i, P_i^{II} and P_j^{II} are the abundances of species i and j in di-association. This follows from a competitive Lotka-Volterra model using log-transformed abundances in place of absolute abundance, described in detail in [159].

One can extend this interaction coefficient to quantify the effect of a single species j on another species i in the five species experiments:

$$C_{ij}^{4-5} = \frac{\log_{10} P_i^{IV} - \log_{10} P_i^{V}}{\log_{10} P_j^{V}} \tag{3.2}$$

These equations can be applied to the invasion experiments where P_i^{II} and P_j^{II} are replaced by the abundances of species i and j in the invasion experiments. Similarly, Eq.3.2 translated to the five species invasion case can be written as:

$$C_{ij}^{5-6} = \frac{\log_{10} P_i^{V} - \log_{10} P_i^{VI}}{\log_{10} P_j^{VI}} \tag{3.3}$$

Where P_i^V is the abundance of species i in the five species (AC, AE, EN, PL and PS) co-inoculation experiment, P_i^{VI} is the population of i post-invasion with species j and P_j^{VI} is the abundance of the invader j. Using equations Eq. 3.1, 3.2 and 3.3, with the experimental abundance data, we can extract the mean and uncertainty of the interaction coefficients for various experiments. We measured the interaction coefficients in the di-association and invasion experiments to be similar with $C_{ij}^{1-2} = -0.64 \pm 0.03$ for the di-association and -0.65 ± 0.03 for the invasion experiments. These signify strong negative interactions with populations of EN dropping by two orders of magnitude relative to mono-association. In the 5

species co-inoculation experiments with AE-MB4, we found $C_{ij}^{4-5} = -0.11 \pm 0.10$, significantly weaker than C_{ij}^{1-2} for di-association. For the invasion experiments we found the magnitude of interactions to be zero within uncertainties $C_{ij}^{5-6} = -0.02 \pm 0.06$. These coefficients affirm implications of previous work that higher order interactions dampen strong pairwise effects and promote co-existence in a diverse community.

To further examine the nature of interactions in a multi-species context and how other species are impacted in the presence of AE-MB4, we returned to characterizing the effects of AE-MB4 on the parental AE strain. In mono-association, challenged by AE-MB4, AE was unable to persist in clusters of n $\geq 10^4$ cells with no likelihood of being in such clusters (Fig 3.4C (ii)). When additional species are present, we see large aggregated populations of AE in the midgut and cells are 53% likely to be found in aggregates of size $\geq 10^4$ cells (Fig 3.6A, B, C). As with EN, greater gut community diversity counteracts the changes induced by the AE-MB4 isolate. Surprisingly, we also found that AE-MB4, highly planktonic on its own, forms aggregates in the invasion experiment with other species present, also altering its localization in the intestine ((Fig 3.6B(ii)D).

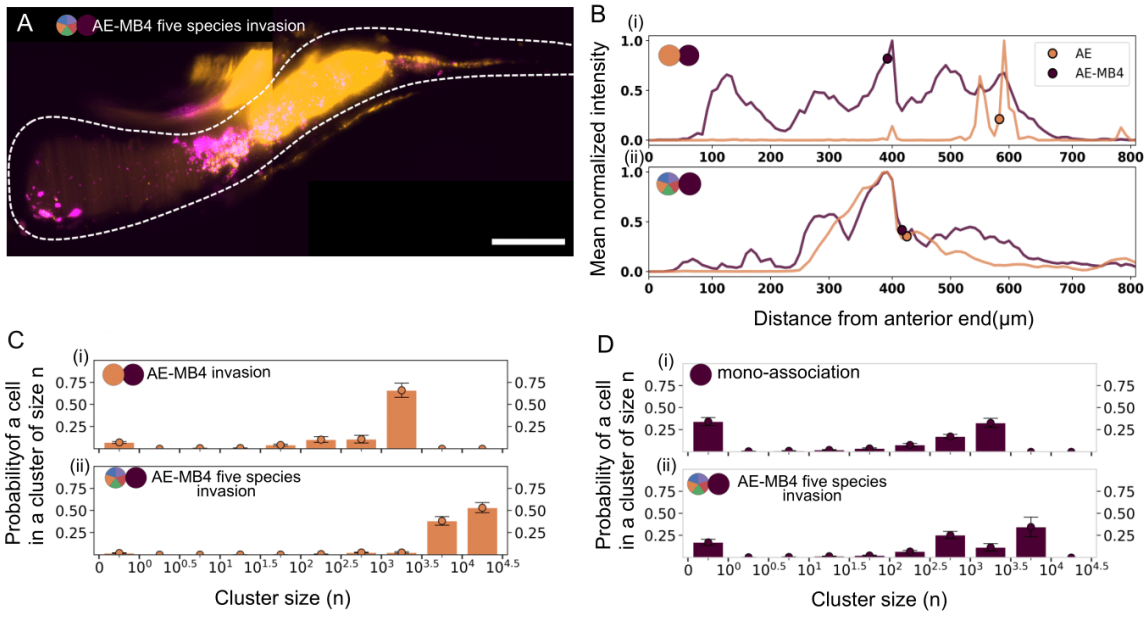

FIGURE 3.6. (A) Maximum intensity projection of a larval zebrafish gut showing a large cluster of AE (orange) after invasion by AE-MB4 (magenta) in the presence of the other four species. Small clumps of AE-MB4 are interspersed in the AE clusters. Bar: 100μm (B) Mean normalized intensity profiles measured along the anterior-posterior axis showing the spatial distribution of AE (orange) and AE-MB4 (magenta) along the intestine when (i) AE and (ii) all five species (including AE) are invaded by AE-MB4. The circular marker indicates the center of mass. Data for (i) and (ii) are from N = 10 and 11 fish respectively.(C) The probability of being in an n-cell cluster for AE when (i) invaded by AE-MB4 (ii) invaded by AE-MB4 in the presence of the other four species. The mean and standard deviation are indicated with circular markers. The x tick marks indicate the bin intervals i.e. the bar between the tick marks 0 and 10^0 corresponds to the probability of being in a cluster within (0-1]. Data are from N = 10 and 14 fish for (i) and (ii) respectively. (D) The probabilities (as in C) for AE-MB4 (i) in mono-association (ii) after invading the five species. The mean and standard deviation are indicated with circular markers. N = 8 and 11 fish for (i) and (ii) respectively.

3.3. Discussion

We report an unexpected mechanism of interactions among gut bacterial species: induced disaggregation. Specifically, in our experiments, the presence of a non-aggregating strain disrupts a different, normally aggregated, commensal

species, lowering its abundance and growth rate and altering its spatial structure in the intestine. Although the AE-MB4 isolate has reduced spatial overlap with EN than the parental strain, we find that this does not attenuate competition, defying the simple expectation that species with different localization characteristics are likely to have weaker interactions.

The molecular mechanism of the observed disaggregation is currently unknown. As described in detail elsewhere [163], the *Aeromonas-MB4* isolate investigated here was derived by directed evolution in media rich in N-Acetylglucosamine (GlcNAc), a sugar prevalent in intestinal mucus [164–167]. *Aeromonas* is normally highly aggregated in the zebrafish gut, with clusters likely held together by extracellular polysaccharides and proteins as is typical for biofilms and other microbial aggregates. It is therefore plausible that in the AE-MB4 isolate, intestinal cues that inhibit production of polysaccharide-digesting enzymes are ignored, and these enzymes act broadly to degrade the extracellular matrix of *Enterobacter*. Testing this hypothesis requires considerable further study and could benefit from experimental assays such as using microfluidics to identify physical and chemical conditions in which dissociation occurs and perhaps the role of geometry of the gut in mediating this competition. Similar phenomena, however, have been reported in non-intestinal contexts. For example, *Streptococcus pyogenes* secretes a protease that disrupts *Staphylococcus aureus* biofilms [168], the algae *C. reinhardtii* can inhibit aggregation of *Escherichia coli* [66], and mucus enhances in vitro biofilm formation by Escherichia coli [169] Given the observed co-aggregation of both *Aeromonas* and *Enterobacter*, it is likely that both species share cues and the disruption of aggregation of one, may directly interfere with aggregation of the other. Universal cues for inter-species bacterial communication such as AI-2 have

been known to promote formation of mixed species biofilms [170, 171]. A study has found that the suppression of AI-2 expression in one of the species in a dual-species biofilm results in sparse co-aggregation and decreased biomass [172].

The *Aeromonas/Enterobacter* interactions we observe in the zebrafish gut differ strikingly from interactions observed in vitro. In minimal media with 0.4% GlcNaC, we find co-aggregates of AE-MB4 and EN (Fig 3.2E), with intermingling of the species at the scale of single cells, a morphology never seen in the gut. The dissimilarity is not surprising, as both the chemical and physical environment of the intestine differ from that of a media-filled petri dish, but it highlights the challenges of inferring in vivo behavior from in vitro assays.

The disaggregation and low abundance induced in *Enterobacter* by *Aeromonas-MB4* in pairwise competition in the zebrafish gut are attenuated in the presence of additional bacterial species. The ability of such higher order interactions to stabilize diverse communities has been noted in many contexts [70, 71, 73, 159], and the observations described here suggest that maintenance of spatial structure is a means by which multi-species coexistence is manifested. It is not currently clear whether this maintenance is facilitated by the biochemical activity of specific members of the community or by more complex spatial organization of species that may emerge. Studies involving labeled subsets of these species, or mutants derived with different aggregation traits, will illuminate the mechanism.

We also note the role of priority effects in determining community composition. It is known that early gut microbiome composition in humans influences whether a new colonizer can establish itself [38]. Studies have linked a diverse and healthy gut microbiome to colonization resistance [173], for example

from invasion by the pathogen *Clostridioides difficile* [174, 175]. In the larval zebrafish, we find that in the presence of a diverse pre-existing community, AE-MB4 interactions with EN and AE are significantly weaker than when all species are inoculated simultaneously. Imaging reveals the spatial signatures that distinguish the outcomes of co-inoculation and invasion: AE-MB4 is more planktonic and less aggregated in the former than the latter, and EN maintains its aggregated phenotype with little fragmentation in invasion but not in co-inoculation studies.

The presence of gut bacterial aggregates [51, 89, 91, 92] and their importance to phenomena such as antibiotic response [53] and resistance to intestinal contractions [52] have been deduced in past work involving live imaging in larval zebrafish. This model system enables exploration of the community-level consequences of altered aggregation of a commensal bacterial species, lending insight into biophysical and biochemical mechanisms that may be at play more broadly, for example in the human gut. We suggest that bacterial manipulation of aggregation state, both their own state and the state of other species, may be a common feature of gut microbiome dynamics.

Moreover, controlled disruption of bacterial aggregates could have therapeutic applications. An engineered disruptor, we speculate, could be introduced to the human gut to displace resident, aggregated microbes, facilitating their replacement by transplanted or otherwise intentionally provided strains. Reaching this end will require a more thorough understanding of inter-species modulation of physical structure.

3.4. Materials and Methods

3.4.1. Animal Care

All experiments with zebrafish were performed in accordance with protocols approved by the University of Oregon Institutional Animal Care and Use Committee and by following standard protocols [147]

3.4.2. Gnotobiology

Wild-type (AB X TU line) larval zebrafish (*Danio rerio*) were derived using protocols described in [47]. The larvae at 0 dpf are washed with antibiotic, bleach and iodine solutions and then moved to tissue culture flasks containing sterile embryo medium solution at a density of approximately 1mL/larva. The flasks are stored in a temperature-controlled room maintained at 28C.

3.4.3. Bacterial strains

Zebrafish gut isolates were previously tagged with green fluorescent protein (GFP) and dTomato [50]. The various isolates used for this study are textitAeromonas sp. (ZOR0001), *Enterobacter sp.* (ZOR0014), *Plesiomonas sp.* (ZOR0011) *Pseudomonas mendocina* (ZWU0006) and *Acinetobacter calcoaceticus* (ZOR0008). *Aeromonas-MB4* strain (JS168), an isolate of *Aeromonas* strain (ZOR0001) was generated through a guided evolution experiment described in [163]. All bacterial stocks were made in 25% glycerol and maintained at -80°C.

3.4.4. Inoculation of tissue culture flasks

The bacteria from frozen stocks were grown in lysogeny broth (LB medium) and shaken overnight for approximately 16 hrs in a temperature controlled room at 30°C. 1mL of the overnight culture was washed twice by centrifuging at 7000g for 2 min and replacing the supernatant with fresh sterile embryo medium each time. For mono-association and co-inoculation experiments, the species were inoculated in fish at 5dpf and for the challenge experiments, the first species was inoculated at 5dpf and the second species is inoculated approximately 24 hrs after, at 6 dpf such that the flask water concentration of species is approximately 10^6 CFUs/mL.

3.4.5. Gut dissections and plating

We determined the abundances of bacterial species in the competition experiments by dissecting and plating the intestine. At 7dpf, zebrafish were euthanized via hypothermic shock, following which gut dissections were done to isolate intestinal contents. The intestine was placed in 500μL of sterile embryo medium and homogenized by blending with 0.5mm zirconium oxide beads. Dilutions of 10^{-1} and 10^{-2} were prepared and 100μ L of these solutions were spread on tryptic soy agar plates. For experiments with zebrafish inoculated with $>$ 2 species, guts were plated on Universal HiChrome agar (Sigma Aldrich) to distinguish species based on a colorimetric indicator. The CFUs on the plates were counted to ascertain the abundances of the inoculated bacterial species.

3.4.6. Live Imaging using light sheet fluorescence microscopy.

3D imaging of the larval zebrafish gut was done on a home-built setup described in [89]. The larvae were anesthetized with MS-222 (Syndel) and mounted

in 0.6% agarose gel in glass capillaries. Each capillary is inserted into an imaging chamber containing sterile embryo medium and MS-222 at a concentration of 20μL/mL of embryo medium. Once mounted, the fish were extruded from the capillaries. Lasers at 488nm and 568nm were used to excite GFP and dTomato bacteria respectively. Image acquisition involves translating the specimen in z-steps of 1 micron to capture the entire volume of the zebrafish gut. For time series experiments, imaging was done overnight at intervals of 20 or 30 minutes. Each acquired image comprises 2-4 regions that are stitched together using software. After imaging, the fish were euthanized by placing in an MS-222 solution of 40μL/mL of sterile embryo medium.

3.4.7. In vitro aggregation assay

AE and EN bacterial cultures were grown over night with shaking at 30°C, normalized to OD600=5.0, then washed 2X in equal volume buffer (sterile embryo medium). Normalized AE and EN cell suspensions were then back diluted 1:10 into 12-well plates containing buffer supplemented with 0.4% GlcNAc and incubated for approximately 6 hours with gentle rotation (115 RPM) at 30°C to allow co-aggregate formation.

3.4.8. Simulation

The model of bacterial cluster dynamics applied to EN is based on earlier work investigating bacterial cluster size distributions in the zebrafish gut [92]. We combine four kinetic processes – growth, aggregation, fragmentation, and expulsion – in a stochastic model simulated with a Gillespie algorithm. Growth is deterministic and occurs at every time step while aggregation, fragmentation

and expulsion are stochastic. Each process is described by a kernel with specific rate parameters described below.

Growth: We model growth of each cluster as deterministic and following a simple logistic growth curve, with the total abundance of all clusters barred from exceeding an overall carrying capacity. The carrying capacity was fixed at 10^4 cells, approximately the mono-association abundance of EN. We use experimentally measured values of the growth rate for both forms of EN, with $r_{pl} = 0.24$ hr^{-1} for planktonic cells (i.e. clusters of size $n = 1$) and $r_{agg} = 0.66$ hr^{-1} for clusters ($n \geq 2$). Growth occurs at every time step with dt being drawn from an exponential distribution with rate governed by the total overall reaction rate.

Aggregation: Aggregation involves a reaction of two clusters of sizes n and m combining to form a cluster of size $n + m$. Aggregation is taken to be size dependent with the rate of clusters n, m coming together given by:

$$K_{agg} = \alpha(n * m)^{1/3} \tag{3.4}$$

where 1/3 indicates that the collision of clusters is dependent on the cluster diameter and $\alpha = 10^{-2.5}$ hr^{-1}. The clusters are randomly grouped in pairs at every time step and the rate of each aggregation reaction is computed.

Fragmentation: Fragmentation or breakup of a single cell from a cluster of size n occurs at a size dependent rate-

$$K_{frag} = \beta(n)^{2/3} \tag{3.5}$$

where 2/3 represents the surface area dependence, i.e. cells only on the surface of clusters can fragment. A value of 0.1 hr^{-1} corresponds to 10 cells fragmenting every hour from a cluster of size 1000.

Expulsion: The expulsion process involves removal of clusters from the intestine. Prior experimental work established that expulsion occurs on average every 10-12 hours, so the expulsion rate set to $\lambda_{agg} = 0.1\ \text{hr}^{-1}$ [51]. The expulsion rate of non-motile individuals occurs at a rate λ_{pl}. The expulsion ratio ($\frac{\lambda_{pl}}{\lambda_{agg}}$) is varied logarithmically with $\frac{\lambda_{pl}}{\lambda_{agg}} \in [0.25, 100]$.

Mono-association simulation: We first generate the initial mono-association cluster configuration for EN. Here, we keep β fixed at $\beta = 0.01\ \text{hr}^{-1}$, since in mono-association we see rare fragmentation of EN and $\log_{10}(\alpha) = -2.5$. The expulsion rates are $\lambda_{pl} = \lambda_{agg} = 0.1\ \text{hr}^{-1}$. Growth of individuals and clusters occurs at rates $r_{pl} = 0.24\ \text{hr}^{-1}$ and $r_{agg} = 0.66\ \text{hr}^{-1}$.

At a given time step, the rates of aggregation, fragmentation and expulsion for all possible cluster reactions are computed. The total reaction rate i.e. the sum of all rates determines the jump interval (dt) when the next reaction occurs. At a given time step, only one cluster reaction is randomly chosen, weighted by the rate. The chosen reaction is executed, following which ($\lambda_{pl} dt$) individual cells are expelled. (Expulsion of individuals is treated deterministically, for computational speed; note that there are large numbers of individuals, so stochasticity is unlikely to be important.) Before proceeding to the next time step, all clusters undergo growth as described previously.

The simulation is carried out until $T = 24$ hrs, the time at which the EN population is invaded by the mutant AE-MB4 species. The configurations with

large ($n > 1000$) clusters are saved as the initial configuration for the invasion simulation.

Invasion simulation: We simulate for different parameters of $\beta \in [0.02, 1]$ hr^{-1} in steps of df=0.02 hr^{-1} and $\frac{\lambda_{pl}}{\lambda_{agg}} \in [0.25, 100]$. Within a simulation run, we choose $\frac{\lambda_{pl}}{\lambda_{agg}}$ and start with the mono-association cluster size distribution. We evolve this distribution until T = 24 hrs (usually when the invasion abundance data is collected). All the processes i.e. growth, fragmentation, expulsion and aggregation are simulated exactly as in generating the initial cluster configuration. The total abundance along with final cluster sizes after 24 hrs are saved. The mean abundance from 500 fish for the full range of parameters of fragmentation rate and expulsion ratio are plotted in Fig 3.3D.

3.4.9. Image analysis

Identification of single cells and clusters in 3D images

Identification of single bacterial cells was done using a combination of machine learning and semi-automated approaches. A convolutional neural network previously trained on 3D images of single bacteria is used to classify potential objects as bacteria or noise blobs [109]. The same network architecture was used and the algorithm was trained on labeled datasets of AE-MB4 and EN cells. Identification of potential bacteria objects in voxels of size (30x30x10) pixels was done by using a local maxima finding algorithm in 2D and stitched in 3D. These potential objects were classified by the network and the classified output was curated manually.

For aggregate segmentation, the zebrafish gut was first segmented in 2D using the U-net algorithm which was previously trained on a hand-labeled dataset

of zebrafish gut images [110]. After segmentation of the gut, bacterial clusters within the gut were segmented by applying a background threshold for each image of the z-stack for segmentation of bacterial aggregates. The total number of cells in an aggregate is determined by dividing the total fluorescence intensity from the segmented object by the median intensity of individuals in the image.

Once the net population in single cells and aggregates was ascertained, these were used to calculate the planktonic fraction, a ratio of the number of individuals to total abundance. To measure the cumulative cluster size distributions, p(n) and cluster size histograms depicting probabilities of finding a cell in an n-celled cluster, we performed a jackknife resampling on the dataset for each experiment to ascertain the mean and uncertainty in our measurements. The distributions shown in Fig 3.1 F reflect pooled distributions with all clusters from all fish in an experiment.

Normalized intensity profiles

After segmentation of the gut using U-net, we defined markers for the foremost point in the anterior in a 3D image. After applying a single background threshold for each 3D image, we computed the total intensity in this thresholded region along the intestinal axis. The normalized intensity profile over several fish is averaged and shown in Fig 3.1D, 3.5D and 3.6B.

Growth rate measurement

To measure growth rates, we select consecutive 3D scans from fish, wherein aggregated or planktonic populations of bacteria are undisturbed and there is no influx or efflux of bacteria from fragmentation or expulsion respectively.

We identify single cells and clumps using the image analysis pipeline described previously. An exponential fit to the abundance of single cells or clusters over time was used to determine the growth rate of cells and clusters respectively. The mean and the standard deviation from several fish are reported in Results. .

CHAPTER IV

IMMUNE RESPONSE FOR DIFFERENT BACTERIAL SPECIES

4.1. Background

Plenty of evidence exists that the microbial residents within our intestines interact with the immune system [176–178]. These interactions are crucial for maintaining intestinal homeostasis. The immune system walks a fine line between tolerating commensal microbiota and sensing and eliminating pathogens [178]. Which biophysical and biochemical features of bacteria may be interpreted by the immune system in its decision-making, need further investigation.

There are different types of immune cells that cooperate to defend us from pathogens. The innate immune system is the body's fast, nonspecific defense mechanism comprising an army of different cell types, namely macrophages, monocytes, dendritic cells, neutrophils, eosinophils. We also have a more specific and sophisticated immune response triggered by components of the adaptive immune system, T cells and B cells. We focus here on innate immune responses, in particular the cytokine TNFα. The adaptive immune response of zebrafish is not activated until approximately 3 weeks into their development, beyond the age examined in our studies [179].

Immune cells communicate using compounds called cytokines that may be pro-inflammatory or anti-inflammatory in nature. Innate immune cells such as macrophages secrete tumor necrosis factor alpha (TNFα), a proinflammatory cytokine. This signaling mechanism has been found to play a role in maintaining

intestinal homeostasis by stimulating cell-proliferation as well as triggering cell-death or apoptosis [180].

In previous work specific to zebrafish, immune responses to several different commensal species have been characterized [90, 101]. In both studies, the highly motile *Vibrio* ZWU0020 strain is observed to cause increased inflammation, showing an influx of neutrophil cells and an almost two orders of magnitude increased activity of TNFα when compared to germ-free hosts [90, 101]. Interestingly in [90], a bacterial mutant deficient in motility induced a TNFα response that was comparable to germ-free levels.

These studies of inflammation and bacterial species reveal that the spatial organization of bacteria impacts their interactions with the immune system. In this chapter, I focus on characterizing the inflammation response in the form of TNFα expression and immune-bacteria co-localization in the form of macrophage localization for a few different commensal bacterial strains. In particular, I focus on two different bacterial species *Aeromonas* (AE) and a strain derived from AE that is resistant to GlcNAc mediated aggregation in the gut, *Aeromonas-MB4* (AE-MB4), also used in the studies described in Chapter III. Simultaneous studies of bacteria and host inflammation in live animals are challenging to perform in different animal models. The zebrafish model system is well-suited for this aspect and allows for recording time-varying immune responses with bacterial dynamics.

A specific transgenic line of zebrafish with a fluorescent reporter for TNFα expression was used in these studies (Tg(*tnfa:gfp*)) [181]. A different transgenic line with a fluorescent reporter for macrophages Tg(*mpeg1:mCherry*) was used to track macrophages [182]. A cross between these two transgenic lines Tg(*tnfa:gfp*)

x Tg(*mpeg1:mCherry*) was often used to conduct experiments for concurrently tracking TNFα expression and macrophage dynamics.

4.2. TNFα response of bacterial strains.

The transgenic fish were derived germ-free as described in Ch. II and III. Culturing of bacteria and inoculations were also done as described in Ch. II and II. The strains that were used to assess the TNFα response were *Aeromonas 01*(ZOR0001) (AE), *Aeromonas-MB4* (AE-MB4), and *Enterobacter* (ZOR0004) (EN). Di-associations were also performed with AE and EN, AE-MB4 and EN. TNFα reporter activity was assessed at 7dpf using light sheet fluorescence microscopy as described in Ch. I and III. For mono-association experiments all dTomato strains were used and excited with a 568nm laser, while for the di-association experiments GFP EN was inoculated along with dTomato AE and AE-MB4. Exemplar images of the spatial distribution and TNFα expression for different strains are shown in Fig. 4.1.

To measure the number of TNFα activated cells, I segmented cells from the images by selecting a user-specified background value for each 3D image. Note that this approach did lose some dim TNFα cells that are likely in a transitory state and a more fine-tuned approach would be necessary if those cells needed to be quantified as well. The numbers of segmented cells for each experiment are plotted in Fig. 4.1. For fish colonized with AE-MB4, either in mono-association or di-association with EN, the number of TNFα positive cells is seen to be 3 times as high as the germ-free condition. In fish colonized with AE and EN strains that form large aggregates in the mid-gut as described in Ch. III, TNFα activity is

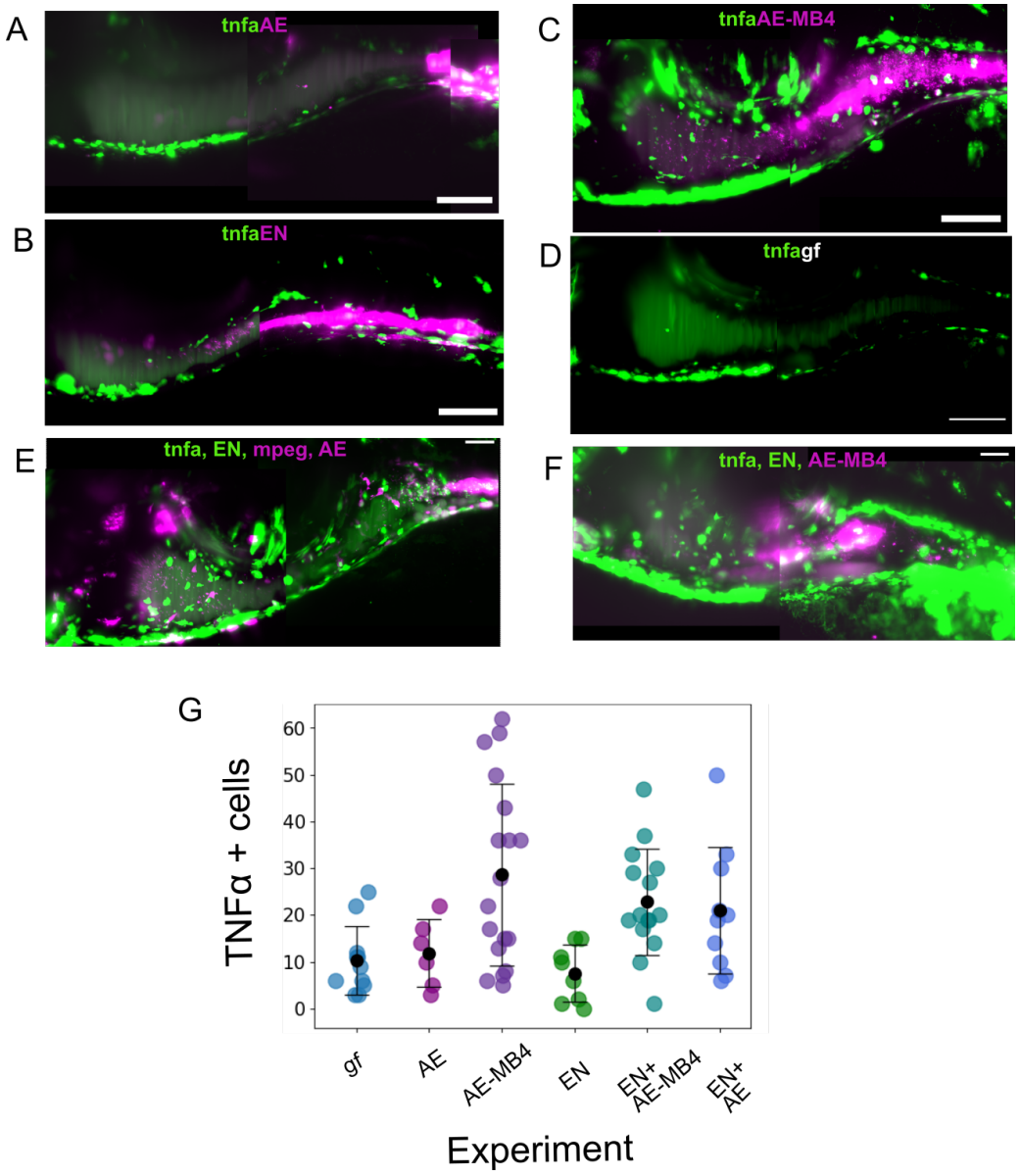

FIGURE 4.1. Exemplar maximum intensity projections of TNFα reporter activity (green) and bacterial spatial distribution (magenta) for (A) AE colonized (B) EN colonized (C) AE-MB4 colonized (D) germ-free tnfa:gfp transgenic fish. (E) and (F) are maximum intensity projections from fish co-inoculated with AE(magenta) EN (green) and AE-MB4(magenta) and EN (green). The TNFα reporter activity and macrophages (only E) are shown in green and magenta respectively. Scale bar: 50μ m (E) The total number of TNFα+ cells in germ-free fish, fish mono-associated with AE, AE-MB4, EN, co-colonized by EN and AE-MB4, EN and AE. N (from left to right) =[10, 6, 17,7,12, 10] fish.

comparable to germ-free fish, suggesting these strains do not produce a strong pro-inflammatory response.

Interestingly, we also found that the TNFα response in the AE-EN diassociation was also around 2-3 times higher compared to fish mono-colonized with AE or EN alone.

Although there seems to be a high degree of variability in TNFα response for fish colonized with AE-MB4, there are clear patterns of greater inflammation compared to the response in fish with AE and EN.The differences in spatial organization of AE and AE-MB4 characterized in Ch II could play a role in AE-MB4 inflammation as reported with *Vibrio* species described in [90]. AE-MB4 is deficient in its mucus sensing pathway that results in its altered aggregation behavior in the gut, which may directly or indirectly be responsible for increased inflammation. More studies investigating AE-MB4 will illuminate the specific conditions wherein this bacterial strain can trigger increased inflammation.

4.3. Macrophage bacteria interactions

Using the double transgenic- Tg(*tnfa:gfp*) x Tg(*mpeg1:mCherry*), I also observed specific macrophage localization patterns in fish mono-associated with AE-MB4 or in di-association with AE-MB4 and EN. We observed several examples of 'macrophage swarms' in the intestinal bulb shown in Fig. 4.2. These swarms are oftentimes localized adjacent to regions where AE-MB4 cells are localized. In rare instances, these swarms show TNFα activity [Fig. 4.2]. Many questions regarding what feature of AE-MB4 triggers such swarm formation and what function these swarms serve, remain to be answered. Recent work by others has explored swarms of innate immune cells, for example neutrophil swarms suppressing fungal

growth [Hopke et al. 2020]. Studies in zebrafish have reported the formation of granulomas or well-organized macrophage aggregates upon infection with Schistosoma eggs [183, 184]. Both the TNFα and macrophage observations open up many more possibilities for deeper exploration.

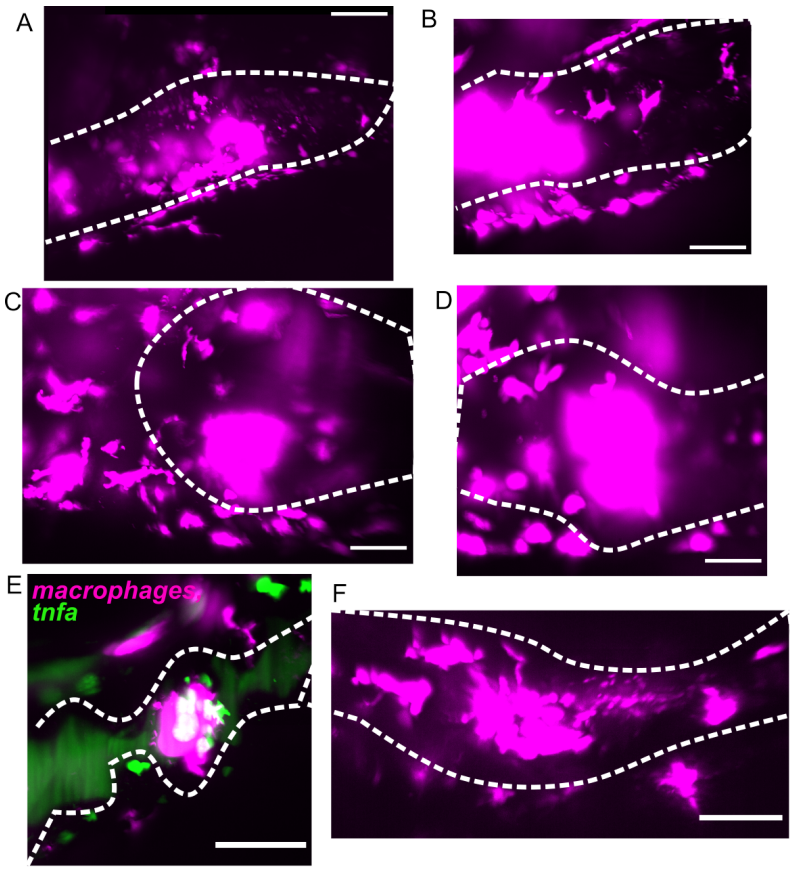

FIGURE 4.2. Examples of macrophage swarms (large clumps in magenta) from maximum intensity projections of the gut of different fish that were initially inoculated with EN and then challenged with AE-MB4 after 24 hrs. The gut outline is shown in dashed white. A, E and F are from the the midgut regions, while B, C and D are from the foregut region of the imaged fish. The region in F shows TNFα+ cells within the macrophage swarm. Scale bar: 50µm

4.4. Conclusion

Visualizing and quantifying immune system dynamics concurrently with bacteria can yield many useful insights into host-microbe interactions. I show that the planktonic species AE-MB4 stimulates increased inflammation compared to its aggregated parental strain AE by measuring TNFα activity, suggesting that the single trait of deficient mucus sensing and all its downstream effects can be sufficient to alter host immune response in the vertebrate intestine. Other recent work submitted for review also corroborates the increased inflammation seen with the AE-MB4 strain [163]. Earlier investigations of inflammation with motile *Vibrio* species showing similar planktonic behavior and localization in the anterior region of the intestine may suggest that generic features of spatial structure and localization of species are determinants of host immune response [90, 101].

Patterns in macrophage spatial dynamics show clustering of macrophages upon colonization by AE-MB4. In some instances, these clusters are TNFα+ as well. It would be useful to visualize the dynamics of swarm formation and dissociation in conjunction with bacterial dynamics. Some recent studies characterize neutrophil migration behaviors in zebrafish, noting pioneer neutrophils in swarms [185]. Further, what timescales dictate the formation of these swarms are indicative of the response times of such dendritic cells and other aspects such as the diffusion of cytokines.

The TNFα response with AE-MB4 translates into di-association experiments with EN, retaining its proinflammatory capacity with this species. It would be interesting to study how previously discovered anti-inflammatory zebrafish isolates such as *Shewenella* [101] interact with AE-MB4 and whether they can suppress

TNFα response. Such studies could help gain insight into whether adding select microbial members can restore TNFα activity to normal levels.

It's unclear why the combination of AE and EN also produced increased inflammation, something not observed in AE and EN mono-colonized fish. What aspects of competition and whether spatial structure changes or altered signaling cues may be contributing to such responses requires a characterization of this competition and spatial structure. These immune cell investigations pave the way for more such studies visualizing and characterizing host immune response in living organisms.

CHAPTER V

CONCLUSIONS AND FUTURE WORK

Combining 3D live imaging, zebrafish transgenics, and the genetic tools developed for commensal bacterial strains has enabled addressing questions regarding interaction dynamics, physical structure, and immune activation that would be impossible to study in humans and other model organisms. There are many directions for future studies that build on insights from this work.

Through mapping interactions between a consortium of five native gut-bacterial isolates, I found the existence of higher order interactions that weaken strong competitive interactions and promote coexistence in the zebrafish gut. A question that arises from this work is how these results translate to communities of a greater number of species or different sets of species. These questions would require more thoughtful experimentation, however the fact that these 4-5 species communities are sufficient to see differences in interaction patterns is telling of the merits of performing such controlled, tractable studies.

The similarity in abundance distributions of both four and five species experiments as well as across different species in these experiments is striking and indicative of species-specific features becoming less apparent in diverse communities. In addition to this, weak competition in five-species communities suggests a shift towards a more neutral community, or a community whose composition is primarily determined by stochastic ecological processes. Studies to specifically uncover the role of these stochastic processes, such as host colonization and transmission between hosts will illuminate to what extent these processes govern composition in complex communities.

One may also ask, whether the addition of a strong competitor can break patterns of coexistence in this model community. Using the interactions mapped in Chapter II, we discovered specific pairs such as *Aeromonas-Enterobacter* showing strong competition. This pair, in combination with an *Aeromonas* isolate (AE-MB4) evolved by colleagues Jarrod Smith and Karen Guillemin that lacks the trait of aggregating in a sugar found in intestinal mucus, was used to test how altered aggregation impacts community structure. Through this study, we found a novel interaction mechanism, namely, induced dissociation of *Enterobacter* aggregates that are prone to intestinal expulsion. The study underscores the ability of a single species to disrupt community structure and for communities to restore themselves in the presence of diverse members. More exploration of how these diverse communities mitigate the dramatic impact AE-MB4 has on two-species communities would be telling of the possible mechanisms of interactions underlying the human gut microbiome. My colleague Jarrod Smith has engineered a genetic switch that converts the bacterial behavior of wild-type *Aeromonas* from aggregated to planktonic. Using powerful genetic tools such as these, one can perturb microbial communities in live fish and visualize community dynamics, an impossible pursuit in humans or other model systems.

Imaging the spatial structure of multi-species communities has shed insights into different mechanisms of co-aggregation of bacterial species in vivo vs in vitro. Along with Jarrod, I observed differences in the structure of bacterial aggregates of AE and EN in vivo and in vitro. For instance, in vivo, these aggregates were often conglomerates of smaller single-species clumps rather than homogeneously distributed cells of both species, suggesting intestinal flow dynamics, especially mixing of isolated clumps is an important factor in co-aggregate formation.

In contrast, imaging in vitro aggregates show that the cells of these individual species are distributed more or less uniformly across the aggregate. More thorough comparative studies of cluster dynamics in vitro and in vivo can illuminate the role of the host in facilitating bacterial aggregation.

Along with the characterization of cluster structure, an understanding of the constituents of these bacterial clusters would reveal the role of possible host-derived structural components such as mucus in aggregation processes. During some recent in vivo imaging studies of live fish stained with WGA (wheat germ agglutinin), a protein that binds to particular sugars, some of which are found in mucus, Jarrod and I found that bacterial aggregates are often times correlated with regions found to be rich in mucus sugars. Such staining experiments can provide details into the composition of these aggregates and perhaps what host cues drive aggregation.

Finally, designing studies to map host immune responses of various members and their aggregation properties illuminate what physical and biochemical factors of microbes are being interpreted by the immune system. Through studies comparing inflammation in fish colonized by AE and AE-MB4, clear differences in TNFα response are observed, similar to the observations in [90]. Such experiments outline the possibility of general spatial structure determinants of immune response. More studies focussing on different species, their inflammation dynamics and macrophage activity would help decipher species-specific and generic characteristics of host-microbe interactions.

Pro-inflammatory bacterial strains such AE-MB4 can be used to address many other questions in microbiome research. Previous studies to study the effects of antibiotic exposure on the microbiota discovered that motile bacteria undergo a

stress response and clump in response to antibiotics [53]. Antibiotics have emerged as a powerful tool to perturb intestinal communities. How antibiotics differentially impact species and can alter species interactions and intestinal community composition remains to be known. Further, studies have shown that after a treatment of tetracycline, zebrafish show suppressed production of cytokines [186]. Investigations of how the immune system responds to pro-inflammatory species such as *Vibrio* and AE-MB4 after antibiotic exposure is unknown, a path that could yield lots of novel information about antibiotic exposure and the immune system.

The combination of using zebrafish as a model system, the exciting avenue of gut microbiome research, novel bacterial engineering approaches, imaging and quantitative modeling leads to an unending set of possibilities for future studies. Specifically in the area of biophysics, the intersection of all of these approaches has the potential to reveal general rules underlying these complex biological systems that can be of great significance to human health. With increasing interest in gut microbiome research, the need for more quantitative approaches and models by physicists to characterize and simplify the complexity in these systems is certain and will only spur more discoveries about the mysteries of intestinal communities.

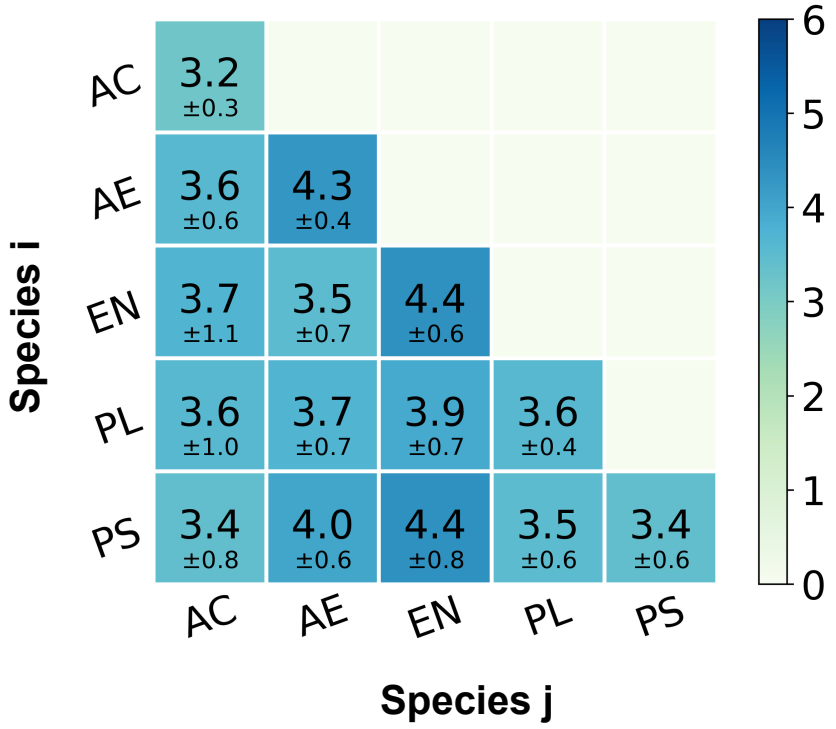

FIGURE A.1. The total bacterial load for different di-association experiments.The total bacterial load for different di-association experiments, expressed as the mean and standard deviation of $\log_{10}$ (total CFUs). The values on the diagonal are the mean load from mono-association experiments.

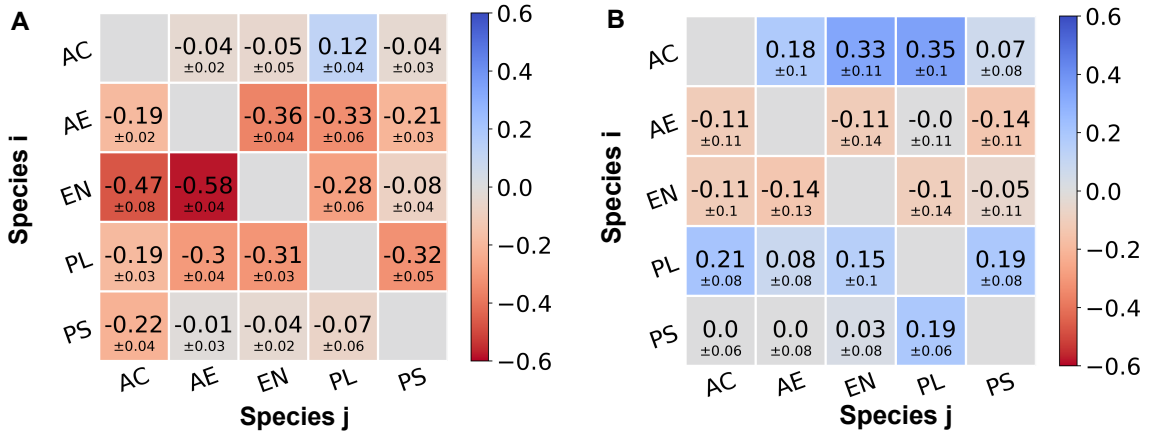

FIGURE A.2. Pairwise interaction coefficients for two-species and five-species experiments using the log-transformed model. The mean pairwise interaction coefficients C_{ij}^{II} (A) and C_{ij}^{V}(B) showing the effect of species j on species i calculated using the log-transformed abundance model. The standard deviations are calculated using a subsampling approach described in Methods.

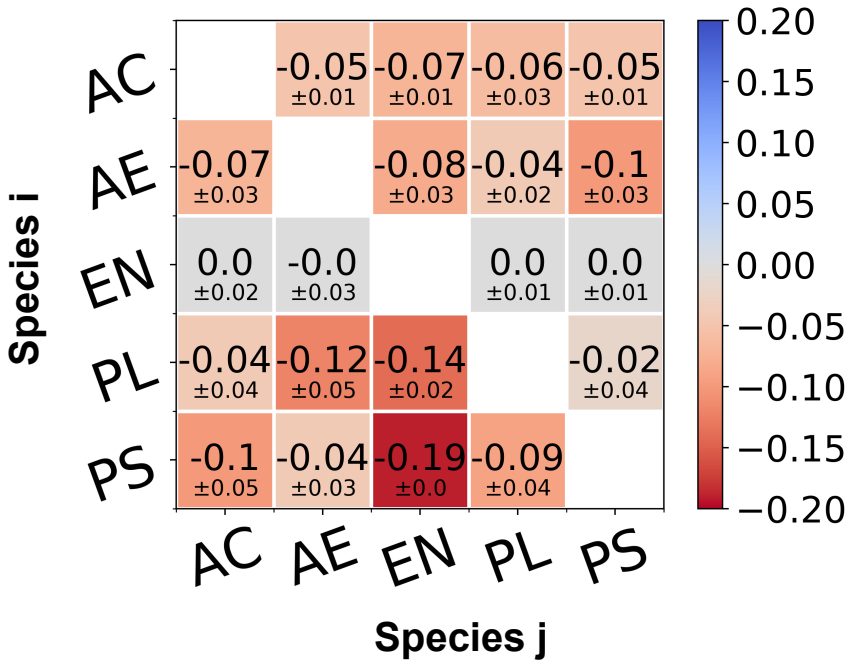

FIGURE A.3. Pairwise interaction coefficients from in vitro two-species experiments calculated using the log-transformed abundance model. The matrix of interaction coefficients showing the mean and standard deviation of C_{ij}^{II} from in vitro competition experiments.

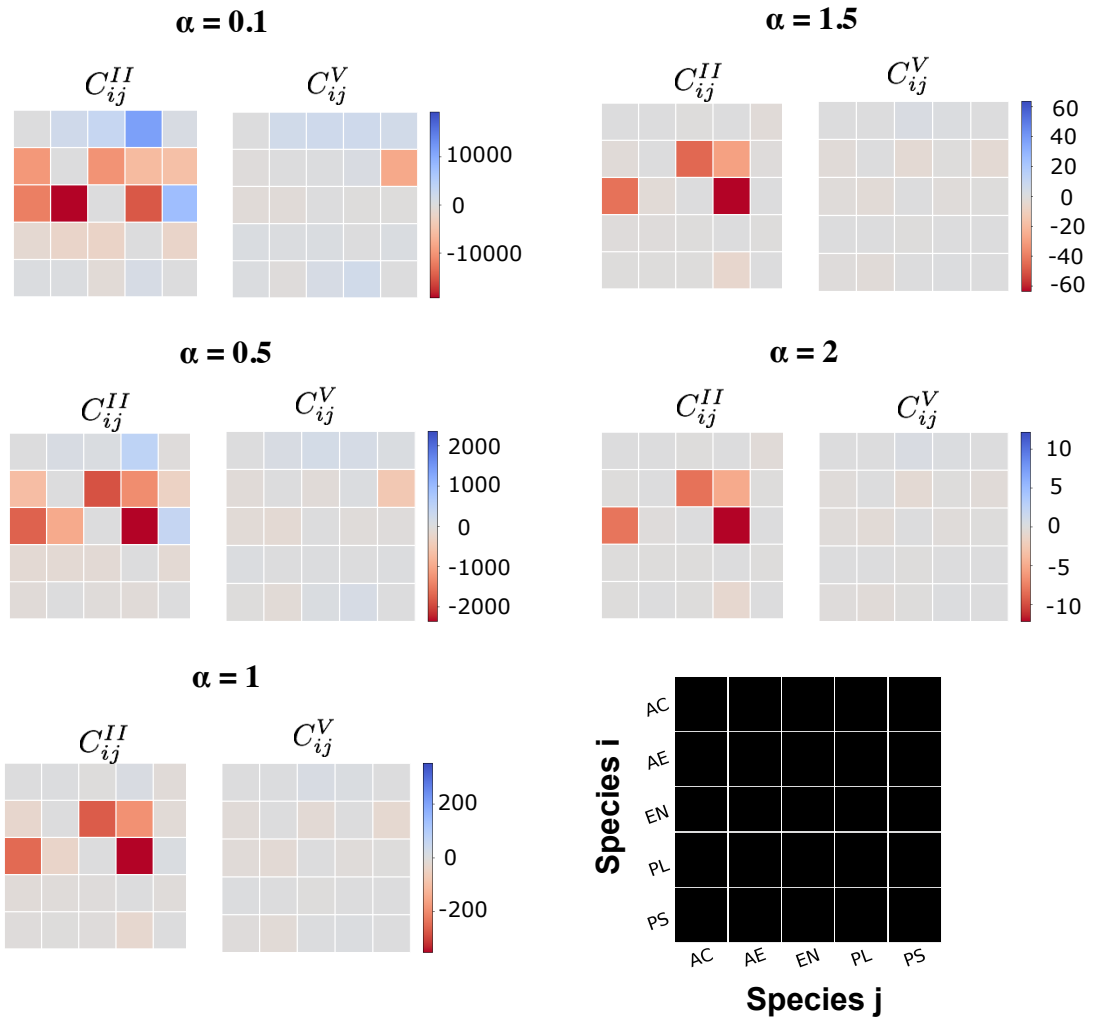

FIGURE A.4. Pairwise interaction coefficients for select α values for two and five-species experiments using the power law model. Interaction coefficients generated from the linear absolute abundance model for are compared for the one-to-two species (left) and four-to-five species (right) experiments. The legend at the bottom-right shows the species labels for the rows and columns.

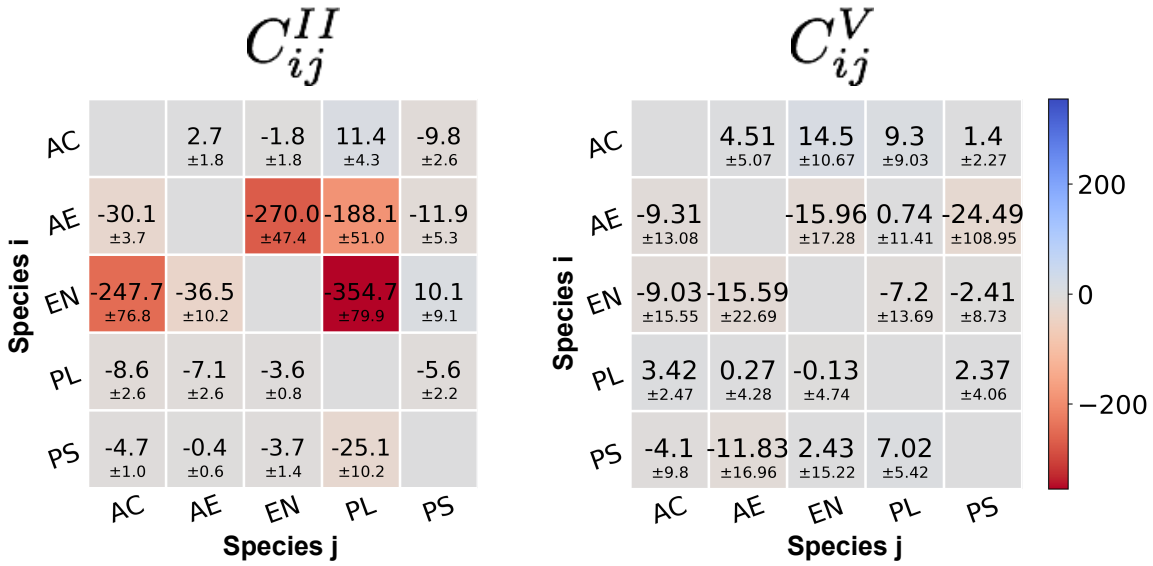

FIGURE A.5. Pairwise interaction coefficients for two and five-species experiments using a linear model. The mean and standard deviation of the interaction coefficients for the two species C_{ij}^{II} and five species C_{ij}^{V} experiments calculated using a model linear in absolute species abundance.

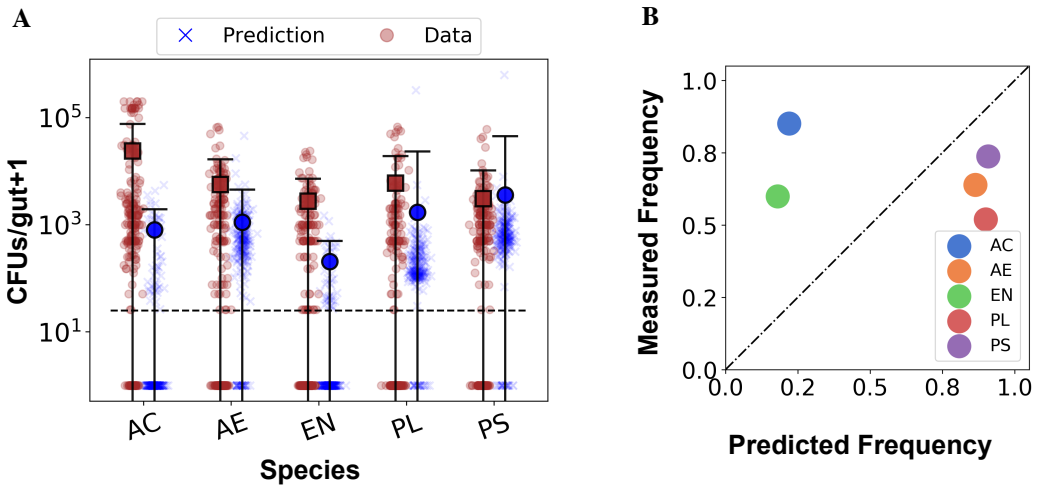

FIGURE A.6. Predicted five species distributions from the linear model. A. Predicted (blue xs) and measured (brown circles) absolute abundance distributions for five-species inoculation experiments calculated from the linear model for pairwise interactions, for each of the five species. The means of the predicted and measured distributions excluding nulls are shown using bold blue circles and brown square markers, respectively, with error bars indicating the standard deviation. The dotted line indicates the experimental detection limit of 25 cells. The predicted distributions are generated from sampling the interaction coefficient distributions as described in Methods, while the experimental distributions comprise abundances from N = 202 fish. B. The observed occurrence frequencies of each species in five-species experiments plotted against the predicted frequencies generated from the linear model.

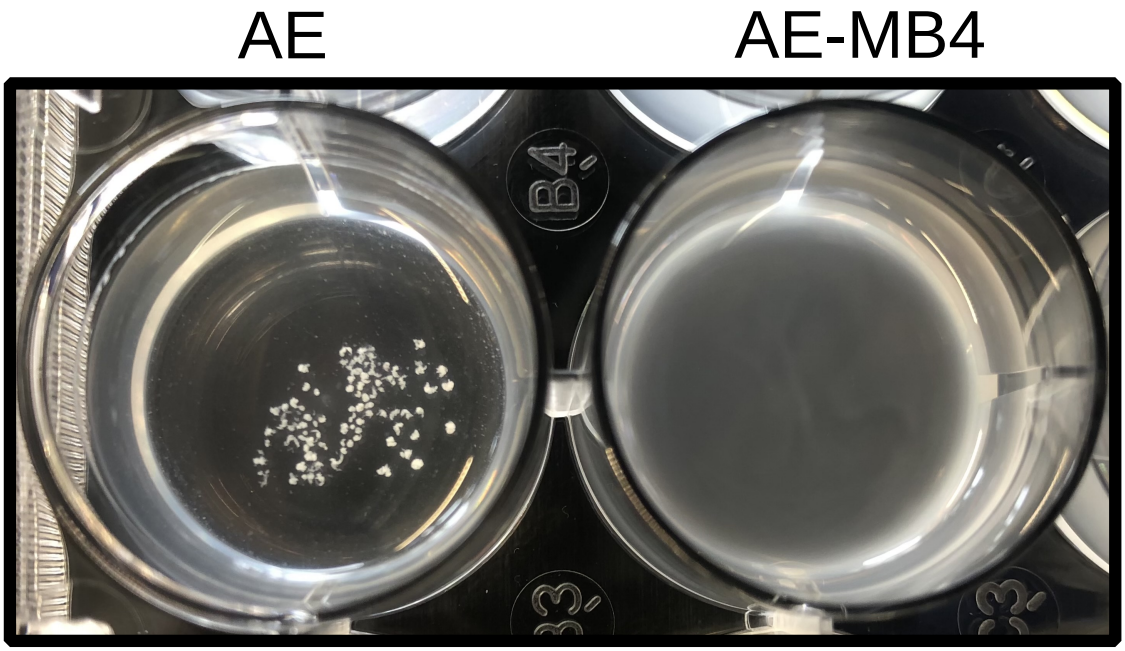

FIGURE A.7. In vitro biofilm assay for AE (top panel) and AE-MB4 (bottom panel) in 0.4% GlcNAc solution. AE forms macroscopic aggregates in 0.4% GlcNAc (top-right) while AE-MB4 (bottom-right) is unable to form biofilms in the same medium.

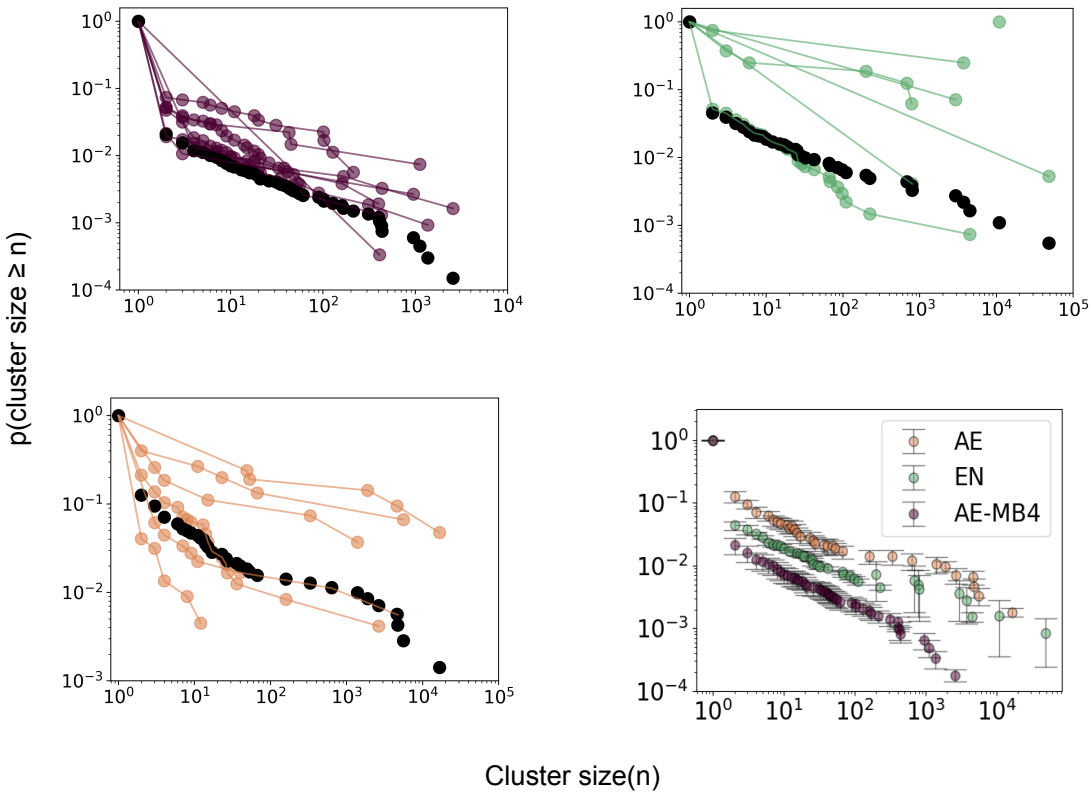

FIGURE A.8. The cumulative cluster size distributions (p(cluster size $\geq$ n)) for (i) AE-MB4 (ii) EN (iii) AE and (iv) all three species in mono-association. The magenta, green and orange curves in (i), (ii) and (iii) are distributions calculated from clusters found in single fish in each mono-association experiment. The black curve in (i)-(iii) shows the pooled distribution calculated from clusters found in all fish. (iv) shows the pooled distribution for each of the species with all three showing power law behavior with slope m = 0.8 $\pm$ 0.1 for AE-MB4 and AE and m = 0.9 $\pm$ 0.2 for EN in the regime $n < 10^2$. Data are from N = 6, 7 and 8 fish for AE, EN and AE-MB4, respectively.

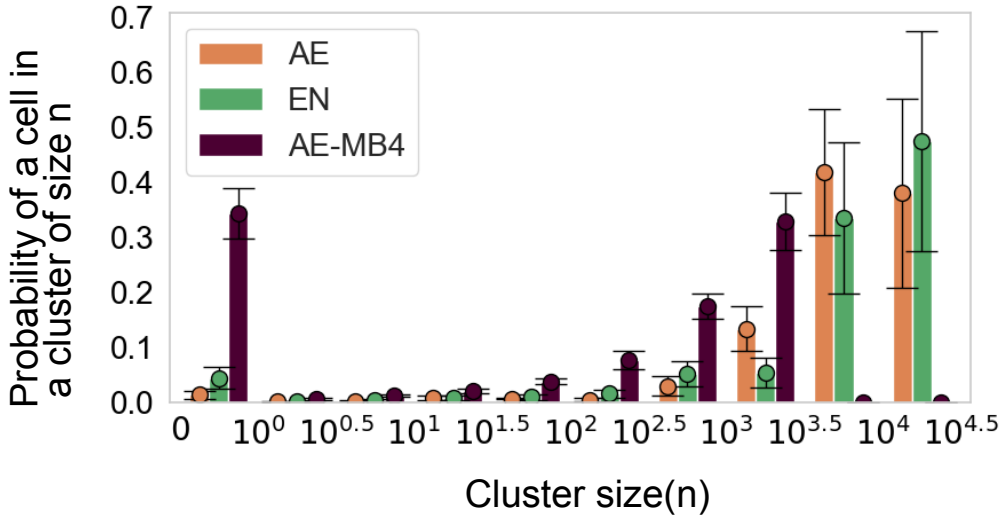

FIGURE A.9. The probability of finding a cell in an n-cell cluster for AE (orange), EN (green) and AE-MB4 (magenta) in mono-association. Circles and error bars indicate the mean and uncertainties, calculated using jack-knife resampling. Tick marks indicate bin intervals, e.g. the three bars between 0 and 10^0 correspond to EN, AE and AE-MB4 probabilities to be in clusters of size n = (0-1]. Data are from N = 6, 7 and 8 fish for AE, EN and AE-MB4, respectively.

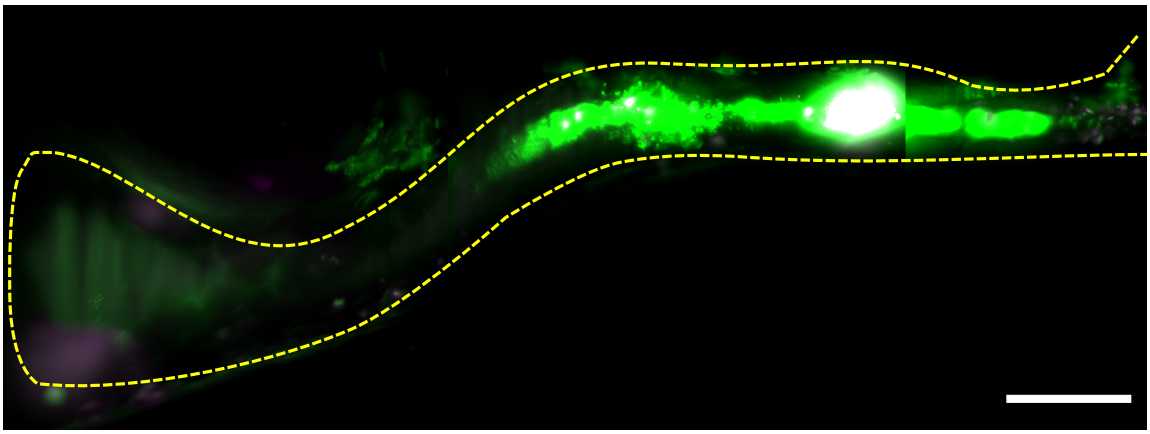

FIGURE A.10. Maximum intensity projection of 3D image of a larval zebrafish gut colonized with EN (green) at 5dpf and challenged with AE (orange) at 6dpf. Overlapping populations are in yellow. Bar:100μm

REFERENCES CITED

[1] R. W. J. Cavicchioli, Ricardo et al. Scientists' warning to humanity: microorganisms and climate change. *Nature Reviews Microbiology*, 17(9), September 2019.

[2] J. U. Scher and S. B. Abramson. The microbiome and rheumatoid arthritis. *Nature Reviews Rheumatology*, 7(10), October 2011.

[3] A. B. Shreiner et al. The gut microbiome in health and in disease. *Current opinion in gastroenterology*, 31(1):69–75, January 2015.

[4] K. J. Pflughoeft and J. Versalovic. Human Microbiome in Health and Disease. *Annual Review of Pathology: Mechanisms of Disease*, 7(1):99–122, 2012.

[5] R. D. Moloney et al. The microbiome: stress, health and disease. *Mammalian Genome: Official Journal of the International Mammalian Genome Society*, 25(1-2):49–74, February 2014.

[6] W. Zhu et al. Precision editing of the gut microbiota ameliorates colitis. *Nature*, 553(7687):208–211, January 2018.

[7] B. Wang et al. The Human Microbiota in Health and Disease. *Engineering*, 3(1):71–82, February 2017.

[8] J. Durack and S. V. Lynch. The gut microbiome: Relationships with disease and opportunities for therapy. *Journal of Experimental Medicine*, 216(1), January 2019.

[9] M. Rajilić, Stojanović et al. Global and Deep Molecular Analysis of Microbiota Signatures in Fecal Samples From Patients With Irritable Bowel Syndrome. *Gastroenterology*, 141(5):1792–1801, November 2011.

[10] K. Honda and D. R. Littman. The microbiome in infectious disease and inflammation. *Annual Review of Immunology*, 30:759–795, 2012.

[11] C. L. Boulangé et al. Impact of the gut microbiota on inflammation, obesity, and metabolic disease. *Genome Medicine*, 8:42, April 2016.

[12] J. H. Hill et al. A conserved bacterial protein induces pancreatic beta cell expansion during zebrafish development. *eLife*, 5, December 2016.

[13] I. Semova et al. Microbiota regulate intestinal absorption and metabolism of fatty acids in the zebrafish. *Cell Host & Microbe*, 12(3):277–288, September 2012.

[14] K. Martinez-Guryn et al. Small Intestine Microbiota Regulate Host Digestive and Absorptive Adaptive Responses to Dietary Lipids. *Cell Host & Microbe*, 23(4):458–469.e5, 2018.

[15] H. Sokol et al. Faecalibacterium prausnitzii is an anti-inflammatory commensal bacterium identified by gut microbiota analysis of Crohn disease patients. *Proceedings of the National Academy of Sciences of the United States of America*, 105(43):16731–16736, October 2008.

[16] N. Arpaia et al. Metabolites produced by commensal bacteria promote peripheral regulatory T-cell generation. *Nature*, 504(7480):451–455, December 2013.

[17] N. Kamada and G. Nunez. Regulation of the Immune System by the Resident Intestinal Bacteria. *Gastroenterology*, 146(6):1477–1488, May 2014.

[18] S. K. Mazmanian et al. An Immunomodulatory Molecule of Symbiotic Bacteria Directs Maturation of the Host Immune System. *Cell*, 122(1):107–118, July 2005.

[19] L. Ye et al. High fat diet induces microbiota-dependent silencing of enteroendocrine cells. *eLife*, 8, December 2019.

[20] J. Yan et al. Gut microbiota induce IGF-1 and promote bone formation and growth. *Proceedings of the National Academy of Sciences*, 113(47):E7554–E7563, November 2016.

[21] C. L. Maynard et al. Reciprocal Interactions of the Intestinal Microbiota and Immune System. *Nature*, 489(7415):231–241, September 2012.

[22] A. Everard et al. Cross-talk between Akkermansia muciniphila and intestinal epithelium controls diet-induced obesity. *Proceedings of the National Academy of Sciences of the United States of America*, 110(22):9066–9071, May 2013.

[23] T. C. Scharschmidt et al. A wave of regulatory T cells into neonatal skin mediates tolerance to commensal microbes. *Immunity*, 43(5):1011–1021, November 2015.

[24] D. Perlman et al. Concepts and Consequences of a Core Gut Microbiota for Animal Growth and Development. *Annual Review of Animal Biosciences*, 10(1), 2022.

[25] D. Haller, editor. *The Gut Microbiome in Health and Disease*. Springer International Publishing, Cham, 2018.

[26] K. D. Kohl and H. V. Carey. A place for hostâmicrobe symbiosis in the comparative physiologist's toolbox. *Journal of Experimental Biology*, 219(22), November 2016.

[27] C. P. Tamboli et al. Dysbiosis in inflammatory bowel disease. *Gut*, 53(1):1–4, January 2004.

[28] D. I. Tedjo et al. The fecal microbiota as a biomarker for disease activity in Crohnâs disease. *Scientific Reports*, 6(1):35216, October 2016.

[29] N. A. Nagalingam and S. V. Lynch. Role of the Microbiota in Inflammatory Bowel Diseases. *Inflammatory Bowel Diseases*, 18(5):968–984, May 2012.

[30] M. Saleh and C. O. Elson. Experimental Inflammatory Bowel Disease: Insights into the Host-Microbiota Dialog. *Immunity*, 34(3):293–302, March 2011.

[31] C. Abraham and R. Medzhitov. Interactions Between the Host Innate Immune System and Microbes in Inflammatory Bowel Disease. *Gastroenterology*, 140(6):1729–1737, 2011.

[32] J. Cremer et al. Effect of flow and peristaltic mixing on bacterial growth in a gut-like channel. *Proceedings of the National Academy of Sciences*, 113(41), October 2016.

[33] M. Arnoldini et al. Bacterial growth, flow, and mixing shape human gut microbiota density and composition. *Gut Microbes*, 9(6), May 2018.

[34] F. Vuik et al. Composition of the mucosa-associated microbiota along the entire gastrointestinal tract of human individuals. *United European Gastroenterology Journal*, 7(7):897–907, 2019.

[35] J. Lloyd-Price et al. The healthy human microbiome. *Genome Medicine*, 8:51, April 2016.

[36] A. Almeida et al. A new genomic blueprint of the human gut microbiota. *Nature*, 568(7753):499–504, 2019.

[37] C. Milani et al. The First Microbial Colonizers of the Human Gut: Composition, Activities, and Health Implications of the Infant Gut Microbiota. *Microbiology and molecular biology reviews: MMBR*, 81(4):e00036–17, December 2017.

[38] D. Sprockett et al. Role of priority effects in the early-life assembly of the gut microbiota. *Nature Reviews Gastroenterology & Hepatology*, 15(4), April 2018.

[39] J. L. Sonnenburg and F. BÃ€ckhed. Dietâmicrobiota interactions as moderators of human metabolism. *Nature*, 535(7610), July 2016.

[40] L. A. David et al. Diet rapidly and reproducibly alters the human gut microbiome. *Nature*, 505, January 2014.

[41] C. De Filippo et al. Impact of diet in shaping gut microbiota revealed by a comparative study in children from Europe and rural Africa. *Proceedings of the National Academy of Science*, 107, August 2010.

[42] G. D. Wu et al. Linking Long-Term Dietary Patterns with Gut Microbial Enterotypes. *Science*, 334, October 2011.

[43] K. A. Dill-McFarland et al. Close social relationships correlate with human gut microbiota composition. *Scientific Reports*, 9(1), January 2019.

[44] P. W. O'Toole and I. B. Jeffery. Gut microbiota and aging. *Science (New York, N.Y.)*, 350(6265):1214–1215, December 2015.

[45] S. J. Jackson et al. Does age matter? The impact of rodent age on study outcomes. *Laboratory Animals*, 51(2).

[46] A. Schlegel and D. Y. R. Stainier. Lessons from âLowerâ Organisms: What Worms, Flies, and Zebrafish Can Teach Us about Human Energy Metabolism. *PLOS Genetics*, 3(11).

[47] E. Melancon et al. Best practices for germ-free derivation and gnotobiotic zebrafish husbandry. *Methods in cell biology*, 138:61–100, 2017.

[48] K. Dooley and L. I. Zon. Zebrafish: a model system for the study of human disease. *Current Opinion in Genetics & Development*, 10(3):252–256, June 2000.

[49] J. F. Rawls et al. Gnotobiotic zebrafish reveal evolutionarily conserved responses to the gut microbiota. *Proceedings of the National Academy of Sciences*, 101(13), March 2004.

[50] T. J. Wiles et al. Modernized Tools for Streamlined Genetic Manipulation and Comparative Study of Wild and Diverse Proteobacterial Lineages. *mBio*, 9(5), November 2018.

[51] T. J. Wiles et al. Host Gut Motility Promotes Competitive Exclusion within a Model Intestinal Microbiota. *PLOS Biology*, 14(7):e1002517, July 2016.

[52] S. L. Logan et al. The Vibrio cholerae type VI secretion system can modulate host intestinal mechanics to displace gut bacterial symbionts. *Proceedings of the National Academy of Sciences*, 115(16):E3779, April 2018.

[53] B. H. Schlomann et al. Sublethal antibiotics collapse gut bacterial populations by enhancing aggregation and expulsion. *Proceedings of the National Academy of Sciences*, 116(43):21392, October 2019.

[54] C. Darwin. *The Origin of Species*. P. F. Collier & son, 1909.

[55] P. J. Morin. *Community Ecology*. Wiley-Blackwell, Chichester, West Sussex ; Hoboken, NJ, 2nd edition edition, August 2011.

[56] F. E. Clements. *Plant succession; an analysis of the development of vegetation,*. Carnegie Institution of Washington,, Washington,, 1916.

[57] C. S. C. S. Elton. *The pattern of animal communities*. Methuen ;, London, 1966.

[58] R. T. Paine. Food Webs: Linkage, Interaction Strength and Community Infrastructure. *Journal of Animal Ecology*, 49(3):667–685, 1980.

[59] R. T. Paine. Food Web Complexity and Species Diversity. *The American Naturalist*, 100(910):65–75, 1966.

[60] R. T. Paine. Energy Flow in a Natural Population of the Herbivorous Gastropod Tegula Funerralis1. *Limnology and Oceanography*, 16(1), 1971.

[61] R. T. Paine. Intertidal community structure : Experimental studies on the relationship between a dominant competitor and its principal predator. *Oecologia*, 15(2):93–120, June 1974.

[62] C. K. Fisher and P. Mehta. Identifying Keystone Species in the Human Gut Microbiome from Metagenomic Timeseries using Sparse Linear Regression. *PLoS ONE*, 9(7), July 2014.

[63] G. G. Mittelbach and B. J. McGill. *Community Ecology*. Oxford University Press, May 2019.

[64] J. H. Vandermeer. The Competitive Structure of Communities: An Experimental Approach with Protozoa. *Ecology*, 50(3):362–371, 1969.

[65] J. Friedman et al. Community structure follows simple assembly rules in microbial microcosms. *Nature Ecology & Evolution*, 1(5):1–7, March 2017.

[66] H. Mickalide and S. Kuehn. Higher-Order Interaction between Species Inhibits Bacterial Invasion of a Phototroph-Predator Microbial Community. *Cell Systems*, 9(6):521–533.e10, December 2019.

[67] M. Morin et al. Changes in the genetic requirements for microbial interactions with increasing community complexity. *eLife*, 7:e37072, September 2018.

[68] A. O. Lopez et al. Interspecies bacterial competition determines community assembly in the c. elegans intestine. *bioRxiv*, pp. 535633, January 2019.

[69] A. L. Gould et al. Microbiome interactions shape host fitness. *Proceedings of the National Academy of Sciences*, 115(51):E11951–E11960, December 2018.

[70] E. Bairey et al. High-order species interactions shape ecosystem diversity. *Nature Communications*, 7(1):1–7, August 2016.

[71] J. M. Levine et al. Beyond pairwise mechanisms of species coexistence in complex communities. *Nature*, 546(7656):56–64, June 2017.

[72] J. Grilli et al. Higher-order interactions stabilize dynamics in competitive network models. *Nature*, 548(7666):210–213, August 2017.

[73] A. Posfai et al. Metabolic Trade-Offs Promote Diversity in a Model Ecosystem. *Physical Review Letters*, 118(2):028103, January 2017.

[74] C. A. Lozupone et al. Diversity, stability and resilience of the human gut microbiota. *Nature*, 489(7415), September 2012.

[75] P. Mehta et al. A high-bias, low-variance introduction to machine learning for physicists. *Physics reports*, 810, 2019.

[76] W. R. Harcombe et al. Metabolic Resource Allocation in Individual Microbes Determines Ecosystem Interactions and Spatial Dynamics. *Cell Reports*, 7(4):1104–1115, May 2014.

[77] T. Taillefumier et al. Microbial consortia at steady supply. *eLife*, 6, May 2017.

[78] B. G. Weiner et al. Spatial ecology of territorial populations. *Proceedings of the National Academy of Sciences*, 116(36), September 2019.

[79] H. J. Kim et al. Defined spatial structure stabilizes a synthetic multispecies bacterial community. *Proceedings of the National Academy of Sciences*, 105(47), November 2008.

[80] V. Torsvik et al. High diversity in DNA of soil bacteria. *Applied and Environmental Microbiology*, 56(3):782–787, March 1990.

[81] D. E. Dykhuizen. Santa Rosalia revisited: Why are there so many species of bacteria? *Antonie van Leeuwenhoek*, 73(1):25–33, January 1998.

[82] C. Tropini et al. The Gut Microbiome: Connecting Spatial Organization to Function. *Cell Host & Microbe*, 21(4), April 2017.

[83] J. Nguyen et al. Cause or effect? The spatial organization of pathogens and the gut microbiota in disease. *Microbes and Infection*, 23(6-7), August 2021.

[84] G. P. Donaldson et al. Gut biogeography of the bacterial microbiota. *Nature Reviews. Microbiology*, 14(1):20–32, January 2016.

[85] T. C. Fung et al. Anatomical localization of commensal bacteria in immune cell homeostasis and disease. *Immunological Reviews*, 260(1), 2014.

[86] T. Bjarnsholt. The role of bacterial biofilms in chronic infections. *APMIS*, 121(s136), 2013.

[87] T. Bjarnsholt et al. Pseudomonas aeruginosa tolerance to tobramycin, hydrogen peroxide and polymorphonuclear leukocytes is quorum-sensing dependent. *Microbiology (Reading, England)*, 151(Pt 2), February 2005.

[88] K. M. Ottemann and J. F. Miller. Roles for motility in bacteria host interactions. *Molecular Microbiology*, 24(6), 1997.

[89] M. Jemielita et al. Spatial and temporal features of the growth of a bacterial species colonizing the zebrafish gut. *MBio*, 5(6):e01751–14, 2014.

[90] T. J. Wiles et al. Swimming motility of a gut bacterial symbiont promotes resistance to intestinal expulsion and enhances inflammation. *PLOS Biology*, 18(3), March 2020.

[91] B. H. Schlomann et al. Bacterial Cohesion Predicts Spatial Distribution in the Larval Zebrafish Intestine. *Biophysical Journal*, 115(11):2271–2277, December 2018.

[92] B. H. Schlomann and R. Parthasarathy. Gut bacterial aggregates as living gels. *eLife*, 10:e71105, September 2021.

[93] N. T. Porter and E. C. Martens. The Critical Roles of Polysaccharides in Gut Microbial Ecology and Physiology. *Annual Review of Microbiology*, 71:349–369, September 2017.

[94] A. J. Silva et al. Haemagglutinin/protease expression and mucin gel penetration in El Tor biotype Vibrio cholerae. *Microbiology (Reading, England)*, 149(Pt 7):1883–1891, 2003.

[95] A. Marcobal et al. A refined palate: Bacterial consumption of host glycans in the gut. *Glycobiology*, 23(9), September 2013.

[96] L. Wrzosek et al. Bacteroides thetaiotaomicron and Faecalibacterium prausnitzii influence the production of mucus glycans and the development of goblet cells in the colonic epithelium of a gnotobiotic model rodent. *BMC biology*, 11:61, May 2013.

[97] T. Rossy et al. Pseudomonas aeruginosa contracts mucus to rapidly form biofilms in tissue-engineered human airways. May 2022.

[98] R. M. Landry et al. MucinâPseudomonas aeruginosa interactions promote biofilm formation and antibiotic resistance. *Molecular Microbiology*, 59(1):142–151, 2006.

[99] S. Pirr and D. Viemann. Host Factors of Favorable Intestinal Microbial Colonization. *Frontiers in Immunology*, 11, 2020.

[100] K. Stagaman et al. The role of adaptive immunity as an ecological filter on the gut microbiota in zebrafish. *The ISME Journal*, 11(7):1630–1639, 2017.

[101] A. S. Rolig et al. Individual members of the microbiota disproportionately modulate host innate immune responses. *Cell host & microbe*, 18(5):613–620, November 2015.

[102] M. Jemielita et al. Comparing phototoxicity during the development of a zebrafish craniofacial bone using confocal and light sheet fluorescence microscopy techniques. *Journal of biophotonics*, 6(0):10.1002/jbio.201200144, December 2013.

[103] R. M. Power and J. Huisken. A guide to light-sheet fluorescence microscopy for multiscale imaging. *Nature Methods*, 14(4):360–373, March 2017.

[104] P. J. Keller et al. Reconstruction of zebrafish early embryonic development by scanned light sheet microscopy. *Science (New York, N.Y.)*, 322(5904):1065–1069, November 2008.

[105] P. J. Keller and H.-U. Dodt. Light sheet microscopy of living or cleared specimens. *Current Opinion in Neurobiology*, 22(1):138–143, February 2012.

[106] R. Parthasarathy. Monitoring microbial communities using light sheet fluorescence microscopy. *Current Opinion in Microbiology*, 43:31–37, June 2018.

[107] Y. Wan et al. Light-Sheet Microscopy and Its Potential for Understanding Developmental Processes. *Annual Review of Cell and Developmental Biology*, 35(1), 2019.

[108] Y. Gong et al. A fully water coupled oblique light-sheet microscope. *Scientific Reports*, 12(1), April 2022.

[109] E. A. Hay and R. Parthasarathy. Performance of convolutional neural networks for identification of bacteria in 3D microscopy datasets. *PLOS Computational Biology*, 14(12), December 2018.

[110] O. Ronneberger et al. U-Net: Convolutional Networks for Biomedical Image Segmentation. *arXiv:1505.04597 [cs]*, May 2015.

[111] E. A. Hay. *Identifying Gut Bacteria and Their Interactions Using Deep Learning Based Image Analysis and Gnotobiotic Experiments*. Ph.D., University of Oregon, Ann Arbor, 2019.

[112] L. Dethlefsen and D. A. Relman. Incomplete recovery and individualized responses of the human distal gut microbiota to repeated antibiotic perturbation. *Proceedings of the National Academy of Sciences*, 108(Supplement 1), March 2011.

[113] S. R. Modi et al. Antibiotics and the gut microbiota. *The Journal of Clinical Investigation*, 124(10):4212–4218, October 2014.

[114] L. Zhao et al. Gut bacteria selectively promoted by dietary fibers alleviate type 2 diabetes. *Science*, 359(6380):1151, March 2018.

[115] R. N. Carmody et al. Diet dominates host genotype in shaping the murine gut microbiota. *Cell host & microbe*, 17(1):72–84, January 2015.

[116] Y. Shang et al. Inferring interactions in complex microbial communities from nucleotide sequence data and environmental parameters. *PloS One*, 12(3):e0173765, 2017.

[117] A. Carr et al. Use and abuse of correlation analyses in microbial ecology. *The ISME Journal*, 13(11):2647–2655, November 2019.

[118] D. Lovell et al. Proportionality: A Valid Alternative to Correlation for Relative Data. *PLOS Computational Biology*, 11(3), March 2015.

[119] N. Zmora et al. Personalized Gut Mucosal Colonization Resistance to Empiric Probiotics Is Associated with Unique Host and Microbiome Features. *Cell*, 174(6):1388–1405.e21, 2018.

[120] A. Aranda-DÃaz et al. Bacterial interspecies interactions modulate pH-mediated antibiotic tolerance. *eLife*, 9, January 2020.

[121] A. R. Burns et al. Contribution of neutral processes to the assembly of gut microbial communities in the zebrafish over host development. *The ISME journal*, 10(3):655–664, March 2016.

[122] E. M. Flores et al. The zebrafish as a model for gastrointestinal tractâmicrobe interactions. *Cellular Microbiology*, 22(3), 2020.

[123] J. T. Wootton. The Nature and Consequences of Indirect Effects in Ecological Communities. *Annual Review of Ecology and Systematics*, 25:443–466, 1994.

[124] I. Billick and T. J. Case. Higher Order Interactions in Ecological Communities: What Are They and How Can They be Detected? *Ecology*, 75(6):1530–1543, 1994.

[125] A. Sanchez. Defining Higher-Order Interactions in Synthetic Ecology: Lessons from Physics and Quantitative Genetics. *Cell Systems*, 9(6):519–520, 2019.

[126] V. C. Ozgen et al. Spatial interference scale as a determinant of microbial range expansion. *Science Advances*, 4(11):eaau0695, November 2018.

[127] R. M. Stubbendieck and P. D. Straight. Multifaceted Interfaces of Bacterial Competition. *Journal of Bacteriology*, 198(16):2145–2155, August 2016.

[128] A. Prindle et al. Ion channels enable electrical communication within bacterial communities. *Nature*, 527(7576):59–63, November 2015.

[129] C. Hoffmann et al. Archaea and Fungi of the Human Gut Microbiome: Correlations with Diet and Bacterial Residents. *PLoS ONE*, 8(6), June 2013.

[130] J. A. Steele et al. Marine bacterial, archaeal and protistan association networks reveal ecological linkages. *The ISME Journal*, 5(9), September 2011.

[131] B. H. Schlomann. Stationary moments, diffusion limits, and extinction times for logistic growth with random catastrophes. *Journal of Theoretical Biology*, 454:154–163, 2018.

[132] R. R. Stein et al. Ecological Modeling from Time-Series Inference: Insight into Dynamics and Stability of Intestinal Microbiota. *PLOS Computational Biology*, 9(12), December 2013.

[133] S. Marino et al. Mathematical modeling of primary succession of murine intestinal microbiota. *Proceedings of the National Academy of Sciences*, 111(1), January 2014.

[134] A. Sanchez-Gorostiaga et al. High-order interactions distort the functional landscape of microbial consortia. *PLOS Biology*, 17(12), December 2019.

[135] L. R. Lawlor. Direct and indirect effects of n-species competition. *Oecologia*, 43(3):355–364, December 1979.

[136] M. Dungan. Three-Way Interactions: Barnacles, Limpets, and Algae in a Sonoran Desert Rocky Intertidal Zone. *American Naturalist - AMER NATURALIST*, 127, March 1986.

[137] J. E. Fauth. Interactive Effects of Predators and Early Larval Dynamics of the Treefrog Hyla Chrysocelis. *Ecology*, 71(4), August 1990.

[138] W. B. Worthen and J. L. Moore. Higher-Order Interactions and Indirect Effects: A Resolution Using Laboratory Drosophila Communities. *The American Naturalist*, 138(5), November 1991.

[139] T. J. Case and E. A. Bender. Testing for Higher Order Interactions. *The American Naturalist*, 118(6), December 1981.

[140] J. E. Losey and R. F. Denno. Positive PredatorâPredator Interactions: Enhanced Predation Rates and Synergistic Suppression of Aphid Populations. *Ecology*, 79(6), 1998.

[141] Z. Zhang et al. Spatial heterogeneity and co-occurrence patterns of human mucosal associated intestinal microbiota. *The ISME journal*, 8(4):881–893, April 2014.

[142] J. Qin et al. A human gut microbial gene catalogue established by metagenomic sequencing. *Nature*, 464(7285):59–65, March 2010.

[143] R. M. May. Will a Large Complex System be Stable? *Nature*, 238(5364):413–414, August 1972.

[144] J. E. Goldford et al. Emergent simplicity in microbial community assembly. *Science*, 361(6401):469, August 2018.

[145] R. DâAndrea et al. Emergent neutrality in consumer-resource dynamics. *bioRxiv*, pp. 710541, January 2019.

[146] G. T.-W. Shaw et al. MetaMIS: a metagenomic microbial interaction simulator based on microbial community profiles. *BMC Bioinformatics*, 17(1):488, November 2016.

[147] M. Westerfield and M. Westernfield. *The zebrafish book : a guide for the laboratory use of zebrafish (Danio rerio)*. University of Oregon, Eugene, 5th ed. edition, 2007.

[148] W. Z. Stephens et al. The composition of the zebrafish intestinal microbial community varies across development. *The ISME journal*, 10(3):644–654, 2016.

[149] C. D. Nadell et al. Spatial structure, cooperation and competition in biofilms. *Nature Reviews Microbiology*, 14(9), September 2016.

[150] E. Trudnowska et al. Marine snow morphology illuminates the evolution of phytoplankton blooms and determines their subsequent vertical export. *Nature Communications*, 12(1), May 2021.

[151] C. M. Flintrop et al. Embedding and slicing of intact in situ collected marine snow. *Limnology and Oceanography: Methods*, 16(6):339–355, 2018.

[152] C. M. Prieto-Barajas et al. Microbial mat ecosystems: Structure types, functional diversity, and biotechnological application. *Electronic Journal of Biotechnology*, 31:48–56, January 2018.

[153] R. Durrett and S. Levin. Spatial Aspects of Interspecific Competition. *Theoretical Population Biology*, 53(1):30–43, February 1998.

[154] P. Amarasekare. Competitive coexistence in spatially structured environments: a synthesis. *Ecology Letters*, 6(12), 2003.

[155] B. Kerr et al. Local dispersal promotes biodiversity in a real-life game of rockâpaperâscissors. *Nature*, 418(6894), July 2002.

[156] B. Shorrocks and M. Bingley. Priority effects and species coexistence: experiments with fungal-breeding Drosophila. 1994.

[157] W. P. Sousa. Experimental Investigations of Disturbance and Ecological Succession in a Rocky Intertidal Algal Community. *Ecological Monographs*, 49(3), 1979.

[158] E. K. Costello et al. The Application of Ecological Theory Toward an Understanding of the Human Microbiome. *Science*, 336(6086), June 2012.

[159] D. Sundarraman et al. Higher-Order Interactions Dampen Pairwise Competition in the Zebrafish Gut Microbiome. *mBio*, 11(5):e01667–20, October 2020.

[160] J.-F. Sicard et al. Interactions of Intestinal Bacteria with Components of the Intestinal Mucus. *Frontiers in Cellular and Infection Microbiology*, 7, 2017.

[161] C. Robbe et al. Structural diversity and specific distribution of O-glycans in normal human mucins along the intestinal tract. *Biochemical Journal*, 384(Pt 2):307–316, December 2004.

[162] J. M. Rhodes. Colonic mucus and mucosal glycoproteins: the key to colitis and cancer? *Gut*, 30(12), December 1989.

[163] T. J. Smith et al. A mucin-regulated adhesin determines the intestinal biogeography and inflammatory character of a bacterial symbiont. *bioRxiv*.

[164] M. A. McGuckin et al. Mucin dynamics and enteric pathogens. *Nature Reviews. Microbiology*, 9(4):265–278, April 2011.

[165] G. C. Hansson. Role of mucus layers in gut infection and inflammation. *Current Opinion in Microbiology*, 15(1):57–62, February 2012.

[166] J. M. H. Larsson et al. A complex, but uniform O-glycosylation of the human MUC2 mucin from colonic biopsies analyzed by nanoLC/MSn. *Glycobiology*, 19(7):756–766, July 2009.

[167] N. Juge. Microbial adhesins to gastrointestinal mucus. *Trends in Microbiology*, 20(1):30–39, January 2012.

[168] K. E. Carothers et al. The Streptococcal Protease SpeB Antagonizes the Biofilms of the Human Pathogen Staphylococcus aureus USA300 through Cleavage of the Staphylococcal SdrC Protein. *Journal of Bacteriology*, 202(11).

[169] R. Randal Bollinger et al. Human secretory immunoglobulin A may contribute to biofilm formation in the gut. *Immunology*, 109(4), 2003.

[170] S. Mukherjee and B. L. Bassler. Bacterial quorum sensing in complex and dynamically changing environments. *Nature Reviews. Microbiology*, 17(6):371–382, June 2019.

[171] S. Elias and E. Banin. Multi-species biofilms: living with friendly neighbors. *FEMS Microbiology Reviews*, 36(5):990–1004, September 2012.

[172] A. H. Rickard et al. Autoinducer 2: a concentration-dependent signal for mutualistic bacterial biofilm growth. *Molecular Microbiology*, 60(6), 2006.

[173] T. D. Lawley and A. W. Walker. Intestinal colonization resistance. *Immunology*, 138(1):1–11, January 2013.

[174] V. Thomas et al. Molecular Characterization and Spatial Analysis of a Simplified Gut Microbiota Displaying Colonization Resistance against Clostridium difficile. *Microbial Ecology in Health and Disease*, 14(4), January 2002.

[175] H. Knecht et al. Effects of Î²-Lactam Antibiotics and Fluoroquinolones on Human Gut Microbiota in Relation to Clostridium difficile Associated Diarrhea. *PLOS ONE*, 9(2), February 2014.

[176] J. Y. Yoo et al. Gut Microbiota and Immune System Interactions. *Microorganisms*, 8(10):1587, 2020.

[177] D. Zheng et al. Interaction between microbiota and immunity in health and disease. *Cell Research*, 30(6), June 2020.

[178] E. M. Brown et al. The role of the immune system in governing host-microbe interactions in the intestine. *Nature Immunology*, 14(7), July 2013.

[179] S. H. Lam et al. Development and maturation of the immune system in zebrafish, Danio rerio: a gene expression profiling, in situ hybridization and immunological study. *Developmental and Comparative Immunology*, 28(1):9–28, January 2004.

[180] B. Ruder et al. Tumour Necrosis Factor Alpha in Intestinal Homeostasis and Gut Related Diseases. *International Journal of Molecular Sciences*, 20(8):E1887, April 2019.

[181] L. Marjoram et al. Epigenetic control of intestinal barrier function and inflammation in zebrafish. *Proceedings of the National Academy of Sciences of the United States of America*, 112(9):2770–2775, March 2015.

[182] F. Ellett et al. mpeg1 promoter transgenes direct macrophage-lineage expression in zebrafish. *Blood*, 117(4):e49–56, January 2011.

[183] K. K. Takaki et al. Schistosoma mansoni Eggs Modulate the Timing of Granuloma Formation to Promote Transmission. *Cell Host & Microbe*, 29(1):58–67.e5, January 2021.

[184] L. Ramakrishnan. Looking Within the Zebrafish to Understand the Tuberculous Granuloma. In M. Divangahi, editor, *The New Paradigm of Immunity to Tuberculosis*, Advances in Experimental Medicine and Biology, pp. 251–266. Springer, New York, NY, 2013.

[185] H. M. Isles et al. Pioneer neutrophils release chromatin within in vivo swarms. *eLife*, 10:e68755, July 2021.

[186] L. Cantas et al. Impact of antibiotic treatments on the expression of the R plasmid tra genes and on the host innate immune activity during pRAS1 bearing Aeromonas hydrophila infection in zebrafish (Danio rerio). *BMC Microbiology*, 12:37, March 2012.